

|| Shri ||

“In-Situ Chemo-Bioremediation for Gas Clean-up”

Thesis submitted to the

UNIVERSITY OF PUNE

For the Degree of

DOCTOR OF PHILOSOPHY

in

CHEMICAL ENGINEERING

BY

ANIRUDDHA SUBHASH DESHPANDE

Research Guide

Dr. B. D. KULKARNI

CHEMICAL ENGINEERING AND PROCESS DEVELOPMENT DIVISION

NATIONAL CHEMICAL LABORATORY

PUNE-411 008, INDIA

March 2009



Dedicated to
Aai & Baba,
Father-in-law & Mother-in-law,

My beloved wife Pallavi

Acknowledgements

I would like to express my sincere gratitude to my guide and guru, Dr. B. D. kulkarni, for his invaluable guidance and help rendered through out the course of my Ph. D. work. He taught, criticized, encouraged and advised all of which have helped me during my Ph.D. work and preparation of the thesis. As an outstanding scientist and guru, he has given me the benefit of his excellent training in abundant measure. His principles and values have always been a source of inspiration for me.

I am grateful to Dr. S. Sivaram, Director, NCL, for this opportunity to work in this prestigious institute. I duly acknowledged CSIR, New Delhi for awarding me Senior Research Fellowship.

I couldn't express my thanks in word to Dr. Ms. S. B. Umbarkar & Dr. M. K. Dongre, for inspiring discussions, constant encouragement, valuable advice and most professional help in crucial time of my work.

I am deeply indebted to Ms. Arti Harle for her guidance, motivation and good wishes.

I greatly appreciate continuous help rendered by Mr. P. P. Barve, Mr. S. N. Nene and Dr. S. S. Tambe to carry out the most vital study of Ph.D. work.

I am very much thankful to scientist Dr. S. P. Gupte, Dr. A. A. Kelkar, Dr. Ms. S. Mayadevi, Dr. Ms. S. Kulkarni, Dr. V. K. Jayaraman. Dr. Ravi Kumar, Dr. R. V. Gadre, Ms. Violet, Dr. U. K. Kharul, Mr. A. B. Gaikwad, Dr. A. G. Gaikwad, Mr. Chaphekar, Dr. Ms. Paradhi, Mr. K. V. Pandare, Mr. G. R. Kale, Dr. S. Pal, Dr. A. K. Lele, Dr. Ms. N. N. Bulakh.

I deeply acknowledge for constant help by Mr. V. Borkar, Mr. S. H. Dure in online data collection system and experimental setup.

I sincerely express my gratitude to my seniors, colleagues and friends; Madhavi, Renuka, Bhalchandra, Ravi, Sonali, Geetanjali, Sandeep Golegaokar, Laxamn, Santosh, Harshada, Dr. Yogesh Bhole, Yogesh Chendake, Sandeep Kothawade, Shubhangi, Mrunal, Ganesh, Dr. Praveen, Dr. Anand, Lalita madam, Savita Madam, Pipalad, Ankush, Trupti, Dr. Ms.

Sujata Mandal, Nikunj, Hemalata, Naren, Dev, Dr. Yogesh Badhe, Prashant, Aniruddha Joshi, Hrishikesh, Prasad, Dr. Narahari Pujari and many more for their support, motivation, help during technical discussion.

I heartily appreciate the constant co-operation of Mr. A. S. Banerjee, Mr. H. Raheja, Mr. S. P. Bhalerao, Mr. S. R. Narwade, Mr. S. B. Wanjale, Mr. D. S. Shinde, Mr. R. M. Murkute, Mr. B. G. Poman, Mr. B. K. Kedari, and Mr. V. L. Rajput.

I am thankful to all staff of NCL facilities, SAIF; Lucknow for providing mass spectrum, Library facility, all other laboratories, Administration and Security.

No words can suffice to acknowledge the encouragement and moral support given by all my family members and relatives.

And finally I appreciate support from all my well wishers.

Aniruddha Subhash Deshpande

Certificate of Guide

Certified that the work incorporated in the thesis entitled “**In-Situ Chemo-Bioremediation for Gas Clean-up**” submitted by Aniruddha Subhash Deshpande was carried out under my supervision. Such material as has been obtained from other sources has been duly acknowledged in this thesis.

March, 2009

National Chemical Laboratory

Pune - 411 008

Dr. B. D. Kulkarni

(Research Guide)

Declaration by the Candidate

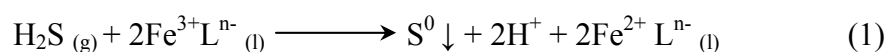
I hereby declare that the thesis entitled “**In-Situ Chemo-Bioremediation for Gas Clean-up**” is my own work conducted under the supervision of Dr. B. D. Kulkarni, at Chemical Engineering and Process Development Division, National Chemical Laboratory, Pune. I further declare that to the best of my knowledge, this thesis does not contain any part of work, which has been submitted for the award of any degree either of this University or any other University without proper citation.

Research Guide
(Dr. B. D. Kulkarni)

Research Student
(Aniruddha Subhash Deshpande)

Abstract

Pollution control is one of the most critical issue in front of developed and developing countries who are facing an immense crisis in this field. Hydrogen sulfide (H₂S) is a highly toxic and an undesirable gaseous component of natural gas and other waste gaseous streams. Abatement of H₂S by Catalytic conversion to elemental sulfur can be achieved by various chemical and biological methods. Liquid redox sulfur recovery processes absorb H₂S from gaseous streams and convert it to elemental sulfur. The gas desulfurization can also be carried out using liquid redox chemistry, where iron complexes are alternately reduced according to the following reactions.



Since the active ferric chelate is converted to inactive ferrous chelate, the later component has to be regenerated by oxidation according to



where 'L' denotes an organic ligands, which is usually a polyaminocarboxylic acids.

Chelating agents (EDTA, HEDTA, DTPA, NTA, CDTA, etc.) reported for iron chelation have very low rate of biodegradation (e.g. EDTA BOD₅²⁰- 0.1%, DTPA BOD₅- 0.7%) thus causing pollution in itself. Alternative chelating agents for gas sweetening should possess high rate of biodegradability along with equal or better complex forming properties compared to commercial chelating agents. It has been reported that carboxylic acids posses good chelating properties and have faster rate of biodegradation (e.g. citric acid BOD₅²⁰- 61% and malic acid BOD₅²⁰- 65%) as compared with commercial chelating agents.

This work, for the first time reports a detailed study involving screening of biodegradable Fe³⁺-chelates for the catalytic conversion of H₂S gas to elemental sulfur. Among various chelates that were screened, the Fe³⁺-MA chelate exhibits

maximum sulfur recovery and purity. Thus, the detail structural characterization of Fe^{3+} -MA chelate was studied. By using this novel biodegradable chelate the synthesis and characterization of sulfur nanoparticles was carried out in w/o microemulsion system and in different aqueous surfactant systems. The performance of mechanically agitated batch reactor (MABR) using Fe^{3+} -MA chelate as a catalyst was also studied extensively. The work done towards achieving this goal has been elaborated into following chapters of the thesis.

Contents

<u>Chapter - 1 Introduction to H₂S Abatement</u>	1
1. Introduction	2
2. Review of Literature	4
3. Motivation	12
4. Objectives	12
<i>Part I – Novel biodegradable iron chelate synthesis and characterization</i>	12
<i>Part II – Sulfur nanoparticles synthesis using novel biodegradable iron chelate</i>	13
<i>Part III – Process modeling and optimization for H₂S abatement in Novel Iron chelate.</i>	13
5. Scheme of the Thesis	13
Reference	16

<u>Chapter – 2 Synthesis and Characterization of Biodegradable Iron (III) Chelate Complexes: Catalytic Oxidation of H₂S</u>	21
Abstract	22
1. Introduction	23
2. Experimental	26
2.1 Chemicals	26
2.2 Characterization	26
2.3 Preparation of Iron chelate solution	27
2.3.1. Iron(III)- carboxylic acid chelate synthesis in acidic medium (at pH-2)	27
2.3.2. Iron(III)- carboxylic acid chelate synthesis in neutral medium (pH 7-7.5)	28
2.3.3. Iron(III)- carboxylic acid chelate synthesis in basic medium (at pH 9)	28
2.4 General method of sulfur recovery from H ₂ S gas	28
3. Results and Discussions	29
3.1 Infrared spectra analysis	31
3.2 TG-DTA analysis	33
3.3 ESI-MS analysis	37

4. Conclusions	44
References	45

Chapter – 3 Sulfur Nanoparticles Synthesis, Characterization and Application 48

Abstract	49
1. Introduction	50
2. Experimental	53
2.1 Materials	53
2.2 Preparation of iron chelate solution for H ₂ S abatement	53
2.3 Selection of optimum iron chelate system	53
2.4 Preparation of FeCl ₃ -malic acid (Fe ³⁺ -malic acid) chelate solution	54
2.5 Instrumentation	55
2.6 Evaluation of antimicrobial activity of sulfur nanoparticles	55
Part-I Synthesis of sulfur nanoparticles in w/o microemulsion system	56
3. Results and Discussion	56
3.1 XRD analysis of the sulfur particles	57
3.2 EDS analysis	58
3.3 TEM analysis	59
3.4 DLS Analysis	61
3.5 IR analysis	62
3.6 Antimicrobial activity of sulfur nanoparticles	63
Part –II Synthesis of sulfur nanoparticles in different aqueous surfactant systems	68
4. Results and Discussion	68
4.1 XRD and EDS analysis	69
4.2 TEM analysis	72
4.3 DLS Analysis	74
4.4 IR analysis	76
4.5 Antimicrobial activity of sulfur nanoparticles	77
5. Conclusions	80
References	81

<u>Chapter – 4 Novel biodegradable iron chelate catalyst for H₂S abatement: Modeling and optimization of batch reactor process using artificial intelligence strategies</u>	84
Abstract	85
1. Introduction	86
2. Materials	88
2.1 Chemicals	88
2.2 Instrumentation	88
2.3 Computational techniques	89
2.4 Screening of Iron chelate solution	89
3. Experimental	90
3.1 General method of sulfur recovery from H ₂ S gas	90
4. Process modeling and optimization using PB-ANN-GA hybrid Model	94
4.1 Plackett-Burman design	94
4.2 ANN-based modeling	95
4.3 GA-Based Optimization of Inputs of ANN-Model	96
5. Results and Discussion	97
5.1 Selection of influential process variables and parameters using Plackett–Burman design	97
5.2 ANN-Based MABR Modeling	99
5.3 GA-based Optimization of the MLP Model	105
6. Part-II Process modeling and optimization using PB-RSM	108
6.1 Plackett-Burman design	108
6.2 Response Surface Method (Central Composite Design)	108
7. Results and Discussion	110
7.1 Selection of influential process variables and parameters using Plackett–Burman design	110
7.2 Response Surface method (Central Composite Design) for process modeling and optimization	111
8. Conclusions	120
References	121
<hr/> <hr/>	
<u>Chapter – 5 Conclusions</u>	124

List of Tables

Chapter – 2

Table 2.1: Various processes and chelating agents used for iron chelation for H₂S abatement

Table 2.2: Screening of iron chelate systems for H₂S abatement

Table 2.3: FTIR data for Fe(III)-malic acid chelate synthesized at different pH conditions

Table 2.4: TG/DTA data for FMI-1, FMI-2, FMI-3

Table 2.5: ESI-MS data for Fe(III)-Malic acid chelate synthesized at different pH condition

Chapter - 3

Table 3.1: Screening of iron chelate systems for H₂S abatement

Table 3.2: Antimicrobial activity of sulfur nanoparticles synthesized in w/o microemulsion system

Table 3.3: The calculation for number of micelles in the solution

Table 3.4: Antimicrobial activity of sulfur nanoparticles synthesized in different aqueous surfactant system

Chapter – 4

Table 4.1: Experiments for Plackett-Burman design

Table 4.2: Statistical calculations for PB design

Table 4.3: H₂S abatement reaction data used in ANN modeling

Table 4.4: GA-optimized solutions and their experimental validation

Table 4.5: The coded values for the independent variables and parameters

Table 4.6: RSM based Central Composite design matrix of independent variables and parameters and their corresponding experimental and predicted % H₂S conversion

Table 4.7: Analysis of variance (ANOVA)

Table 4.8: RSM-optimized solutions and their experimental validation

List of Figures

Chapter – 1

Scheme 1.1: Schematic representation of the approach of Ph.D. work

Chapter – 2

Figure 2.1: Simplified process flow diagram for catalytic conversion of H₂S to elemental sulfur

Figure 2.2: Comparison of FTIR spectra of malic acid (MA) with iron chelates at pH 2 (FMI-1) at pH 7-7.5 (FMI-2) and at pH 9 (FMI-3)

Figure 2.3a: TG-DTA curve for Fe(III)-Malic acid chelate synthesized at pH 2 (FMI-1)

Figure 2.3b: TG-DTA curve for Fe(III)-Malic acid chelate synthesized at pH 7-7.5 (FMI-2)

Figure 2.3c: TG-DTA curve for Fe(III)-Malic acid chelate synthesized at pH 9 (FMI-3)

Figure 2.4: ESI-MS for Fe(III)-Malic acid chelate at pH 2 (FMI-1)

Figure 2.5: ESI-MS spectra for Fe(III)-Malic acid chelate (FMI-2) at pH 7.5

Figure 2.6: ESI-MS spectra for Fe(III)-Malic acid chelate (FMI-2) at pH 7.5

Figure 2.7: ESI-MS spectra Fe(III)-Malic acid chelate at pH 9 (FMI-3)

Figure 2.8: ESI-MS spectra Fe(III)-Malic acid chelate at pH 9 (FMI-3)

Scheme 2.1: Fragmentation pattern for the Fe(III)-Malic acid chelate synthesized at pH 2 (FMI-1)

Scheme 2.2: Fragmentation pattern for the Fe(III)-Malic acid chelate synthesized at pH 7-7.5 (FMI-2) and at pH 9 (FMI-3)

Chapter - 3

Figure 3.1: Schematic representation of synthesis of sulfur nanoparticles in w/o microemulsion system

Figure 3.2: XRD of sulfur particle synthesis in: a) aqueous phase; b) w/o microemulsion

Figure 3.3: EDAX of sulfur nanoparticles synthesized in: a) aqueous phase; b) w/o microemulsion

Figure 3.4: TEM analysis for sulfur nanoparticles synthesized in different systems: a-1) aqueous phase system; a-2) diffraction pattern of aqueous phase sulfur;

b-1 to b-3) W/O microemulsion at various magnification; b-4) diffraction pattern of sulfur nanoparticle

Figure 3.5: Histogram for particles size distribution for sulfur nanoparticles synthesized in w/o microemulsion

Figure 3.6: DLS analysis for sulfur nanoparticles synthesized in w/o microemulsion system

Figure 3.7: Diffused Reflectance Infra-red Fourier Transform analysis: a) sulfur nanoparticles; b) Std IR of rhombic sulfur

Figure 3.8: BET isotherm for the sulfur nanoparticles synthesized in w/o microemulsion

Figure 3.9: BET isotherm for the sulfur synthesized in aqueous phase only

Figure 3.10: Schematic representation of synthesis of sulfur nanoparticles in various aqueous surfactant systems

Figure 3.11: XRD of sulfur particle synthesis in: a) aqueous phase; b) CTAB; c) SDS; d) Tween-80

Figure 3.12: EDAX of sulfur nanoparticles synthesized in: a) aqueous phase; b) CTAB; c) SDS; d) Tween-80

Figure 3.13: TEM analysis for sulfur nanoparticles synthesized in different systems: a) aqueous phase; b) Tween-80; c) CTAB; d) SDS surfactant

Figure 3.14: Histogram for particles size distribution for sulfur nanoparticles synthesized in different aqueous surfactant systems using: a) CTAB; b) Tween-80; c) SDS surfactant system

Figure 3.15: DLS analysis for sulfur nanoparticles synthesized in different systems: a) CTAB; b) Tween-80; c) SDS aqueous surfactant system

Figure 3.16: Diffused Reflectance Infra-red Fourier Transform analysis for sulfur nanoparticles synthesized in aqueous surfactant system using: a)CTAB surfactant; b) Tween-80 surfactant; c) SDS surfactant

Figure 3.17: Photographs of plate assay for antimicrobial and antifungal activity of sulfur nanoparticles and sulfur synthesized in aqueous phase

Chapter – 4

Figure 4.1: Simplified process flow diagram for catalytic conversion of H₂S to elemental sulfur

Figure 4.2: H₂S gas cylinders along with gas reservoir

Figure 4.3: Mechanically agitated batch reactor

Figure 4.4: Online data acquisition system used for H₂S abatement

Figure 4.5: Parity plot of model-predicted and experimental H₂S conversion.

Figure 4.6: Plot of RSM model predicted H₂S % conversion v/s experimental Results

Contour plot 4.1: Response for H₂S conversion - Initial H₂S concentration v/s Temp

Contour plot 4.2: Response for H₂S conversion - Stirring speed of impeller v/s Initial H₂S concentration

Contour plot 4.3: Response for H₂S conversion - Temperature v/s Pressure

Contour plot 4.4: Response for H₂S conversion-
Stirring speed of impeller v/s Pressure

Contour plot 4.5: Response for H₂S conversion- Stirring speed of impeller v/s Temp

||shri||

CHAPTER-1

INTRODUCTION TO H₂S ABATEMENT

1. Introduction

The massive pace of industrialization and advanced commercial activity over the last few years has influenced the growth and development of mankind. This advancement has brought along with it a parallel series of fallouts and negative impacts that endanger the very basics of environmental safety and human existence. It is not easy for the earth to replenish her at a pace that she may be relieved of all the stresses (pollution) we impose upon her. Pollution control is one of the most important and critical issue to catch the attention of the developed and developing countries who are facing an immense crisis in the field. Air pollution is one of the many forms of pollution that plagues mankind everyday.

In the last few decades, concerns have been raised about release of toxic or smog-forming compounds. Objectionable air emissions are generally categorized as **volatile organic carbons (VOCs)** or as **odorous hazardous air pollutants (HAPs)**. Installation of an air purification system for the removal of odor is normally carried out to eliminate the nuisance factor of noxious odors and the impact on workers and the surrounding population, while VOC removal is often triggered by health and regulatory issues or localized damage caused by the emissions. Several technologies have been developed or improved recently to control odors from various industries. The best method for controlling odorous compounds is by eliminating the odor before it is formed thus eliminating the need for further processing of the air. However, this is not an easy task. Many manufacturers cannot control all of the volatile released during processing.

Processes like catalytic conversion of odorous HAP's go a long way in ensuring clean and healthy environment for the benefit of one and all in all parts of the world. The process being operated at atmospheric pressure and ambient

temperature with easy monitoring of process parameters will help small, medium and large industries with their pollution abatement needs. Technologies for controlling odorous HAP's must meet the following criteria to be effective in the processing industry.

- 1) Stable and predictable performance in the removal of odorous compounds from the contaminated air stream
- 2) Easy adaptability for applications experiencing large variations of air-flow rates and odor control intensity
- 3) No or low generation of environmentally harmful chemical by-products
- 4) Low generation of solid and/or liquid waste materials and
- 5) Low equipment costs and low operational and maintenance requirement

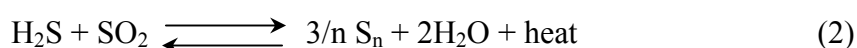
Hydrogen sulfide (H₂S) is a naturally occurring highly toxic and undesirable gas. It occurs in many natural gas wells and is also produced in large quantities in the desulfurization of petroleum stocks and other waste gaseous streams. The hydrogen sulfide concentration in natural gas ranges from 3.76 to 8.55% (v/v). The natural gas wells having more than 10% of hydrogen sulfide are closed down, as it is very difficult to operate them. The biogas contains 1.2 to 2.5% (v/v) H₂S. The co-generated gaseous fuel from crude oil is mainly refinery fuel gas that contains H₂S ranging from 4.5 to 7.5% (v/v). The H₂S content of coke oven gas varies from 0.30 to 4.8% (v/v). The gaseous fuels generated during the gasification of coal also contain appreciable concentrations of H₂S ranging from 0.6 to 2.0% (v/v).¹

2. Literature review

H₂S abatement processes also known as sulfur recovery processes were developed as back as in late 1800. Some of the processes reported are based on the absorption of H₂S gas with inorganic compounds solutions and suspensions namely potassium phosphates and carbonates, sodium carbonates, iron compounds, alkali metal hydroxides, arsenic compounds and many others. Removal of H₂S gas using various organic compounds like alkanolamines, amines, ethers and esters have also reported.² Catalytic conversion of H₂S to elemental sulfur can be achieved by various chemical³⁻⁵ and biological methods.^{6,7} Traditional method for removing H₂S from sour natural gas was to first treat the gas with a solvent to remove the H₂S and then recover the H₂S as molten sulfur in sulfur plant. C. F. Claus patented ‘Claus Process’ for H₂S removal which was developed in 1883.⁸ The Claus process was the most widely used method for sulfur recovery form acid gases. Conversion was achieved by partial oxidation of H₂S obtained by desulfurization of natural gases, refinery gas or other industrial gases. In the standard form of the process the reaction takes place in two successive steps. In the first thermal stage one-third of the H₂S gas is burned at 1,188°C to produce SO₂ according to following reaction,



The remaining part of H₂S gas reacts subsequently with the SO₂ to form S in the thermal and catalytic stages according to following reaction,



Where n is average molecular species of the sulfur vapour product, with n = 2 to 8 and possibly more. The most widely used Claus catalyst is non-promoted spherical activated alumina,⁹⁻¹¹ however some other catalysts were also reported e.g. Co-Mo/Al₂O₃¹²⁻¹⁴, Fe/SiO₂, Fe-Cr/SiO₂¹⁵, V/SiO₂¹⁶ etc. Sulfur recovery in traditional

Claus plants varies from 90-96% for two stage plant and up to 97% of the sulfur recovery can be achieved when three stage Claus sulfur recovery units was employed.¹⁷ Higher sulfur recoveries can not be achieved for three reasons.

- 1) The Claus reaction is an equilibrium reaction and thus complete H₂S and SO₂ conversion is not possible.
- 2) Process water produced in the Claus reaction can not be practically removed and hinders conversion and limits total sulfur recovery.
- 3) The critical H₂S:SO₂ ratio of 2:1 is, in practice, extremely difficult to achieve.

The modified Claus process, SuperClaus 99 and SuperClaus 99.5 process, MOST process¹⁸ were the new developments which achieve sulfur conversion up to 99%.

There are many other commercial processes which are the further development and/or modification of the existing Claus process e.g. AMOCO sulfur recovery,^{19,20} Giammarco Vetrocoke-Sulfur,²¹ Stretford,^{22,23} Takahax,²⁴ Sulfox,²⁵ Beavon,²⁶ IFP,^{27,28} Shell Claus off-Gas Treating (SCOT),^{29,30} Sulfreen,³¹ W-L SO₂ recovery³² and Claus Tail-gas treatment process.³³

Khol and Riensenfeld reported the Liquid redox sulfur recovery (LRSR)³⁴⁻³⁸ processes which absorb H₂S from gaseous streams and convert it to elemental sulfur. Six processes have been reported in the literature that are used for desulfurization of refinery fuel gases and sour off gases, natural gases, process and off gas streams in coal gasification plants, geothermal vent gases, shale oil and underground gasification plant gases, Claus tail gas and enhanced oil recovery vent gas. These processes have occupied a major place in the world market. The first three processes, viz., Stretford,²⁹ Unisulf, and Sulfolin, are vanadium-based processes in which vanadium is the primary catalyst interacting with the sulfur species. The two other processes, LOCAT

and Sulferox, are iron based. While the Hiperion process uses iron and quinone as catalysts.^{40, 41}

The first LRSR process reported is based on the ammonium sulfide / ammonium sulfate couple. This process involved a number of ammonium polythionates. The next development in the LRSR process is the involvement of iron oxide particles suspended in alkaline Na₂CO₃ solution. The Fe₂O₃ and Fe(OH)₃ suspension were used in American Ferrox process, the German Gluud process and in the British Manchester process. The process efficiency was affected by various side reactions. The formation of sulfur compounds such as thiosulfate and sulfate hampered the process efficiency.⁴² The Fe(III)/Fe(II) redox couple technology was further developed on the basis of use of hexacyanoferrate and is known as “Staatsmijnen-Otto process”. The use of toxic Fe(CN)₆ⁿ⁻ (n=3 or 4) and ammonia raised serious environmental issues.⁴³ The use of As(V)/As(III) in Giammarco-Vetrocoke process was another attempt for desulfurization, but the toxicity of As(V)/As(III) lost its significance during 1950’s.^{44, 45}

The Stretford process was developed by M/s North Wester USA and has been available for desulfurization of gas since 1959. Stretford solution contains pentavalent vanadium ion as a catalyst which is reduced to a tetravalent state during reaction with H₂S.⁴⁶ One or more ventury tower or packed tower as contactor may be used in various configurations for contacting the Stretford liquid and acid gas. Solution leaving the contactor was held in a reaction tank to allow sufficient time for bisulfide ion to be oxidized to elemental sulfur. Then the solution was routed through the oxidizer, where anthraquinone disulfonic acid (ADA) is used to catalyze the oxygen transfer in regeneration of reduced vanadium. Subsequently air was passed through the solution that causes reoxidation of vanadium (V⁴⁺) to vanadium (V⁵⁺) and causes

sulfur to agglomerate and float on the surface. The regenerated solution was returned to the contactor, while sulfur froth was separated from the oxidizer and sent to a filter or centrifuge. The sulfur froth was dewatered to get 50% solids and then washed to recover the Stretford solution. The sulfur may be further purified by autoclaving or sulfur cake may be disposed as solid waste.⁴⁷

The first commercial test of the Unisulf solution was made at SASOL in late 1981 developed by Union Oil's Science and Technology Division at Brea, California. The process was based on use of vanadium catalyst along with thiocyanate, carboxylate and aromatic sulfonates as complexing agents. The process claims that they avoid salt byproduct formation. The Unisulf Process can remove only H₂S but not the other sulfur compounds such as COS, CS₂, and SO₂. For feeds containing these other sulfur compounds, such as the Claus plant tail gas, a variation of this process called the BSR/Unisulf Process can be used.⁴⁸ Sulfolin process was marketed by M/s Lindane A.G. This process also uses vanadium based catalyst. The H₂S in the feed gas is absorbed by and reacts with alkaline washing liquor in absorber unit followed by reactions,



The NaHS formed in the absorber was oxidized by sodium vanadate to elemental sulfur according to following reaction,

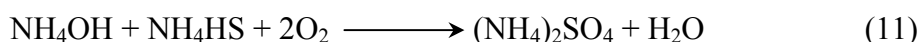
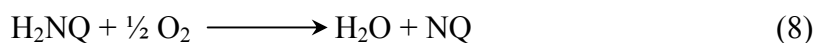


After oxidation of H₂S the reduced vanadium (V⁴⁺) must be reoxidized. In sulfolin process the oxidation rate was accelerated by addition of a promoter, which increases the reactivity of reduced vanadium. The promoter used was organic nitrogen compound, but exact composition was proprietary.

For removal of up to 99.9% of H₂S from gas streams particularly those with low initial H₂S concentration and/or high CO₂/H₂S ratios, the Takahax process was developed by Hasebe of the Tokyo gas company limited.⁴⁹ The main objective of the process is to devise a liquid redox H₂S removal process comparable to Streford, Sulfolin process and to eliminate the use of heavy metals to oxidize H₂S. Takahax process utilizes alkaline solution (pH 8.5) containing sodium 1,4-naphthoquinone, 2-sulfonate as a redox catalyst which contacts feed gas in an absorber tower. H₂S reacts with sodium carbonate to form sodium bisulfide and sodium bicarbonate. The bisulfide is oxidized by the catalyst to precipitate very finely divided solid sulfur (2 μm).



During this reaction naphthoquinone sulfonate was reduced to naphtho-hydroquinone sulfate, which was further oxidized by bubbling air to regenerate and reuse. A major drawback of this process was the very slow rate of reoxidation of the hydro-naphthoquinine sodium salt. This increases the regenerator residence time requirements and capital cost.⁵⁰

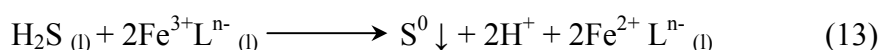


The modified version of Takahax process was Hiperion Process developed in 1994. In this HS⁻ ions were oxidized by naphthoquinone (NQ) chelate to elemental sulfur & the quinone was reduced to hydroquinone form (HNQ). The hydroquinone

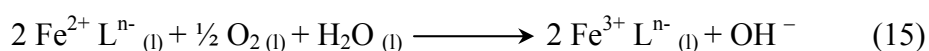
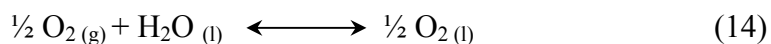
chelate was subsequently reacted with oxygen in the atmospheric air to form the quinone chelate and hydrogen peroxide. The benefit of hydrogen peroxide produced in the reaction is that it is extremely active oxidation agent, which reacts readily with residual unreacted bisulfide ion to form sulfur and water.⁴⁰

The environmental concern about vanadium content of the blow down streams has resulted in the selection of iron based processes for most recent application of H₂S removal. Iron is an excellent oxidizing agent for the H₂S to elemental sulfur conversion however, due to the very low solubility of iron in aqueous solutions, the iron had to be present in dry state or in suspension form (Ferrox process) or compounded with toxic materials such as cyanides.⁴³ To increase the solubility of elemental iron in aqueous solution the ‘Chelated Iron Process’ (CIP), was introduced in late 1960’s in United Kingdom. Iron chelation means the encapsulation of iron metal with chelating agents in liquid solution, such as amino and polyaminopolycaobxylic acids e.g. nitrilotriacetic acid (NTA), ethylene diamine tertaacetic acid (EDTA), hydroxy ethylethylene diamine triacetic acid (HEDTA), etc. This CIP process however failed miserably due to severe ligand loss and/or iron precipitated out with sulfur as FeS. The problem was that the chelation strength of many chelating agents varies with solution pH.

In the iron chelate-based processes following reaction usually represent the absorption of hydrogen sulfide and conversion into elemental sulfur; iron complexes are alternately reduced according to the following reactions.⁵¹⁻⁵⁵



Since, the active ferric chelate is converted to inactive ferrous chelate, the later component has to be regenerated by oxidation according to



where, 'n' denotes the charge of an organic ligand 'L', which is usually a polyaminocarboxylic acid such as EDTA, HEDTA, NTA, cyclohexane-1,2-diaminetetraacetic-(CDTA), etc. It is interesting to note that the chelating agents do not appear in the process chemistry, and in the overall chemical reaction no iron chelate is consumed. So the obvious question is why chelated iron is required at all, if it does not take part in overall reaction. The iron serves two purposes in the process chemistry. First, it serves as an electron donor and acceptor or in other words, a reagent. Secondly it serves as a catalyst in accelerating the overall reaction. Because of this dual purpose it was called as catalytic reagent. Thus it may also be considered as a pseudocatalyst. In late 1970's LOCAT process was introduced by M/s ARI technologies. In this process the problem of iron chelate precipitation and the strength of iron chelates were increased. All the LOCAT plants were operated under mildly alkaline conditions ($7 \leq \text{pH} \leq 9$),⁵⁶ and iron concentrations are in the order of 0.02M, temperatures may be within the range of $5 \leq T \leq 75$ °C. The sour gas was passed through the gas liquid contactor e.g. ventury scrubber, spray tower and liquid-filled contactors, depending on the required efficiencies for sour gas removal. LOCAT process uses ARI-310 catalytic reagent, a proprietary chemical, which uses EDTA as a chelating agent to form iron chelation (iron solution concentration was 500-1800 ppm). Addition of a polyhydroxylated sugar to the EDTA overcomes the stability problem. High activity of the catalytic reagents allow operation with very low concentrations of iron in solutions. It also requires very high solution circulation rate.⁵⁷ The second 'Autocirculation LOCAT' process was introduced in 1983 which can handle amine acid gases and other high H₂S concentration streams. This design

suggests circulation of very large volumes of catalyst and in turn allows very low iron concentrations and minimizes the cost of solution lost from the unit with sulfur product and/or as blow down. The byproduct formation like thiosulfate production however was very high. The next Aqua-Cat process was introduced in 1990, which requires a special mechanical configuration to allow the use of ultra low catalyst concentrations. All the three processes differ from each other. It was very difficult to translate the advantageous characteristics of one system into the other. The development of LOCAT-II process overcomes all the disadvantages of the three processes.^{58,59} This new configuration of LOCAT-II permits circulation at controlled rates through vessels with inherently improved oxygen mass transfer. The reduction in initial cost is achieved by reducing unit size, initial inventory cost of chemicals and air blower size. As the byproduct formation of thiosulfate was reduced the chemical makeup cost is also reduced. In the LOCAT and Autocirculation LOCAT processes, the molar ratio of iron in the scrubbing solution to H₂S in the feed was typically 4:1, twice the stoichiometric requirement. In the LOCAT-II process (both the conventional and Autocirculation versions) this ratio was typically less than 2:1.^{59,60}

In 1987 M/s Shell Oil and M/s Dow Chemical, U.S. jointly introduced a new process named "Sulferox process". Fe-NTA chelate system at pH 3.5 - 4.5 was introduced for H₂S removal. Iron concentration in Sulferox process is around 1 -3%,⁶¹ where as in LOCAT it was about 0.1 - 0.05%. The presence of NTA serves two functions; 1) to solubilize the ferric ion and 2) prevent formation of hydroxide at the pH of operation and catalyze the reaction of Fe²⁺ with O₂. It also inhibits the formation of salt of sulfoxy compounds such as thiosulfate.

3. Motivation

From the literature search the iron chelate process for H₂S abatement reported various chelating agents e.g. EDTA, HEDTA, DTPA, NTA, CDTA, etc. These chelating agents were having very low rate of biodegradation (e.g. EDTA BOD₅²⁰- 0.1%, DTPA BOD₅²⁰- 0.7%) thus causing pollution.⁶² Alternative chelating agents for gas sweetening should meet three main criteria, viz. (i) should possess equal or better complex forming properties compared to commercial chelating agents, (ii) should possess better biodegradability and (iii) should contain low nitrogen so as to minimize the nitrogen content in effluents. It has been reported that carboxylic acids (e.g. citric acid,⁶³ malic acid, gluconic acid, etc.) possess good chelating properties and have faster rate of biodegradation (e.g. citric acid BOD₅²⁰- 61% and malic acid BOD₅²⁰- 65%) as compared to commercial chelating agents.⁶²⁻⁶⁴ The complex forming properties of these carboxylic acids needs to be studied and improved if they have to replace commercial chelating agents.

With this background, specific objectives of the present work are listed as follows.

4. Objectives

The work presented in this thesis was carried out with the following objectives:

Part I – Novel biodegradable iron chelate synthesis and characterization

- ❖ Screening of carboxylic acids for iron chelation
- ❖ Synthesis of iron chelates using carboxylic acids
- ❖ Detail analysis for H₂S to elemental sulfur conversion based on quantitative and qualitative analysis of sulfur produced
- ❖ Detail structural characterization of screened iron chelates

Part II – Sulfur nanoparticles synthesis using novel biodegradable iron chelate

- ❖ Synthesis and characterization of sulfur nanoparticles using biodegradable iron chelate
- ❖ Synthesis in reverse microemulsion and in different aqueous surfactant systems
- ❖ Detailed characterization of sulfur nanoparticles using XRD, EDAX, TEM, DLS, DRIFT analysis techniques
- ❖ Statistical analysis of the data on the application of sulfur nanoparticles as antimicrobial and antifungal agent

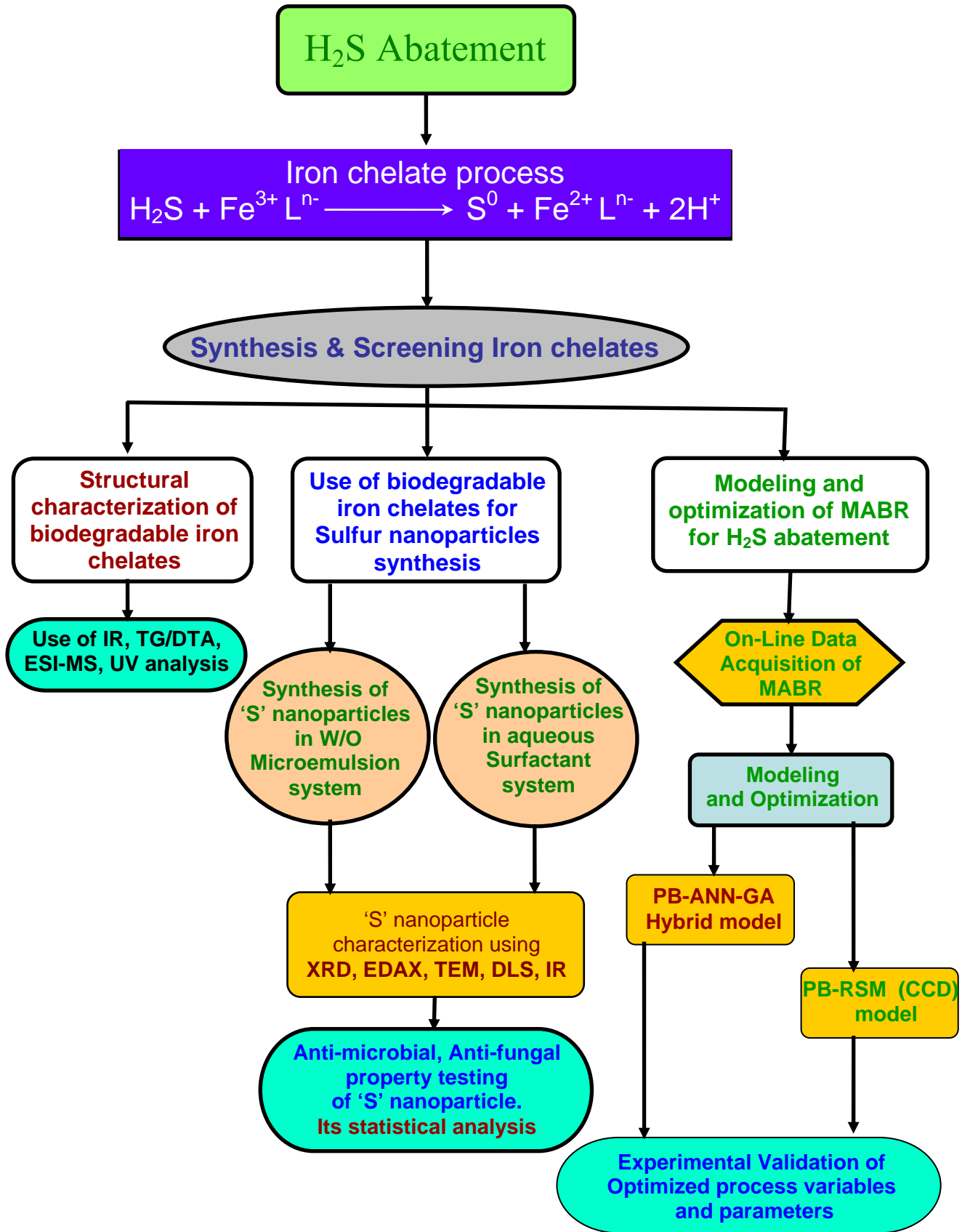
Part III – Process modeling and optimization for H₂S abatement in Novel Iron chelate.

- ❖ Design of experiments for optimization and modeling to study the reactive chemical absorption of H₂S in biodegradable iron chelate system
- ❖ Experimental setup for online data acquisition of mechanically agitated batch reactor (MABR) for the measurement of various operating process variables and parameters
- ❖ Use of PB-ANN-GA hybrid model for modeling and optimization of MABR. Analysis of system using PB-RSM (CCD) methods
- ❖ Experimental validation of mathematically optimized process variables and parameters conditions for H₂S abatement

5. Scheme of the Thesis

The present work introduces the use of biodegradable iron chelates for catalytic conversion of H₂S to elemental sulfur. The first chapter emphasis is on the introduction of novel biodegradable iron chelates along with detailed literature review for H₂S abatement processes. The details of the objective of work are elaborated. In

the second chapter the screening and selection of various iron chelates and their detailed structural characterization are discussed. The third chapter deals with the use of the biodegradable Fe³⁺-MA chelate scheme for synthesis, structural characterization of sulfur nanoparticles in reverse microemulsion and in aqueous surfactant system. The application of synthesized sulfur nanoparticles as an antimicrobial and antifungal agent is also discussed. In the fourth chapter mechanically agitated batch reactor (MABR) using Fe³⁺-MA chelate as a catalyst was studied extensively. The modeling and optimization of process variables and parameters using hybrid PB-ANN-GA technique and PB-RSM (CCD) model for nonlinear system of catalytic conversion of H₂S to elemental sulfur are studied. The experimental validation of optimized conditions is carried out. Overall summary of the work and some suggestions for further work is given at the end.



Schematic representation of the approach of Ph.D. work.

Reference

- [1] Pandey, R. A.; Malhotra, S. “Desulphurization of Gaseous Fuels with Recovery of Elemental Sulfur: An Overview”. *Crit. Rev. Env. Sci .Tec.* **1999**, Vol. 29, issue 3, p. 229.
- [2] Stecher, P.G. “Hydrogen sulfide removal processes”. Noyes Data Corporation, New Jersey, **1972**.
- [3] John, S. E. “Recovery of Sulfur from Sour acid Gas: A Review of the Technology”. *Environ. Prog.* **2002**, Vol. 21, p. 143.
- [4] Gaa, D.; Lagas, J. “Sulfur Recovery Solutions Global Trends”. *Chem. Eng. World.* **2004**, Vol. 39, p. 43.
- [5] Asai, S.; Konishi, Y.; Yabu, T. “Kinetics of Absorption of Hydrogen Sulfide into Aqueous Ferric Sulfate Solutions”. *AIChE J.* **1990**, Vol. 36, p. 1331.
- [6] Pagella, C.; De Faveri, D. M. “H₂S gas Treatment by Iron Bioprocess”. *Chem. Eng. Sci.* **2000**, Vol. 55, p. 2185.
- [7] Jensen, A. B.; Webb, C. “Treatment of H₂S Containing Gases: A review of microbiological alternatives”. *Enzyme. Microb. Technol.* **1995**, Vol. 17, p. 2.
- [8] Claus C. F. British Patent No. 5958, **1883**.
- [9] Mora, R. L. “Sulfur Condensation Influence in Claus Catalyst Performance”. *J. Hazardous Materials A.* **2000**, Vol. 79, p. 103.
- [10] Burns, R. A.; Lippert, R. B.; Kerr, R. K. “Choose Catalystst Objectively”. *Hydrocarbon Processing.* November **1974**, p. 181.
- [11] Gens, T. A. “Decrease in Carbonyl Sulfide in the Feed to Claus Convertors by Shift Catalysts”. *Ind. Eng. Chem. Res.* **1994**, Vol. 33, issue 7, p. 1654.
- [12] Paik, S. C.; Chung, J. S. “Selective Catalytic Reduction of Sulfur Dioxide with Hydrogen to Elemental Sulfur over Co-Mo/Al₂O₃”. *Applied Catalysis B:Environment.* **1995**, Vol. 5, p. 233.
- [13] Paik, S. C.; Chung, J. S. “Selective Hydrogenation of SO₂ to Elemental Sulfur Over Transition Metal Sulfides Supported on Al₂O₃”. *Applied Catalysis B:Environment.* **1996**, Vol. 8, p. 267.
- [14] Burns, R. A.; Lippert, R. B.; Kerr, R. K. “Choose Catalyst Objectively”. *Hydrocarbon Processing.* Nov. **1974**, p. 181.
- [15] Terorde, R. J. A. M.; Van den Brink, P. J.; Visser, L. M.; Van Dillen, A. J.; Geus, J. W. “ Selective Oxidation of Hydrogen Sulfide to Elemental Sulfur

- using Iron Oxide Catalysts on Various Supports”. *Catalysis Today*. **1993**, Vol. 17, p. 217.
- [16] Chung, J. S.; Paik, S. C.; Kim, H. S.; Lee, D. S.; Nam, I. S. “Removal of H₂S and or SO₂ by Catalytic Conversion Technologies”. *Catalysis Today*. **1997**, Vol. 35, p. 37.
- [17] Lagas, J. A.; Borsboom, J.; Heijkoop, G. “Claus Process Gets Extra Boost”. *Hydrocarbon Processing*. April **1989**, p. 40.
- [18] Stern, D. L.; Nariman, K.E.; Buchanan, J. S.; Bhore, N. A.; Johnson, D. L.; Grasselli, R. K. “ The Mobile Oil SO_x Treatment Process (MOST). Catalytic Removal of SO_x and H₂S from Refinery Tailgas”. *Catalysis Today*. **2000**, Vol. 55, p. 311.
- [19] Palm, J. W. “Watch these Trends in Sulfur Plant Design”. *Hydrocarbon Processing*. March **1972**, p. 105.
- [20] “AMOCO”. *Hydrocarbon Processing*. April **1975**, p. 102.
- [21] “Giammarco Vetrocoke – Sulfur”. *Hydrocarbon Processing*. April **1975**, p. 103.
- [22] Ellwood, P. “Meta-Vanadates Scrub Manufactured Gas”. *Chemical Engineering*. **1964**, Vol. 71, issue 15, p. 128.
- [23] “Stretford”. *Hydrocarbon Processing*. April **1975**, p. 104.
- [24] “Takahax”. *Hydrocarbon Processing*. April **1975**, p. 105.
- [25] “Sulfox”. *Hydrocarbon Processing*. April **1975**, p. 106.
- [26] “Beavon”. *Hydrocarbon Processing*. April **1975**, p. 107.
- [27] Bonnifay, P.; Dutriau, R.; Frankowiak, S.; Deschamps, A. “Pollution Abatement: Partial & Total Sulfur Recovery”. *Chemical Engineering Progress*. August **1972**, Vol. 68, issue. 8, p. 51.
- [28] “IFP”. *Hydrocarbon Processing*. April **1975**, p. 108.
- [29] Naber, J. E.; Wesselingh, J. A. Groenendaal, W. “Sulfur Developments: New Shell Process Treats Claus Off-gas”. *Chemical Engineering Progress*. December **1973**, Vol. 69, issue 12, p. 29.
- [30] “SCOT”. *Hydrocarbon Processing*, April **1975**, p. 109.
- [31] “Sulfreen”. *Hydrocarbon Processing*. April **1975**, p. 110.
- [32] “W-L SO₂ Recovery”. *Hydrocarbon Processing*. April **1975**, p. 111.
- [33] Granchar, P. “Advances in Claus Technology”. *Hydrocarbon Processing*. July **1978**, p. 155.
- [34] Khol, A. K.; Riesenfeld, F. C. Gas purification. McGraw-Hill, New York, **1960**.

- [35] Dalrymple, D. A.; Trofe, T. W. "An Overview of Liquid Redox Sulfur Recovery". *Chem. Eng. Prog.* **1989**, Vol. 85, p. 43.
- [36] McManus, D.; Martell, A. E. "The Evolution, Chemistry and Application of Chelated Iron Hydrogen Sulfide Removal and Oxidation Processes". In 6th International Symposium on the Activation of Dioxygen and Homogenous Oxidation, Noordwijkerhout, The Netherlands, **1996**.
- [37] Oostwouder, S. P.; Hodge, V. B. "Sulferox Process Technology and Application update". In *Sulfur Recovery Conference*. GRI, **1995**.
- [38] Hua, G. X.; Mcmanus, D.; Woollins, J. D. "The Evolution, Chemistry and Applications of Homogeneous Liquid Redox Sulfur Recovery Techniques". *Comments in Inorganis Chemistry*. **2001**, Vol. 22, p. 327.
- [39] Wilson, B. M.; Newell, R. D. "H₂S removal by Stretford process — further development by British Gas Corporation". Presented at National *AICHE*, Meeting Atlanta, G. A. **1984**.
- [40] Douglas, R. A. "Applications of the Hiperion Sulfur Removal Process", Presentation at the 1987 Stretford Conference, October 5, **1987**, Austin, Texas.
- [41] Douglas, R. A. "Hiperion Process Update - Commercial and Pilot Plant Experience", Presentation at the 1989 Liquid Redox Conference, May 7-9, **1989**, Austin, Texas.
- [42] McManus, D.; Martell, A. E. "The Evolution, Chemistry and Applications of Chelated Iron Hydrogen Sulfide Removal and Oxidation Processes". *J.Mol. Catal. A-Chem.* **1996**, Vol. 117, p. 289.
- [43] Pieters, H. A. J.; Krevelen, D. W. "The Wet Purification of Coal Gas and similar Gases by the Staatsmijnen-otto-process": Elsevier, **1946**.
- [44] Hartely, W.; Craig, R. S.; Sapiro, R. H. British Patent 855421, **1960**.
- [45] Gollmar, H. A. "Chemistry of the Thylox Gas-Purification Process" *Ind. Eng. Chem.* **1934**, Vol. 26, p. 130.
- [46] Ellwood, P. "Meta-Vanadates Scrub Manufactured Gas". *Chemical Engineering*. **1964**, Vol. 71, issue 15, p. 128.
- [47] Trofe, T. W., Dalrymple, D.A., Scheffel, F.A., "Stretford Process - Status and R & D Needs", Topical Report Prepared for Gas Research Institute, February, **1987**.
- [48] Gas Processing Handbook, "Unisulf". *Hydrocarbon Processing*. April **1984**, Vol. 63, issue 4, p. 51.

- [49] "Takahax". *Hydrocarbon Processing*, April **1975**, P. 105.
- [50] Khol, A. L.; Nielsen, R. "Gas Purification". 5th edition, Gulf Publishing Company, Houston. p.765.
- [51] Bedell, S. A.; Kriby, L. H.; Buenger, C. W.; McGaugh, M. C. "Chelates' Role in Gas Treating". *Hydrocarb. Process.* **1988**, Vol. 67, p. 63.
- [52] McManus, D.; Martell, A. E. "The Evolution, Chemistry and Applications of Chelated Iron Hydrogen Sulfide Removal and Oxidation Processes". *J.Mol. Catal. A-Chem.* **1997**, Vol. 117, p. 289.
- [53] Demmink, J. F.; Wubs, H. J.; Beenackers, A. A. C. M. "Oxidative Absorption of Hydrogen Sulfide by a Solution of Ferric Nitrilotriacetic Acid Complex in a Cocurrent Down Flow Column Packed with SMV-4 Static Mixers". *Ind. Eng. Chem. Res.* **1994**, Vol. 33, p. 2989.
- [54] Pandey, R. A.; Malhotra, S. "Desulphurization of Gaseous Fuels with Recovery of Elemental Sulphur: an overview". *Crit. Rev. Env.Sci.Tec.* **1999**, Vol. 29, p. 229.
- [55] Nagal, G. Controlling H₂S Emissions. *Chem Eng.* **1997**, Vol. 104, p. 125.
- [56] McManus, D.; Martell, A. E. "The Evolution, Chemistry and Applications of Chelated Iron Hydrogen Sulfide Removal and Oxidation Processes". 6th International Symposium on the Activation of Dioxygen and Homogenous Oxidation. Noordwijkerhout, The Netherlands, **1997**.
- [57] Hardison; L. C. "Go from H₂S to S in one unit". *Hydrocarbon Processing*. April **1985**, p.70.
- [58] Hardison, L.C. "LO-CAT-II: Big Step Forward in Iron Redox Chemistry". In *GRI Liquid Redox Sulfur Recovery Conference*. GRI **1991**.
- [59] Hardison, L. C.; Ramshaw, D. E. "H₂S to S: process improves". *Hydrocarbon Processing*. January **1992**, p. 89.
- [60] Cantrall, R. "LO-CAT and LO-CAT-II Application of Technology Update". In *Sulfur recovery conference*. GRI **1997**.
- [61] Pirtle, L.L., Allen, M.C., Hammond, C.A., Anderson, K.D., **1994**. Proceedings of the GRI Liquid Redox Sulfur Recovery Conference, mai 15–17, Austin, TX.
- [62] Karel, V. *Handbook of Environmental Data on organic chemicals*; Van Nostrand Reinhold an international Thomson Publishing company, New York: **1996**.

- [63] Gautier-Luneau, I.; Merle, C.; Phanon, D.; Lebrun, C.; Biaso, F.; Serratrice, G.; Pierre, J. New Trends in the Chemistry of Iron (iii) Citrate Complexes: Correlations between X-ray Structures and Solution Species Probed by Electrospray Mass Spectrometry and Kinetics of Iron Uptake from Citrate by Iron Chelators. *Chem. Eur. J.* **2005**, Vol. 11, p. 2207.
- [64] Deshpande, A. S.; Sankpal, N. V.; Kulkarni, B. D. Indian Patent application number 1366/DEL/**2003**.

||shri||

CHAPTER-2

SYNTHESIS AND CHARACTERIZATION OF BIODEGRADABLE IRON (III) CHELATE COMPLEXES: CATALYTIC OXIDATION OF H₂S

Abstract

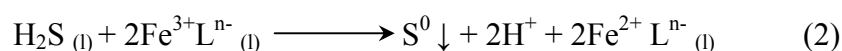
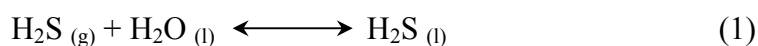
In this study we report the synthesis and structural characterization of biodegradable iron chelates synthesized using carboxylic acids as chelating agent with various iron salts as iron sources. These chelates were synthesized in the pH range of 2-9.5 and used for catalytic conversion of H₂S gas to sulfur. The screening of iron chelates was carried out on the basis of qualitative and quantitative analysis of the sulfur recovery. The structural characterizations of ferric chloride and malic acid chelate complex have been systematically studied by Electrospray mass spectroscopy (ESI-MS), Fourier transform infra-red technique (FTIR), Differential thermal analysis (DTA). It was concluded that ferric ion coordinated with bidentate malic acid to form chelate complex that gives maximum recovery of sulfur (499 mg/g of iron chelate) along with high purity (>99%) and reasonable extent of reaction time over other systems.

Key words: H₂S abatement; Biodegradable iron chelates; ESI-MS, TG/DTA

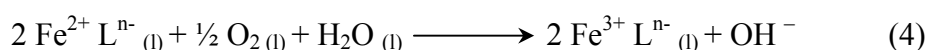
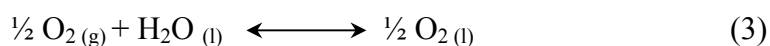
1. Introduction

Abatement of H₂S gas by catalytic conversion to elemental sulfur can be achieved by various chemical¹⁻⁴ and biological^{5,6} methods. Liquid redox sulfur recovery processes absorb H₂S from gaseous streams and convert it to elemental sulfur. For desulfurization, a number of processes have been reported in the literature. Stretford, Unisulf, and Sulfolin processes⁷ are vanadium-based, in which vanadium is the primary catalyst interacting with the sulfur. The other two processes, LO-CAT and Sulferox, are iron based.^{8,9,11} The Hiperion process⁷ uses iron and quinone as catalysts.

The gas desulfurization can also be carried out using liquid redox chemistry, where iron complexes are alternately reduced according to following reactions,¹⁰⁻¹⁸



Since the active ferric chelate is converted to inactive ferrous chelate, the later component has to be regenerated by oxidation according to



Where, 'n' denotes the charge of an organic ligand 'L', which is usually a polyaminocarboxylic acid such as ethylenediamine tetraacetic acid (EDTA), hydroxy ethylethylene diamine triacetic acid (HEDTA), diethylenetriamine pentaacetic acid (DTPA), nitrilotriacetic acid (NTA), cyclohexane-1,2-diaminetetraacetic-(CDTA), etc. Here, no iron chelate is consumed in the overall reaction; it may be considered as a pseudocatalyst.

The experimental records of the oxidative scrubbing of H₂S by ferric chelates are available in the open literature.

Table 2.1 Various processes and chelating agents used for iron chelation for H₂S abatement

Sr. No.	Chelating agent	Process	Author and Year
1	Iron cyanide	Gesellschaft fur Kohlentechnik and Fischer process	Fischer. 1932
2	Ferricyanide/ ferrocynaide	Staatsmijnen-Otto	Pieters. 1946
3	Ethylene diamine tetraacetic acid (EDTA)	-	Hartley. 1960
4	ethylenediamine disuccinic acid (EDDS)	-	Kezerian. 1964
5	Cataban reagent	Cataban Process	Meuly. 1972
6	Na ₂ FeO ₄	Konox Process	Kasai. 1975
7	Ethylene diamine tetraacetic acid (EDTA), N-hydroxyethylethylene diamine triacetate acid (NHEDTA)	LOCAT-I and LOCAT-II	Hardison. 1985 Hardison.1991
8	Triethanolamine (TEA), Diethylene tramine penta acetic acid (DEPTA), Citric acid	-	Naraghi. 1989
9	Nitrilotriacetic acid (NTA)	Sulferox Process	Pirtle. 1994
10	2,6-pyridnedicarboxylic acid	-	Sawyer. 1993
11	2-car-boxy-8-hydroxyquinoline	-	Hancock. 1997
12	Pyridine-2-phosphonic-6-carboxylic acid	-	McManus. 1997
13	Acetylacetonate, Benzoylacetonate, 1,1,1-trifluoro-2,4-pentaneadione, 1-phenyl-4,4,4-trifluoro-1,3-butanedione	-	Ferm. 1997 Eng. 1998
14	Polyamino disuccinic acids	-	Wilson. 1998
15	2,6-pyridinediphosphonic acid	-	Chen. 1998
16	Cyclohexane-1,2-diaminetetraacetic	-	Piché. 2005

The Fe³⁺ redox couple process using hexacyanoferrate known as “Staatsmijnen-Otto” process was reported by Pieters et al.²¹ Problems with this process are usage of toxic solutions containing Fe(CN)₆ⁿ⁻ (n = 3 or 4) and ammonia, and occurrence of side reactions. Deemink et al.,¹⁷ studied oxidative absorption of

H₂S by ferric-NTA solutions in a cocurrent down-flow column. Here, synthetic H₂S/air mixture having an inlet concentration of 4000-8000 ppm was introduced in the column. The H₂S content at the outlet was measured in the 230-2400 ppm range. The use of ethylenediamine tetraacetic acid (EDTA), hydroxy ethylethylene diamine triacetic acid (HEDTA), and diethylenetriamine pentaacetic acid (DTPA) as chelating agents for iron chelation has also been reported.^{14,16} Piche et al.,¹⁷ used cyclohexane-1,2-diaminetetraacetic-(CDTA) as an iron chelating agent for the removal of dilute H₂S in the 100-400 ppm concentration range. The maximum H₂S conversion observed in the counter-current packed bed reactor approached 91%.

Chelating agents (EDTA, HEDTA, DTPA, NTA, CDTA, etc.) reported for iron chelation have very low rate of biodegradation (e.g. EDTA BOD₅²⁰ - 0.1%, DTPA BOD₅ - 0.7%) thus causing pollution.³⁴ Alternative chelating agents for gas sweetening should meet three main criteria, viz., (i) should possess equal or better complex forming properties compared to commercial chelating agents, (ii) should possess better biodegradability and (iii) should contain low nitrogen so as to minimize the nitrogen content in effluents. It has been reported that carboxylic acids (e.g. citric acid,^{35,36} malic acid,³⁷ gluconic acid,³⁷ etc.) possess good chelating properties and have faster rate of biodegradation (e.g. citric acid BOD₅²⁰ - 61% and malic acid BOD₅²⁰ - 65%) as compared with commercial chelating agents. The complex forming properties of these carboxylic acids needs to be studied and improved if they have to replace commercial chelating agents.

In this study, we report the synthesis and structural characterization of biodegradable iron chelates using carboxylic acids (e.g. citric acid, malic acid, gluconic acid, etc.) as chelating agent with various iron salts (e.g. ferric chloride, ferric nitrate and ferric sulphate, etc.) as iron sources in the pH range (2-9.5) used for

catalytic conversion of H₂S gas to sulfur. The screening of iron chelates was carried out on the basis of qualitative and quantitative analysis of the sulfur.

Various Iron(III) salts have been used as iron source and the complexes have been synthesized in different pH range at ambient temperature and atmospheric pressure. The conversion of H₂S to elemental sulfur has been studied using all the iron(III) chelates and the results are reported here. The structural characterizations of ferric chloride and malic acid chelate complex have been systematically studied by Electrospray Mass Spectroscopy ESI-MS, Fourier Transform Infra-red technique (FTIR), Differential Thermal analysis (DTA). It was concluded that ferric ion is coordinated with bidentate malic acid to form chelate complex that gives maximum recovery of sulfur (499 mg/g of iron chelate) along with high purity (>99%) and reasonable extent of reaction time over other systems.

2. Experimental

2.1 Chemicals

All chemicals were of analytical grade and used without further purification. Ferric chloride, ferric sulfate, ferric nitrate, gluconic acid, malic acid, citric acid and sodium hydroxide pellets were purchased from Merck India. All solutions were prepared in deionized Milli-Q water (H₂O with 18.2 Milli-Q cm resistivity, Millipore Corporation). The H₂S cylinders 99.6% pure were procured from Vadilal chemicals.

2.2 Characterization

The iron chelates were characterized for their structural analysis using FTIR, TG-DTA, ESI-MS and UV analysis.

Infrared Spectra were recorded in the region 4000-400 cm⁻¹ on Shimadzu 8300 series spectrophotometer using KBr pellets.

The TG/DTA analysis was recorded on Perkin-Elmer Diamond TG/DTA analyzer. Samples were heated in platinum crucibles with $\alpha\text{-Al}_2\text{O}_3$ as reference compound in static nitrogen atmosphere, in the temperature range 30-1200 °C. The heating rate was 5 °C min⁻¹ and the samples mass range was from 12-20 mg.

The electrospray mass spectra were recorded on a MICROMASS QUATTRO II triple quadrupole mass spectrometer. The sample dissolved in water was introduced into ESI source through syringe pump at the rate of 5 μl per min. The ESI capillary was set at 3.5 kV. The spectrum was collected in 6 s scans. For each sample the spectra were recorded at a cone voltage of 30 V and 80 V.

UV analysis of the various Iron(III) chelates was carried out on double beam UV spectrophotometer of Chemito make model Spectroscan 2700.

2.3 Preparation of Iron chelate solution

Typically iron chelates were synthesized using various ferric salts in combination with different carboxylic acids as a chelating agent in various molar ratios as given in Table 2.2.

2.3.1. Iron(III)- carboxylic acid chelate synthesis in acidic medium (at pH-2)

All the iron (III) chelates were synthesized by dissolving iron salts (1 mol) into 15 ml deionized water. The chelating agents are added to the iron salt solutions in the molar ratio of 1:2 or 1:3, depending on the coordination number of iron and availability of ligand sites in the respective chelating agent. The solution was stirred for 2 h at room temperature. The pH of the resulting solution was 2. Water was removed by heating the solution at 90 °C in the oven. The dry powder obtained was kept in vacuum oven at 70 °C for two days for complete removal of moisture. The sample was cooled in desiccator.

2.3.2. Iron(III)- carboxylic acid chelate synthesis in neutral medium (pH 7-7.5)

The aqueous solution of various Fe(III) salt and carboxylic acid chelating agent were stirred at room temperature for 2 h. The pH of the solution was adjusted to 7-7.5 by drop wise addition of 5N NaOH solution. Orange red coloured solution was obtained. To prepare the dried powder of this chelate water content was removed as described in the above section.

2.3.3. Iron(III)- carboxylic acid chelate synthesis in basic medium (at pH 9)

The Iron(III)- carboxylic acid chelate at pH 9 was synthesized by the same procedure as described above. The drop wise addition of 5N NaOH solution was continued till the pH reached 9. The dry powder of the Fe-chelates was obtained by following the same procedure as described in above section.

The various Iron(III)-carboxylic acid chelates prepared in-situ at pH 7-7.5 at ambient conditions of temperature, and pressure were used in the Fe(III)concentration range of 500-20,000 ppm for catalytic conversion of H₂S to elemental sulfur.

2.4 General method of sulfur recovery from H₂S gas

Figure 2.1 shows schematic flow diagram for catalytic conversion of H₂S to elemental sulfur. Pure H₂S gas (99.9%) was sparged in the absorber unit. In the absorber unit, Fe³⁺-chelate solution oxidized H₂S gas to elemental sulfur and simultaneously active ferric chelate was reduced to inactive ferrous chelate (Reaction 2). After complete reduction of ferric chelate, H₂S conversion to elemental sulfur ceases. The completion of the reaction was confirmed by confirming the presence of unreacted H₂S gas by 0.1N AgNO₃ test. After completion of the reaction the regeneration of inactive ferrous chelate to active ferric chelate was carried out by sparging pure oxygen (Reaction 4) till the original colour of solution regained. The regenerated ferric chelate was recycled for further H₂S conversion.

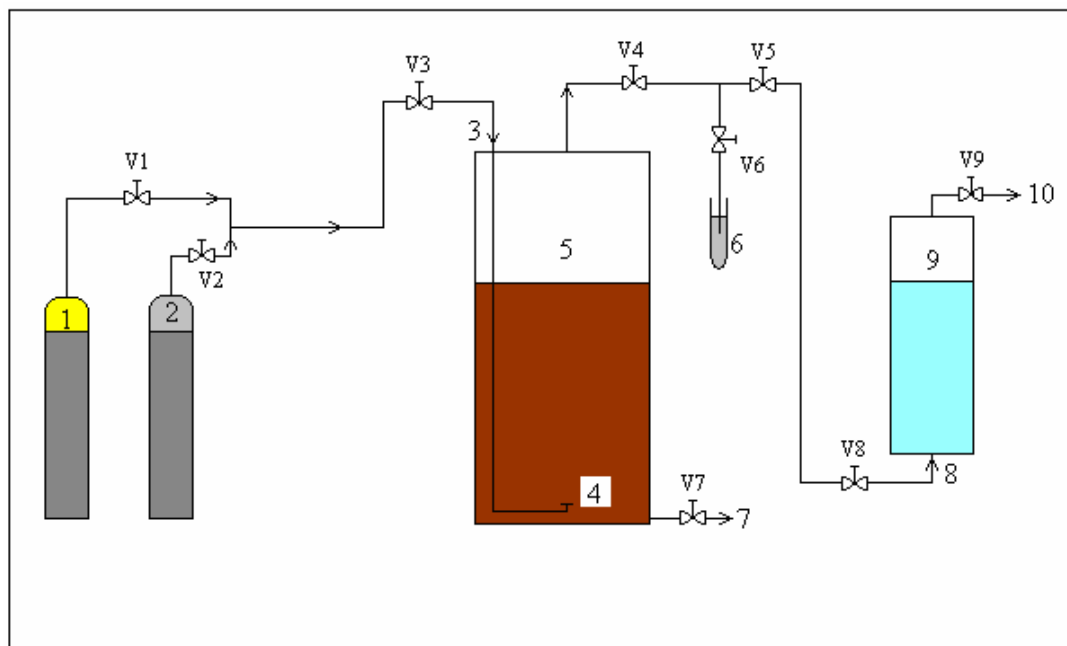


Figure 2.1 Simplified process flow diagram for catalytic conversion of H₂S to elemental sulfur (1: H₂S cylinder; 2: O₂ cylinder; 3: gas inlet; 4: sparger; 5: absorber/regenerator; 6: outlet gas checking port; 7: sulfur recovery; 8: gas inlet; 9: NaOH scrubber; 10: sweet gases; V1-V9: valves)

3. Results and Discussions

Iron chelates using different carboxylic acids were synthesized by varying the molar ratios of metal to ligand as shown in Table 2.2. All the synthesized iron chelates were evaluated for catalytic conversion of H₂S gas to elemental sulfur during all the experiments and the results are reported in Table 2.2. The volume of the reaction mixture and the rate of H₂S gas addition was kept constant. The reaction time for completion of the reaction gives a measure of the rate of reaction for various iron chelates.

The trend of different carboxylic acid- Fe chelate follows the following order for catalytic activity, malic acid > citric acid > gluconic acid. Among various iron chelates, FeCl₃-gluconic acid chelate system required much less reaction time (5 min.) compared to the FeCl₃- malic acid (15 min) and FeCl₃-citric acid (36 min.) however,

the purity and recovery of product was very poor (83% only) compared to FeCl₃-citric acid (>99%).

Table 2.2 Screening of iron chelate systems for H₂S abatement

Iron salt	Chelating agent	Molar ratio	Reaction Time (min)	sulfur recovered mg/gm of iron chelate	% purity Sulfur ^a
FeCl₃	Citric acid	1:2	36	184.20	>99
	Malic acid	1:3	15	499	>99
	Gluconic acid	1:3	5	27.7	83.71
Fe₂(SO₄)₃	Citric acid	1:2	25	137.8	97.5
	Malic acid	1:3	37	235	>99
	Gluconic acid	1:3	39	51	88.44
Fe₂(NO₃)₃	Citric acid	1:2	10	116.83	75.96
	Malic acid	1:3	5	290.88	94
	Gluconic acid	1:3	20	90	99

^a The precipitate also contains C, N, H, and Fe as confirmed by elemental analysis.

The purity of sulfur is very high for the Fe(NO₃)₃-gluconic acid chelate system compared to Fe(NO₃)₃-malic acid chelate system (94%) and Fe(NO₃)₃-citric acid chelate system (75%), but recovery of sulfur is maximum for Fe(NO₃)₃-malic acid chelate system compared to other chelate system. This trend is followed by all other iron salts in combination with different chelating agents. From Table 2.2 it is observed that all iron salts with malic acid as chelating agent shows better compared to other chelating agents such as citric acid and gluconic acid. FeCl₃-malic acid chelate system has been observed to give maximum recovery of sulfur (499 mg/g of iron chelate) with high purity (> 99%) in relatively less time (15 min.). As FeCl₃-

malic acid chelate among all the studied Fe-salts and different chelating ligand combination gave maximum recovery of >99% purity of sulfur it was therefore selected for detail structural characterization studies.

3.1 Infrared spectra analysis

IR spectra of malic acid (MA), FeCl₃-malic acid chelate at pH 2 (FMI-1), at pH 7-7.5 (FMI-2) and at pH 9 (FMI-3) was described by Figure 2.2 In the spectrum of MA, prominent peaks due to C=O stretching at 1737.7 and 1687.6 cm⁻¹, sharp α-OH stretching at 3444.6 cm⁻¹, C-O stretching at 1218.9 cm⁻¹, and weak O-H deformation at 1442.7, 1409.9 and 950.8 cm⁻¹ are seen. Broad peak at 3058.8 cm⁻¹ is attributed to carboxylic O-H stretching. The IR spectrum of chelates under acidic (FMI-1), neutral (FMI-2) and basic conditions (FMI-3) shows remarkable shifts in the C=O, C-O, and α-OH stretching region compared to neat MA (Table 2.3). From ESIMS and TG/DTA studies the plausible structures for FMI-1, FMI-2 and FMI-3 are suggested (see Scheme 2.1 and 2.2). From the structures of FMI-2 and FMI-3 it can be seen that two MA molecules are bonded to Fe³⁺ through C=O group of acid and four MA molecules via C-O of hydroxyl group of -COOH. Whereas in FMI-1 all the three MA groups are bonded to Fe³⁺ through C=O group of acid. This fact is evident from IR of MA and FMI-1 in which the two C=O groups show shift from 1737.7 to 1733.9 cm⁻¹ and from 1687.6 to 1614.3 cm⁻¹ respectively indicating C=O bonding with Fe³⁺. Also sharp α-OH stretching at 3444.6 cm⁻¹ in MA is found to be diminished and merged with carboxylic O-H stretching in spectrum of FMI-1 which can be seen at higher frequency of 3201cm⁻¹. Also major shift is observed in C-O stretching and O-H deformation bands supporting the C-O bonding with Fe³⁺. C-O stretching frequencies in MA shows shift by 14 cm⁻¹ to higher side and 10 cm⁻¹ to

lower side in FMI-1 appearing at 1232 and 1174 cm^{-1} . The O-H deformation bands also show shift by 15 and 46 cm^{-1} and appear at lower frequency 1427 and 904 cm^{-1} in FMI-1.

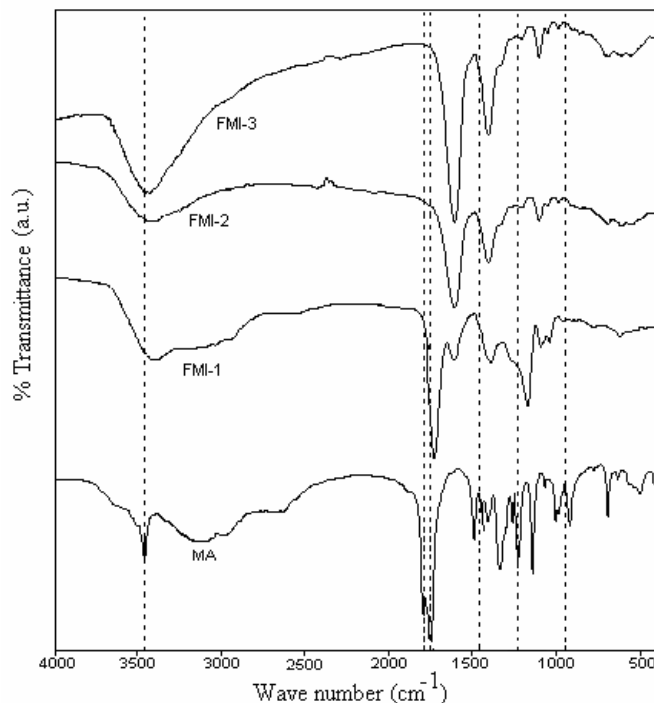


Figure 2.2 Comparison of FTIR spectra of malic acid (MA) with iron chelates at pH 2 (FMI-1) at pH 7-7.5 (FMI-2) and at pH 9 (FMI-3)

Table 2.3 FTIR data for Fe(III)-malic acid chelate synthesized at different pH conditions

Ligand	Assignments	Standard Malic acid	(FMI1) pH-2	(FMI2) pH-7.5	(FMI3) pH-9
$\text{C}_4\text{H}_4\text{O}_5^{-2}$	V O-H	3450-2900	3201	3402.2	3419.6
	$\text{V}_{\text{as}} \text{COO}^-$	1737 _s	1733.9	1598.9	1595
	$\text{V}_{\text{s}} \text{COO}^-$	1687 _s	1614.3	-	-
	V O-H	1442	1427	1392.5	1392.5
	V C-O	1218	1174	1197	1199
	V O-H	950	904	895	893

as – asymmetric; s- symmetric

In the spectra of FMI-2 and FMI-3 only single band for C=O stretching is seen at 1598.9 and 1595 cm^{-1} in contrast to two C=O bands in MA at 1733.9 and 1614.3 cm^{-1} respectively. This shift to lower frequency indicates decrease in C=O strength. Another evidence for Fe^{3+} bonding through C-O is disappearance of –OH deformation peaks of lower frequency 950 cm^{-1} and appearance of single bands at lower frequency for –OH deformation at 1392.5 cm^{-1} to that of MA. The shifts in C-O stretching band by 50 cm^{-1} to lower frequency also supports this bonding. In MA the bands due to –OH stretching vibration of carboxylic acid is seen at 3026 cm^{-1} but in FMI-2 and FMI-3 this band appears at higher frequency region 3402-3419 cm^{-1} indicating frequency shift due to inductive effect of bond between Fe^{3+} and C=O. Sharp α -OH stretching vibration at 3444.6 cm^{-1} which is prominent in MA is now found to be merged with –OH frequency of carboxylic group and is indistinguishable in FMI-2 and FMI-3 at 3402 and 3419 cm^{-1} , respectively.

3.2 TG-DTA analysis

The iron chelate complex formed at different pH were subjected to TG-DTA analysis from 30 °C to 1200 °C in nitrogen atmosphere at the heating rate of 5°C/min. Thermo-analytical curves of FMI-1, FMI-2, FMI-3 are presented in Figure 2.3a, 2.3b and 2.3c, respectively. TG/DTA data for the weight loss as a function of temperature has been summarized in Table 2.4.

The DTA endotherm at 157 °C, 232 °C and 231 °C indicates that the melting takes place just before decomposition of the iron chelates synthesized at acidic, neutral and basic condition, respectively. While the well defined degradation stages are accompanied by exothermic and endothermic effects.

Table 2.4 TG/DTA data for FMI-1, FMI-2, FMI-3

Compound	Stage	Temp (°C)	DTA		Mass % loss	Mass loss Calculated %	Evolved moiety formula
			Endo (-)	Exo (+)			
FMI1	1	30-200	87	-	93.8	93.7	Cl ⁻
			-	172	86.1	86.0	CO ₂
	2	200-400	212	-	72.6	73.4	2Cl ⁻
			222	-	68.3	68.4	CO
			262	-	55.0	55.3	2CO, H ₂ O
			-	327	47.0	47.5	CO ₂
	3	400-600	-	462	31.0	31.6	-MA-
4	600-800	777	-	20.7	21.8	2CO	
5	800-1100	-	1002	9.4	9.1	H ₂ O, CO ₂	
6	1022	-	-	7.8	7.8	FeO	
FMI2	1	200-300	237	-	96.9	96.9	CO
	2	300-500	-	407	77.4	77.5	MA, 3CO ₂ ,
			457	-	65.4	64.4	2CO
	3	500-800	637	-	61.4	61.1	CO
	4	800-1100	-	1087	27.6	27.5	3MA, 2CO ₂ , CO
5	1100-1200	-	-	23.8	24	CO	
FMI3	1	200-300	181	-	92.447	92.386	2CO
			-	261	84.646	84.362	-MA-
	2	300-500	-	476	70.592	70.576	MA
			581	-	67.649	67.695	CO
			631	-	63.703	64.814	CO
			-	731	56.820	56.995	-MA-
	3	500-800	-	781	52.475	52.469	CO ₂
			-	861	43.627	43.416	2 CO ₂
-			881	39.371	38.992	CO ₂	
-			916	29.257	29.733	-MA-	
-			951	18.007	18.313	MA.2Na ⁺	
-			-	-	-	-	

The initial decomposition temperatures indicate the thermal stabilities of the complexes. The complex formed in the acidic condition was thermally unstable as compared to the complex formed at neutral and basic pH condition.

The dehydration takes place above 50 °C and continues till all weakly and adsorbed water molecules are removed. At higher temperatures, coordinated water is

removed step wise. After the melting point temperature, the decomposition of the chelates starts. For the $[\text{Fe}^{+3} (\text{L}^{-n})_3] 3\text{Cl}^-$ complex at pH-2 (shown in Figure 3a), the first decomposition stage proceeds with a sudden and considerable mass loss (70%) , which shows the rupture of the ligand bonds along with the rupture of bonds inside the ligand (removal of Cl^- , CO_2 , CO and H_2O moieties form the ligand with increase in temperature). Intermediates formed which are unstable and under go further decomposition till stable FeO is formed above $1000\text{ }^\circ\text{C}$.

For the Iron- malic acid chelate $([\text{Fe}^{+3}_2 (\text{L}^{-n})_4(\text{L})_2]^{-2} 2\text{Na}^+\text{H}_2\text{O})$ formed at pH-7 to7.5 and pH-9, the first decomposition stage gives mass loss of 30% and 35% respectively (as shown in Figure 2.3b and 2.3c). First the water molecule is released form the chelate structure. The major mass loss at this stages is due to rupture of first coordination bond between the two Fe^{+3} which forms the bimetallic structure (as shown in the Scheme 2.2). The rupture of the second coordination bond of ligand to metal under goes the further decomposition.

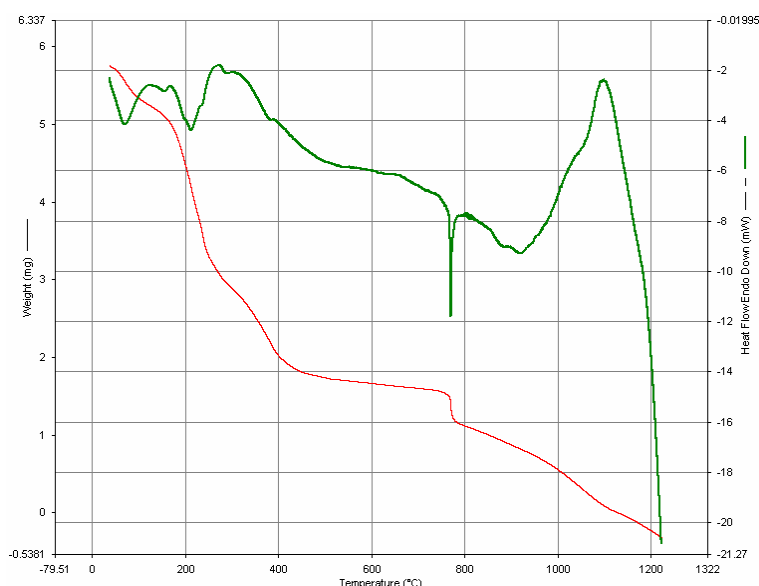


Figure 2.3a TG-DTA curves for Fe(III)-Malic acid chelate synthesized at pH 2 (FMI-1)

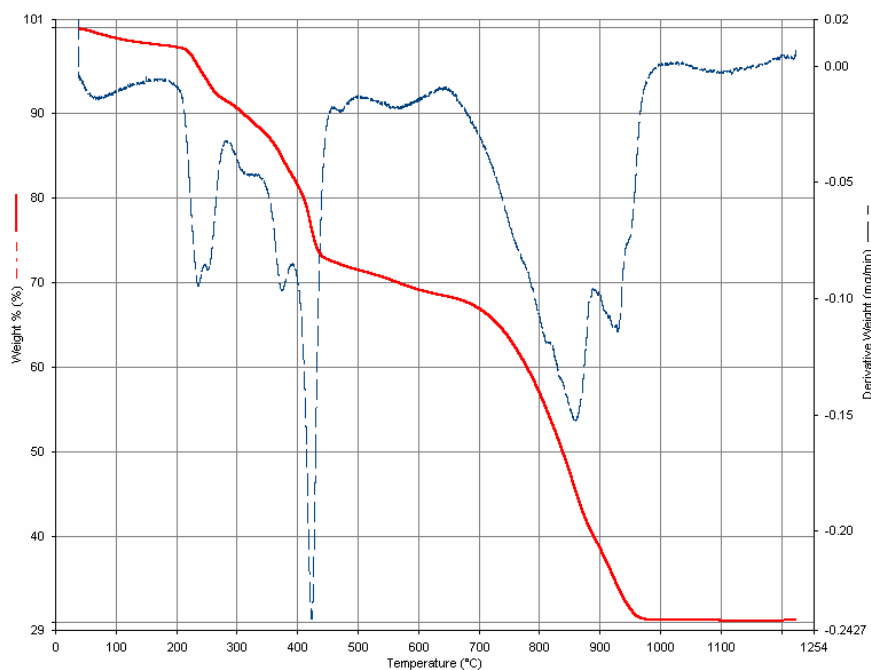


Figure 2.3b TG-DTA curves for Fe(III)-Malic acid chelate synthesized at pH 7.5 (FMI-2)

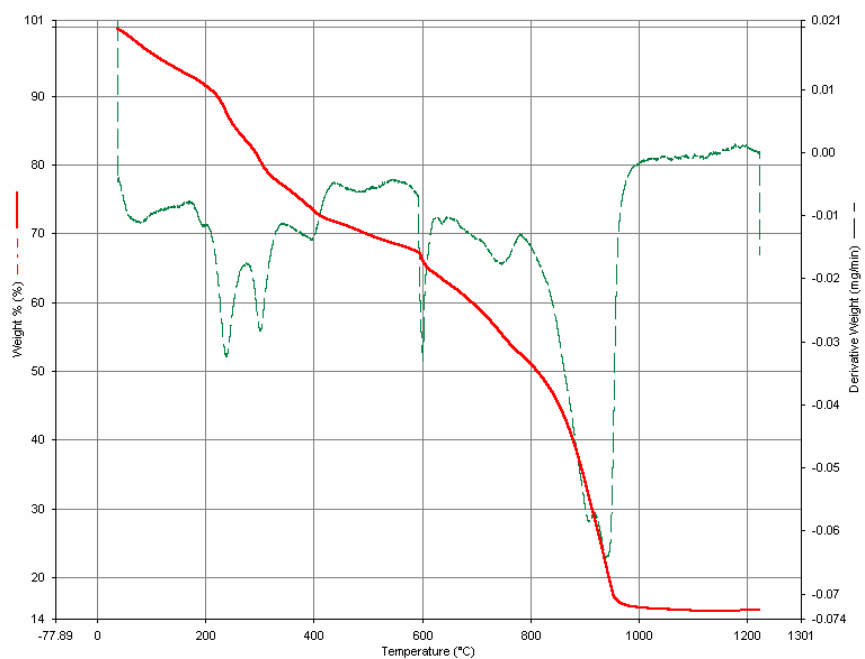


Figure 2.3c TG-DTA curves for Fe(III)-Malic acid chelate synthesized at pH 9 (FMI-3)

In the second decomposition stage the major mass loss of 70% above 425 °C and 85% above 600 °C occurs. During this decomposition stage the mass loss is due to rupture of coordination bonds between metal to ligand along with the rupture of the

bonds inside the ligand with exothermic and endothermic effects (possibly elimination of CO₂, CO, H₂O and unstable intermediates of malic acid). At higher temperature the decomposition of intermediates continuous till all malic acid part will get decomposed and gives Fe only above 1000 °C as expected.

3.3 ESI-MS analysis

Mass spectra were obtained for three different iron chelates at various pH values. At three different pH values the ferric chloride –malic acid gives different complex structures. The most prominent mass spectral peaks of the studied compounds are given in Table 2.5.

Table 2.5 ESI-MS data for Fe(III)-Malic acid chelate synthesized at different pH condition

Sr. No.	Compound	m/e (R/I) ^a
1	[Fe ⁺³ L ₃] 3Cl ⁻	43(25), 51(7), 56(10) , 57(13), 65(79), 71(14), 77(31), 89(10), 91(100), 92(7), 111(19), 115(53), 128(85), 149(96), 166(74), 178(12) , 180(38), 189(33) , 198(52), 215(21), 233(31) , 251(21) , 268(76) , 282(30), 295(15), 312(20) , 313(8), 331(18), 349(20), 367(6), 377(10), 384(30) , 389(18), 398(80), 414(5) , 419(3), 447(3), 474(2), 485(4) , 493(4), 500(10), 520(7), 529(6) , 550(8), 552(13), 564(4) , 576(7), 578(18), 600(2), 602(10), 604(31), 605(12), 606(7), 616(3), 618(3) , 648(3), 664(7), 665(3), 690(1) .
2	[2Fe ⁺³ L ⁻² ₂ L] ⁻² 2Na ⁺ . H ₂ O	43(26), 56(20) , 63(90), 81(27), 88(21), 91(13), 112(13) , 133(9), 157(14), 159(55) , 179(20) , 201(100), 223(27), 255(1), 259(9), 275(20), 288(55) , 317(12), 319(23), 357(4), 379(55) , 407(10), 422(4) , 437(23), 438(5), 475(3), 497(10), 498(1), 510(1) , 554(2) , 557(49), 558(7), 579(20), 589(12), 604(12), 612(11), 615(6), 626(4), 639(8), 645(8), 658(3), 675(5), 686(6) , 687(7), 698(7), 705(6), 715(10), 718(9), 735(100), 736(21), 737(6), 757(18), 773(9), 786(14), 798(9), 800(15), 812(10), 815(16), 820(12) , 826(19), 828(25), 830(10), 842(10), 854(15), 872(8), 880(17), 882(50), 883(35), 884(15), 905(6), 906(27), 908(66) , 909(39), 913(23), 915(7), 933(7), 940(3), 954(6) , 960(4), 971(11), 972(11) .

3	$[2\text{Fe}^{+3}\text{L}^{-2}_2\text{L}]^{-2} 2\text{Na}^+ \cdot \text{H}_2\text{O}$	43(2), 56(11) , 63(69), 81(100), 83(34), 88(10), 106(5), 119(11), 133(39), 159(38) , 179(6) , 201(67), 203(38), 223(21), 245(2), 259(15), 275(13), 288(5) , 317(27), 319(14), 331(4), 357(2), 379(33) , 380(3), 407(24), 422(3) , 437(18), 439(4), 495(1), 497(6), 509(1) , 557(13) , 558(2), 590(4), 604(6), 615(12), 618(6), 635(4), 643(7), 644(15), 646(6), 653(2), 658(7), 663(8), 673(5), 686(6) , 709(5), 719(4), 735(12), 744(4), 761(4), 772(12), 774(9), 786(14), 798(14), 800(24), 814(17), 820(15) , 828(21), 830(15), 854(20), 856(27), 857(16), 868(7), 880(33), 882(74), 883(44), 884(23), 885(11), 896(5), 904(16), 906(36), 908(100) , 909(54), 910(37), 911(17), 912(8), 927(4), 940(7), 954(3) , 967(6), 972(3) , 990(5).
---	---	---

^a (R/I) – Relative Intensity

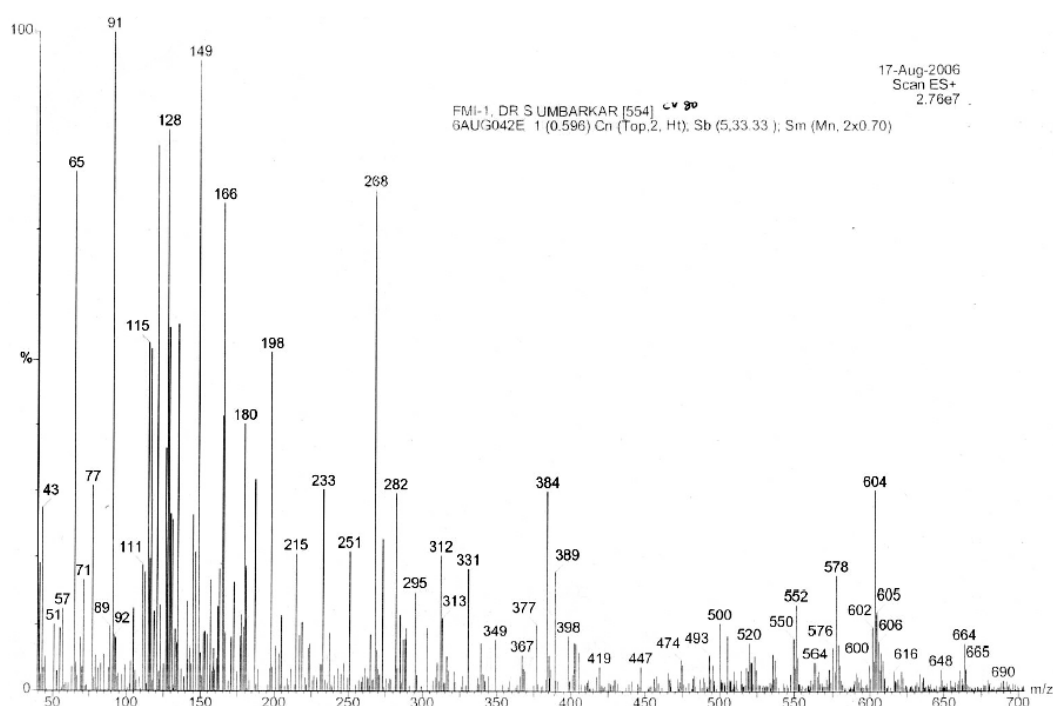
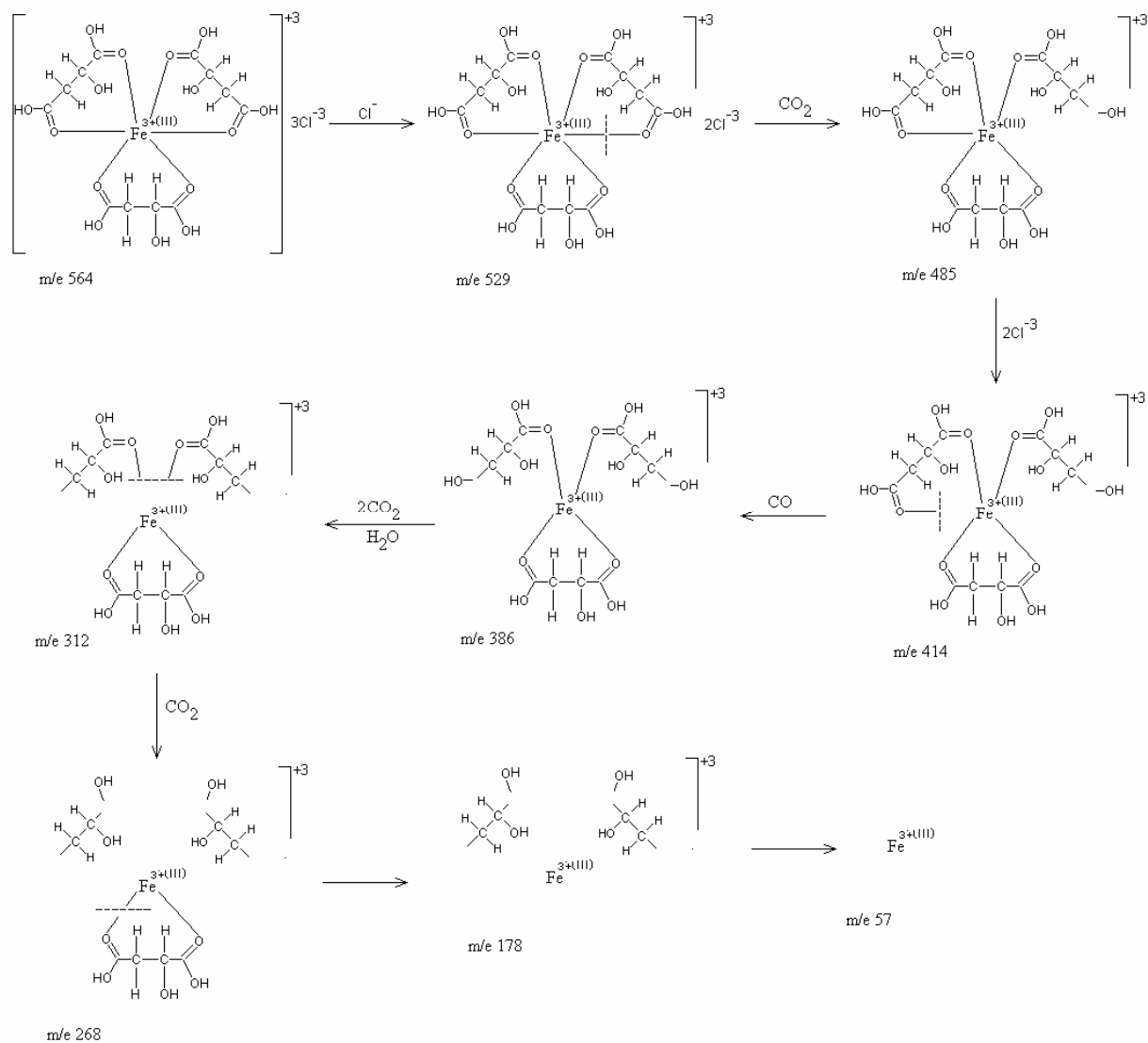


Figure 2.4 ESI-MS for Fe(III)-Malic acid chelate at pH 2 (FMI-1)

Figure 2.4 gives the formation of complex of Ferric chloride – malic acid in the acidic pH condition. The peak at m/e 564 assigned to the $[\text{Fe}^{+3}(\text{L}^{-n})_3] 3\text{Cl}^-$, where $n = 2$, complex. The elimination of Cl^- , CO_2 , CO and H_2O group gives the

fragmentation of the complex which is shown by the peaks at m/e 529, 485, 414, 386, 312, etc as shown in fragmentation scheme 2.1. The m/e peak at 57 shows the Fe^{+3} ion only.



Scheme 2.1 Fragmentation pattern for the Fe(III)-Malic acid chelate synthesized at pH 2 (FMI-1)

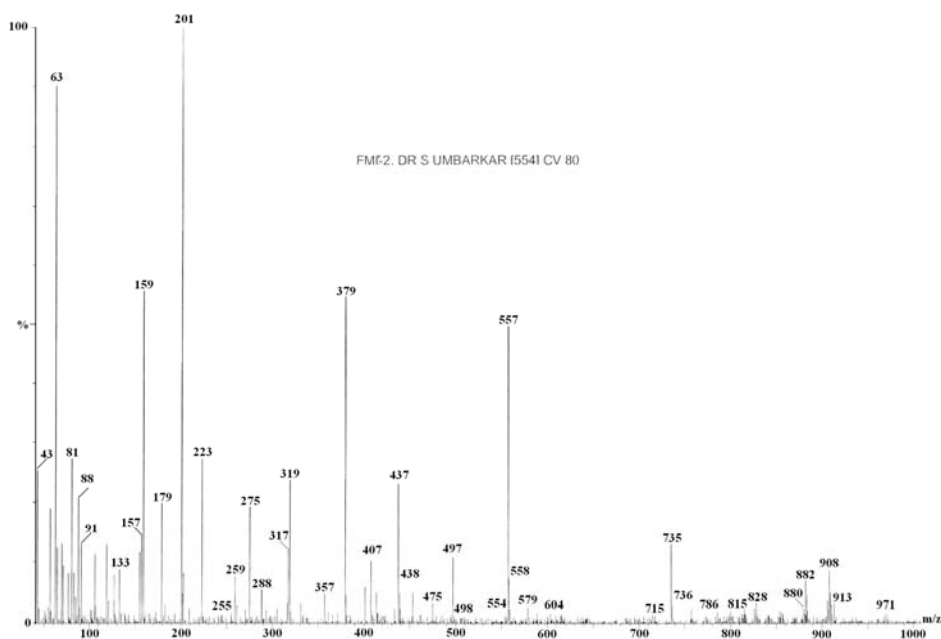


Figure 2.5 ESI-MS spectra for Fe(III)-Malic acid chelate (FMI-2) at pH 7.5

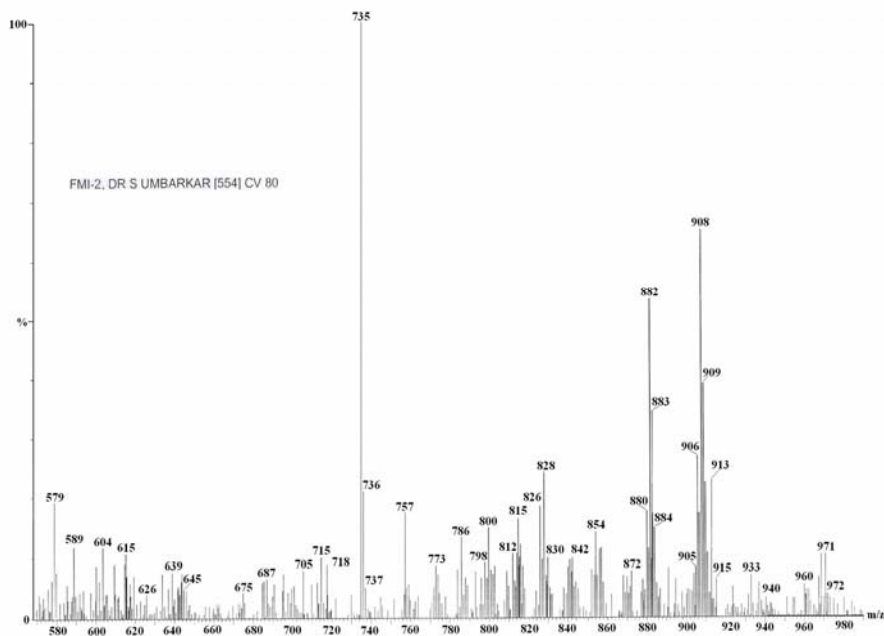


Figure 2.6 ESI-MS spectra for Fe(III)-Malic acid chelate (FMI-2) at pH 7.5

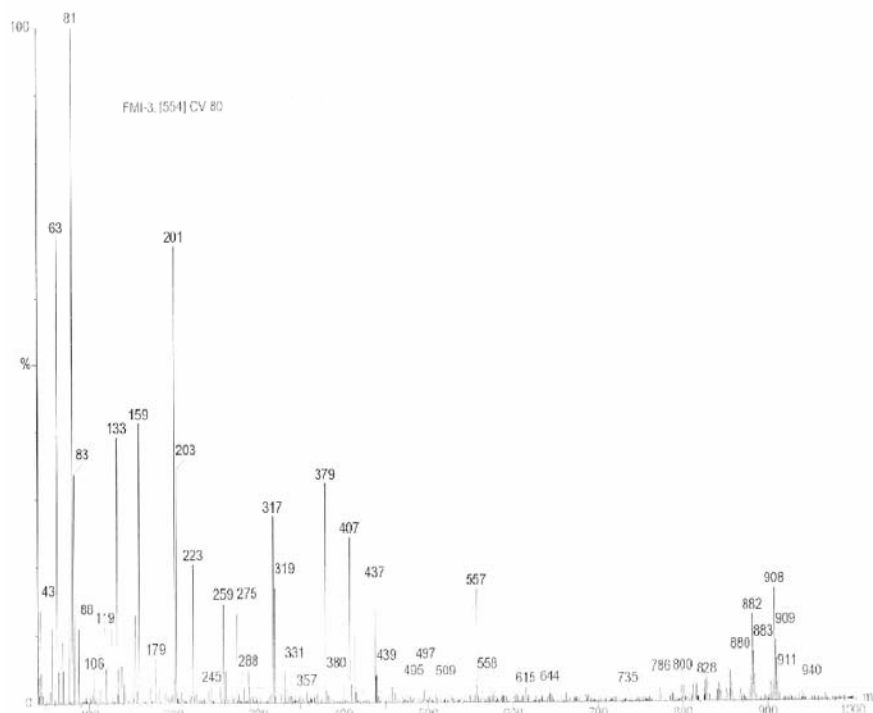


Figure 2.7 ESI-MS spectra Fe(III)-Malic acid chelate at pH 9 (FMI-3)

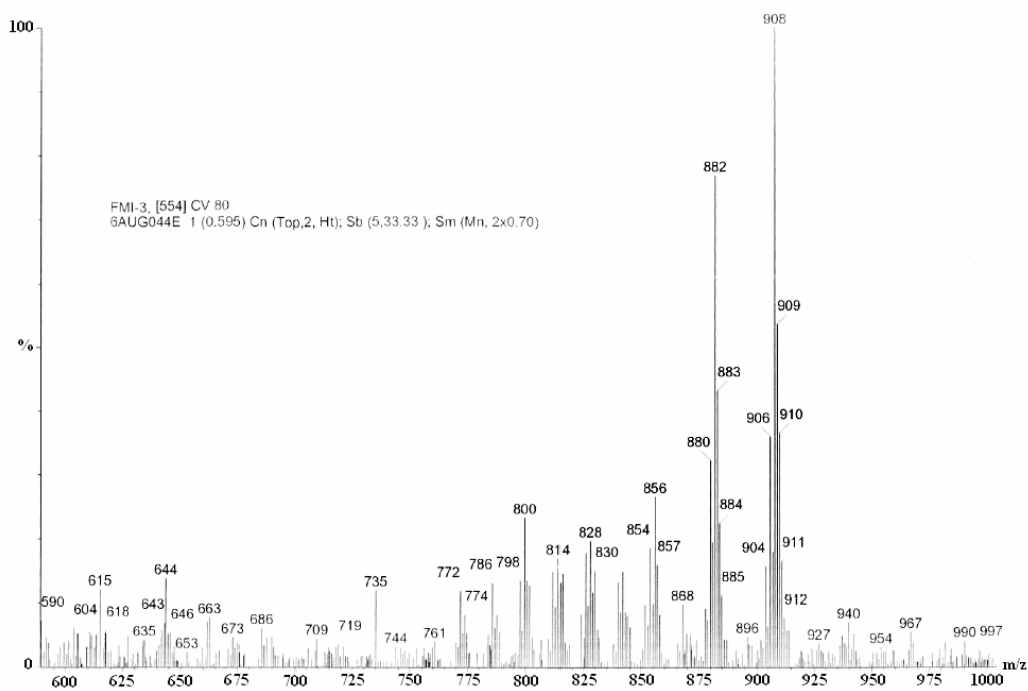


Figure 2.8 ESI-MS spectra Fe(III)-Malic acid chelate at pH 9 (FMI-3)

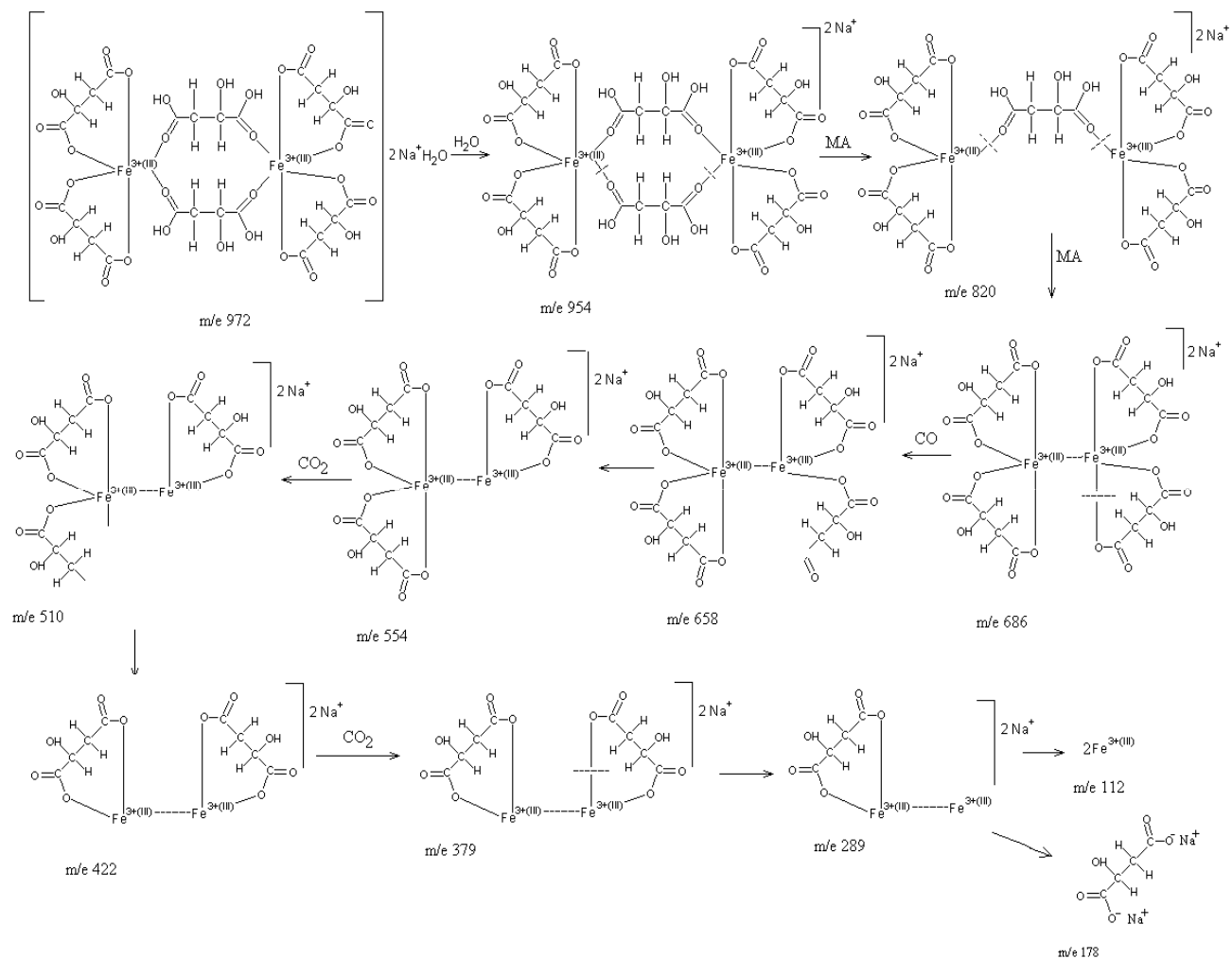
This gives bi-metallic complex formation with the malic acid where pH is adjusted by addition of NaOH. As the pH increases the deprotonation of the carboxylic group takes place and it will get coordinated with the Fe^{+3} to form metal

chelate The peak at m/e 972 attributed to the $[\text{Fe}^{+3}_2 (\text{L}^{-n})_4(\text{L})_2]^{-2} 2\text{Na}^+\text{H}_2\text{O}$, where $n = 2$ and $\text{L} = \text{C}_4\text{H}_6\text{O}_5$. The elimination of H_2O gives the peak at m/e 954 and the elimination of 2Na^+ gives the high intensity peak at m/e 908 attributed to complex $[\text{Fe}^{+3}_2 (\text{L}^{-n})_4(\text{L})_2]^{-2}$, where $n = 2$ and $\text{L} = \text{C}_4\text{H}_6\text{O}_5$, which is the expected iron chelate complex. The scheme 2.2 gives the representation of structural fragmentation of the complex. Further peak at m/e 820 and 686 assigned to the elimination of one $\text{C}_4\text{H}_6\text{O}_5$ to form $[\text{Fe}^{+3}_2 (\text{L}^{-n})_4(\text{L})]^{-2} 2\text{Na}^+$ and another $\text{C}_4\text{H}_6\text{O}_5$ which gives $[\text{Fe}^{+3}_2 (\text{L}^{-n})_4]^{-2} 2\text{Na}^+$. As the fragmentation goes on the m/e peak at 554 and 422 gives elimination of $\text{C}_4\text{H}_6\text{O}_5$ groups one by one giving the complex fragment $[\text{Fe}^{+3}_2 (\text{L}^{-n})_2]^{-2} 2\text{Na}^+$. The further decomposition gives the stable Fe_2O_3 formation which gives the m/e peak at 159 as expected. Also the peak at m/e 112 and 178 are attributed to the 2Fe^{+3} ions and $\text{C}_4\text{H}_4\text{O}_5\text{Na}$ formation respectively.

Our ESIMS study gives the good evidence for chelation of iron with malic acid. As the pH of the solution increases the coordination bond formation takes place between the metal ion and ligand, which gives the formation of bimetallic iron malic acid chelate complex with the metal to ligand ratio, as 1:3.

ESIMS analysis of the iron chelates reported here is in well accordance with the TG-DTA analysis

The UV-Vis spectra exhibited a strong absorbance characteristic of iron(III) malic acid complex (λ_{max} at 329.2 nm).



Scheme 2.2 Fragmentation pattern for the Fe(III)-Malic acid chelate synthesized at pH 7-7.5 (FMI-2) and at pH 9 (FMI-3)

4. Conclusions

The most notable feature of this work is, several different biodegradable iron chelates were synthesized and characterized. The iron chelates so synthesized were tested for catalytic conversion of hazardous H₂S gas to elemental sulfur. Due to low biodegradability (e.g. BOD₅ of EDTA: 0.01%, BOD₅ of DTPA: 0.7%), the disposal of iron chelating agents used in LO-CAT process raised serious environmental concern [28]. In order to overcome this environmental pollution, there is a need to look for alternative iron chelating agents. The carboxylic acids are known to possess high rate of biodegradation (e.g. BOD₅²⁰ of malic acid: 65%) along with good iron chelating property. From the screening of synthesized different iron chelates, FeCl₃-malic acid chelate system has been observed to give maximum recovery of sulfur (499 mg/g of iron chelate) along with high purity (> 99%) and reasonable extent of reaction time (15 min). To the best of our knowledge, the detail study of iron chelating property of malic acid has not yet been reported. The detail structural characterization of Fe⁺³-MA chelate was carried out using ESI-MS, TG/DTA and IR technique. The formation of bimetallic iron chelate complex with six malic acid molecules was characterized and reported. The reported biodegradable iron chelates serves many objectives; as reduction of aqueous pollution (by using biodegradable iron chelate), treatment for gaseous waste (removal of H₂S) and recovery of commercially important product (sulfur recovery).

References

- [1] John, S. E. "Recovery of Sulfur from Sour acid Gas: A Review of the Technology". *Environ. Prog.* **2002**, Vol. 21, p. 143.
- [2] Gaa, D.; Lagas, J. "Sulfur Recovery Solutions Global Trends." *Chem. Eng. World.* **2004**, Vol. 39, p. 43.
- [3] Yu, W. C.; Astarita, G.; "Selective Absorption of Hydrogen Sulphide in Tertiary Amine Solutions". *Chem. Eng. Sci.*, **1987**, Vol. 42. issue 3, p. 419.
- [4] Asai, S.; Konishi, Y.; Yabu, T. "Kinetics of Absorption of Hydrogen Sulfide into Aqueous Ferric Sulfate Solutions." *AIChE J.* **1990**, Vol. 36, p. 1331.
- [5] Pagella, C.; De Faveri, D. M. "H₂S Gas Treatment by Iron Bioprocess." *Chem. Eng. Sci.* **2000**, Vol. 55, p. 2185.
- [6] Jensen, A. B.; Webb, C. "Treatment of H₂S Containing Gases: A Review of Microbiological Alternatives." *Enzyme. Microb. Technol.* **1995**, Vol. 17, p. 2.
- [7] Khol, A. K.; Riesenfeld, F. C. Gas purification. McGraw-Hill, New York, **1960**.
- [8] Hardison; L. C. "Go from H₂S to S in one unit". *Hydrocarbon Processing.* April **1985**, p.70.
- [9] Hardison, L.C. "LO-CAT-II: Big Step Forward in Iron Redox Chemistry". *In GRI Liquid Redox Sulfur Recovery Conference.* GRI **1991**.
- [10] Pirtle, L.L., Allen, M.C., Hammond, C.A., Anderson, K.D., **1994**. Proceedings of the GRI Liquid Redox Sulfur Recovery Conference, mai 15–17, Austin, TX.
- [11] Hua, G. X.; Mcmanus, D.; Woollins, J. D. "The Evolution, Chemistry and Applications of Homogeneous Liquid Redox Sulfur Recovery Techeniques." *Comments in Inorganis Chemistry.* **2001**, Vol. 22, p. 327.
- [12] Bedell, S. A.; Kriby, L. H.; Buenger, C. W.; McGaugh, M. C. "Chelates' Role in Gas Treating." *Hydrocarb. Process.* **1988**, Vol. 67, p. 63.
- [13] McManus, D.; Martell, A. E. "The Evolution, Chemistry and Applications of Chelated Iron Hydrogen Sulfide Removal and Oxidation Processes." *J.Mol. Catal. A-Chem.* **1997**, Vol. 117, p. 289.
- [14] Demmink, J. F.; Wubs, H. J.; Beenackers, A. A. C. M. "Oxidative Absorption of Hydrogen Sulfide by a Solution of Ferric Nitrilotriacetic Acid Complex in a Cocurrent Down Flow Column Packed with SMV-4 Static Mixers." *Ind. Eng. Chem. Res.* **1994**, Vol. 33, p. 2989.

- [15] Pandey, R. A.; Malhotra, S. Desulphurization of Gaseous Fuels with Recovery of Elemental Sulphur: an overview. *Crit. Rev. Env.Sci.Tec.* **1999**, Vol. 29, p. 229.
- [16] Nagal, G. "Controlling H₂S Emissions." *Chem Eng.* **1997**, Vol. 104, p. 125.
- [17] J. F. Demmink, A. Mehra, A.A.C.M. Beenackers, "Absorption of Hydrogen Sulfide into Aqueous Solutions of Ferric Nitritotriacetic Acid: Local Auto-Catalytic Effects." *Chem. Eng. Sci.* **2002**, Vol. 57, p. 1723.
- [18] Iliuta, I.; Larachi, F. "Concept of Bifunctional Redox Iron-Chelate Process for H₂S Removal in Pulp and Paper Atmospheric Emissions". *Chem. Eng. Sci.* **2003**, Vol. 58, p. 5305.
- [19] Fischer, F. US Patent 1,891,974. **1932**.
- [20] Gómez, J. M.; Cantero, D.; "Hydrogen Sulfide Removal from Gaseous Effluents". *Microbial Processing of Metal Sulfides*, **2007**, p. 287.
- [21] Pieters, H. A. J.; Krevelen, D. W. "The Wet Purification of Coal Gas and similar Gases by the Staatsmijnen-otto-process": Elsevier, **1946**.
- [22] Hartley, W. Craig, R. S. Sapiro, R. H. British Patent 855421. **1960**.
- [23] Kezerian. C.; Ramsey, W. M.; Calif, D. "Bis-adduction Products and Methods Preparing Same". U.S. Pat. No.– 3,158,635, **1964**.
- [24] Meuly, W. C.; Ruff, C. D. *Paper Trade Journal*. **1972**.
- [25] Kasai, T. "Konox Process Removes H₂S". *Hydrocarbon Processing*. **1975**, Vol. 54, issue 2, p. 93.
- [26] Naraghi, A. R. "Chelate Catalyst System for H₂S Removal from a Gas Stream". U.S. Pat. No.– 4,880,609, **1989**.
- [27] Sawyer, D. T.; Sobkowiak, A. "Conversion of H₂S to sulfur". U.S. Pat. No.– 5,273,734. **1993**.
- [28] Hancock, R. D.; Martell, A. E.; Chen, D. "Design of Ligands for the Complexation of Fe(II)/Fe(III) in the catalytic Oxidation of H₂S to sulfur." *Can. J. Chem.* **1997**, Vol. 75, issue 5, p. 591.
- [29] McManus, D. Martell, A. E.; Chen, D. "Oxidation-reduction process". U.S. Pat. No.– 5,591,419. **1997**.
- [30] Ferm, B; Freivald, W. A.; McManus, D. Reicher, M. "Sulfur Recovery using Non-Aqueous Chelated Iron, Redox Catalyst Solution". *In Sulfur Recovery Conference*. GRI **1997**, Vol. 8.

- [31] Wilson, D. L.; Crump, D. K. "Succinic Acid Derivative Degradable Chelants, Uses and Compositions Thereof". U.S. Pat. No.– 5,741,555, **1998**.
- [32] Chen, D.; Martell, A. E.; Motekaitis, R. J.; McManus, D. "Syntheses and Fe(II)/Fe(III) Equilibria of the New Multidentate Ligands Pyridine-2-phosphonic- 6-carboxylic Acid and 2,6-pyridinediphosphonic Acid for the Use of Their Iron Chelates as Catalysts for the Oxidation of H₂S to S₈ by Air". *Can. J. Chem.* **1998**, Vol. 76. issue 4, p. 445.
- [33] Eng, S. J.; Motekaitis, R. J.; Martell, A. E. "The Effect of End-Group Substitutions and Use of a Mixed Solvent System on B-Diketones and their Iron Complexes". *Inorg. Chem. Acta.* **1998**, Vol. 278. p. 170.
- [34] Karel, V. Handbook of Environmental Data on organic chemicals, third ed. Van Nostrand Reinhold an international Thomson Publishing company, **1996**.
- [35] Gautier-Luneau, I.; Merle, C.; Phanon, D.; Lebrun, C.; Biaso, F.; Serratrice, G.; Pierre, J.-L. "New Trends in the Chemistry of Iron(III) Citrate Complexes: Correlations between X-ray Structures and Solution Species Probed by Electrospray Mass Spectrometry and Kinetics of Iron Uptake from Citrate by Iron Chelators." *Chem. Eur. J.* **2005**, Vol. 11, p. 2207.
- [36] Matzapetakis, M.; Raptopoulou, C. P.; Tsohos, A.; Papaefthymiou, V.; Moon, N.; Salifoglou, A. "Synthesis, Spectroscopic and Structural Characterization of the First Mononuclear, Water Soluble Iron-Citrate Complex, (NH₄)₅Fe(C₆H₄O₇)₂·2H₂O." *J. Am. Chem. Soc.* **1998**, Vol. 120, p. 13266.
- [37] Deshpande, A.S.; Sankpal, N.V.; Kulkarni, B.D. Indian Patent application number 1366/DEL/**2003**.

||shri||

CHAPTER-3

SULFUR NANOPARTICLES SYNTHESIS, CHARACTERIZATION AND APPLICATION

Abstract

Sulfur nanoparticles were synthesized from hazardous H₂S gas using novel biodegradable iron chelates in w/o microemulsion system and in different aqueous surfactant systems. Fe³⁺-malic acid chelate (0.05M aqueous solution) was used for catalytic oxidation of H₂S gas at ambient conditions of temperature, pressure and neutral pH for synthesis of sulfur nanoparticles in w/o microemulsion containing cyclohexane, Triton X-100 and n-hexanol as oil phase, surfactant and co-surfactant respectively and in aqueous surfactant system using CTAB, Tween-80 and SDS surfactants. The structural features of sulfur nanoparticles have been characterized by XRD, TEM, EDS, DLS, DRIFT-IR and BET surface area measurements. XRD analysis indicates the presence of α -sulfur. TEM analysis shows that the morphology of sulfur nanoparticles synthesized in w/o microemulsion system is nearly uniform in size (average particle size 10 nm) with narrow particle size distribution (in range of 5-15 nm), where as sulfur nanoparticles synthesized in aqueous surfactant systems of CTAB, Tween-80 and also SDS shows nearly uniform size (average particle size 7nm, 12nm, 15nm respectively). DLS analysis shows the monodispersity of the synthesized nanoparticles as compared to that synthesized only in aqueous phase. The EDS analysis indicated high purity of sulfur (>99%). Sulfur nanoparticles synthesized in w/o microemulsion system and in aqueous surfactant system exhibit higher antimicrobial activity (against bacteria, yeast and fungi) than that of colloidal sulfur synthesized only in aqueous phase.

Key words: Sulfur nanoparticles; H₂S gas; Iron chelates; w/o microemulsion; Antimicrobial activity

1. Introduction

Sulfur finds extensive technological applications such as in production of sulfuric acid, plastics, enamels, antimicrobial agent, insecticide, fumigant, metal glass cements, in manufacture of dyes, phosphate fertilizers, gun-powder and in the vulcanization of rubber etc.¹⁻⁴ Sulfur nanostructures are also used in synthesis of sulfur nano-composites for lithium battery,^{5,6} modification of carbon nanostructure,^{7,8} in synthesis of sulfur nano-wires with carbon to form hybrid materials with useful properties for gas sensor and catalytic applications,⁹ metal-sulfur compounds like ZnS, CdS, play important role in nonlinear optical and electroluminescent devices respectively. Lead sulfide nanostructures find wide variety of applications in lasers, light emitting devices, detectors, optical switches and optical amplification, telecommunication, etc. Similarly Ag₂S, Cu₂S, HgS nanocomposite, (Sn_{1-x}Ge_x)S mixed crystal semiconductors, iron sulfide nanoparticles are used in high-energy density batteries, diagnostic material, materials of photoelectrolysis, etc.¹⁰⁻¹⁵

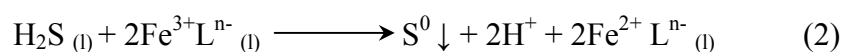
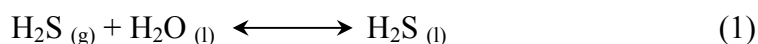
The synthesis of nanoparticles can be carried out by various methods. Igor et al.¹⁶ reported synthesis of sulfur microtubules in acetone solution in presence of (NH₄)₂Mo₂S₁₂ without any organic structure directing agent. SEM images show the aggregates of microtubules of 5-100 μm length and 100-400 nm outer diameter. The use of anodic alumina membranes (AAM) was reported by Jia et al.¹⁷ for the synthesis of sulfur nanotubes. In a common two-electrode electrochemical cell, and a common graphite plate this electrodeposition was carried out. The Zn nanowire was electrochemically deposited at room temperature, after which the AAM template along with Zn nanowires covered with sulfur powder and CS₂ solvent was autoclaved at 150 °C. The liquid sulfur was injected into gaps between Zn nanowires and the walls of AAM under CS₂ high vapor pressure forming nanotubes of sulfur which are

further purified. The outer diameter of the nanotubes was about 50 nm and thickness is about 5-8 nm. Synthesis of sulfur nanowires using anodic alumina nanoporous templates (AANTs) using S-CS₂ solution as precursor was reported by Santiago et al.⁹ The nanowires thus synthesized are of 15-20 nm diameter and 1000 nm length.

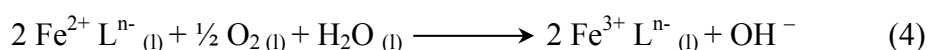
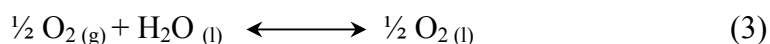
The monoclinic sulfur nanoparticles synthesis by liquid phase precipitation method was carried out by Guo et al.¹⁸ The average particles size was reported to be 50-80 nm with spherical shape. The use of microemulsion system is an attractive and simple method as it allows greater control over nanoparticle morphology (size and shape).^{19,20} Recently, Guo et al.²¹ reported the synthesis of monoclinic sulfur nanoparticles using the mixture of two w/o microemulsion systems. The two w/o microemulsions consisting of sodium polysulfide/ammonium polysulfide and hydrochloric acid as aqueous phase and Theolin/(Span80-Tween80)/butanol as oil phase were mixed together to form insoluble sulfur nanoparticles. However, during synthesis the H₂S gas was released as hazardous by-product. The 20 nm sulfur nanoparticles were prepared using sodium polysulfide as reactant where as ammonium polysulfide gave 35 nm sulfur nanoparticles.

In the present work we report for the first time synthesis of sulfur nanoparticles in the range of 5-15 nm from hazardous H₂S gas by catalytic conversion using biodegradable iron chelates in w/o microemulsion system and in aqueous surfactant systems.

The numerous gas sweetening processes are reported in open literature. Nagal²⁸ has reported the gas desulfurization based on liquid redox chemistry, as follows



where 'L' denotes an organic ligand, which are usually a polyaminocarboxylic acid, such as ethylenediamine tetraacetic acid (EDTA), nitrilotriacetic acid (NTA), hydroxy, diethylenetriamine pentaacetic acid (DTPA), etc.²⁹ and 'n' denotes the charge on the organic ligand. Since the active ferric chelate is converted to inactive ferrous chelate, the later component has to be regenerated by oxidation according to the reactions,



At present, use of iron chelates has been extensively commercialized in Lo-CAT, Sulferox process.³⁰ However, these chelating agents [e.g. EDTA, DTPA, NTA, cyclohexane-1,2-diaminetetraacetic-(CDTA), etc.] have very low rate of biodegradation and therefore cause environmental pollution. Therefore it is necessary to study the alternative chelating agents for iron chelation. It has been reported that carboxylic acids (e.g. citric acid, malic acid, gluconic acid etc.) have good chelating properties and have faster rate of biodegradation.^{31, 32}

In the present study use of novel biodegradable iron chelates, in particular, FeCl₃-malic acid chelate system has been extensively studied in w/o microemulsion (cyclohexane-n-hexanol/TritonX-100/water) and in different aqueous surfactant systems using CTAB, Tween-80 and SDS surfactant, for the catalytic conversion of H₂S gas to sulfur nanoparticles. The sulfur nanoparticles have been systematically characterized by X-ray diffraction (XRD), transmission electron microscope (TEM), energy dispersive spectroscopy (EDS), dynamic light scattering (DLS), diffused

reflectance infra-red fourier transform technique (DRIFT-IR) and BET surface area measurements. Furthermore, the potency of antimicrobial activity of sulfur nanoparticles has been determined by plate assay and compared with that of colloidal sulfur.

2. Experimental

2.1 Materials

All chemicals were of analytical grade and used without further purification. Ferric chloride, ferric sulfate, ferric nitrate, gluconic acid, malic acid, citric acid, sodium hydroxide, sodium sulfide, cyclohexane, n-hexanol, Triton X-100, Tween-80, CTAB, and SDS were purchased from Merck India. All solutions were prepared by deionized milli-Q water (Q-H₂O with 18.2 MQ cm resistivity, Millipore corporation).

All microbial cultures (*Pseudomonas areuginosa* NCIM 2036 and *Styphylococcus aureus* NCIM 2079; *Candida albicans* NCIM 3102, *Candida albicans* NCIM 3466, *Aspergillus flavus* NCIM 535 and *Aspergillus niger* 545) were procured from National Collection of Industrial Micro-organisms (NCIM), NCL-Pune (India).

2.2 Preparation of iron chelate solution for H₂S abatement

The synthesis of iron chelates and the experimental method for H₂S removal and sulfur recovery was discussed in detail in chapter 2, section 2.3 and 2.4.

2.3 Selection of optimum iron chelate system

Different iron chelates were evaluated for catalytic conversion of H₂S gas to elemental sulfur. Table 3.1 reports the values of reaction time indicating the breakthrough of H₂S uptake since the beginning of experiments. In all experiments, the volume of the reaction mixture and the rate of H₂S gas addition were kept constant. The values of 'reaction time' therefore give a measure of the rate of reaction for various iron chelates. Besides the reaction time; purity and recovery of sulfur also

need to be considered to establish the best iron chelate system. Among various iron chelates, FeCl₃-gluconic acid chelate system required much less reaction time than the others (5 min.); however, the purity and recovery of product was very poor. Over all, FeCl₃-malic acid chelate system has been observed to give maximum recovery of sulfur (499 mg/g of iron chelate) along with high purity (> 99%) and reasonable extent of reaction time (15 min.). Hence it was selected for further evaluation in different systems.

Table 3.1 Screening of iron chelate systems for H₂S abatement

Iron salt	Chelating agent	Molar ratio	Reaction Time (min)	sulfur recovered mg/gm of iron chelate	% purity Sulfur ^a
FeCl ₃	Citric acid	1:2	36	184.20	>99
	Malic acid	1:3	15	499	>99
	Gluconic acid	1:3	5	27.7	83.71
Fe ₂ (SO ₄) ₃	Citric acid	1:2	25	137.8	97.5
	Malic acid	1:3	37	235	>99
	Gluconic acid	1:3	39	51	88.44
Fe ₂ (NO ₃) ₃	Citric acid	1:2	10	116.83	75.96
	Malic acid	1:3	5	290.88	94
	Gluconic acid	1:3	20	90	99

^a The precipitate also contains C, N, H, and Fe as confirmed by elemental analysis

2.4 Preparation of FeCl₃-malic acid (Fe³⁺-malic acid) chelate solution

Iron chelate solution (0.05M) was prepared by dissolving ferric chloride and malic acid (1:3 mole ratio) in deionized water. The pH of the solution was adjusted to 7.0-7.5 with sodium hydroxide solution. This aqueous chelate solution was used in the w/o microemulsion system and in different aqueous surfactant systems for synthesis of sulfur nanoparticles.

2.5 Instrumentation

The sulfur nanoparticles were characterized by X-ray diffraction (XRD) using Rigaku Dmax 2500 diffractometer equipped with graphite monochromatized CuK α radiation ($\lambda = 1.5406 \text{ \AA}$) employing a scanning rate of $5^\circ/\text{min}$ in the 2θ range from 10° to 80° . The energy dispersive spectroscopy (EDS) was carried out by using EDAX of Phoenix Company. The morphology of the sulfur nanoparticles was observed by transmission electron microscope (TEM). The samples for TEM analysis were prepared by deposition of an ultrasonically dispersed suspension of the sulfur product in methanol on collidon and carbon coated copper grids. The TEM measurements were performed on a JEOL model 1200EX instrument. Dynamic light scattering (DLS) measurements were performed on the 90 PLUS particle size analyzer from Brookhaven Instruments Corporation. Infrared (IR) spectra were recorded by Parkin Elmer system 2000 Infrared spectrometer employing a potassium bromide (KBr) using diffused reflectance infra-red fourier transform technique (DRIFT-IR).

2.6 Evaluation of antimicrobial activity of sulfur nanoparticles

The antimicrobial activity of sulfur nanoparticles was determined by plate assay and compared with that of colloidal sulfur. Nutrient agar [HiMedia, India], MGYP [malt extract (0.3 g), glucose (1.0g), yeast extract (0.3g), peptone (0.5g) and agar (2.0g) per 100mL medium] and potato dextrose agar [HiMedia, India] were used as growth media for bacterial, yeast and fungal strains respectively. The antimicrobial activity of sulfur nanoparticles and colloidal sulfur was determined by measuring the inhibition zones on agar plates inoculated with bacterial (*Pseudomonas areuginosa*, *Styphylococcus aureus*), yeast (*Candida albicans*) and fungal strains (*Aspergillus flavus*, *Aspergillus niger*). Freshly prepared microbial cell suspension (0.5 ml) was

added on sterile petri plates containing solidified agar medium. 30 μ l of sulfur suspension was added on agar plates followed by incubation at specified temperature (28 °C for yeast and fungi, 30 °C for bacteria). Being antimicrobial agent, sulfur inhibited the growth of microorganism and inhibition zones were formed. The inhibition zones were measured after 24 h for bacteria and after 48 h for yeast and fungi. The efficiency of antimicrobial activity is expressed in terms of average diameter of inhibition zones obtained by triplicate results.

Part-I Synthesis of sulfur nanoparticles in w/o microemulsion

system

3. Results and Discussion

The oil phase was prepared by mixing 52 wt% of cyclohexane, 22 wt% Triton X-100 (as surfactant) and 11 wt% n-hexanol (as co-surfactant) under constant stirring. Then 15% (0.05M) aqueous Fe³⁺-malic acid chelate solution was added drop wise to the oil phase under vigorous stirring, to prepare optically clear and stable system. The sulfur nanoparticles synthesis was carried out by the procedure described earlier in section 2.2 and 2.3. The oxidation of H₂S occurred inside aqueous micelle containing iron chelate as shown in Figure 3.1. The precipitated sulfur was separated by centrifugation at 8000 rpm for 20 mins and washed with water, methanol and dried under vacuum at 60 °C for 4 h.

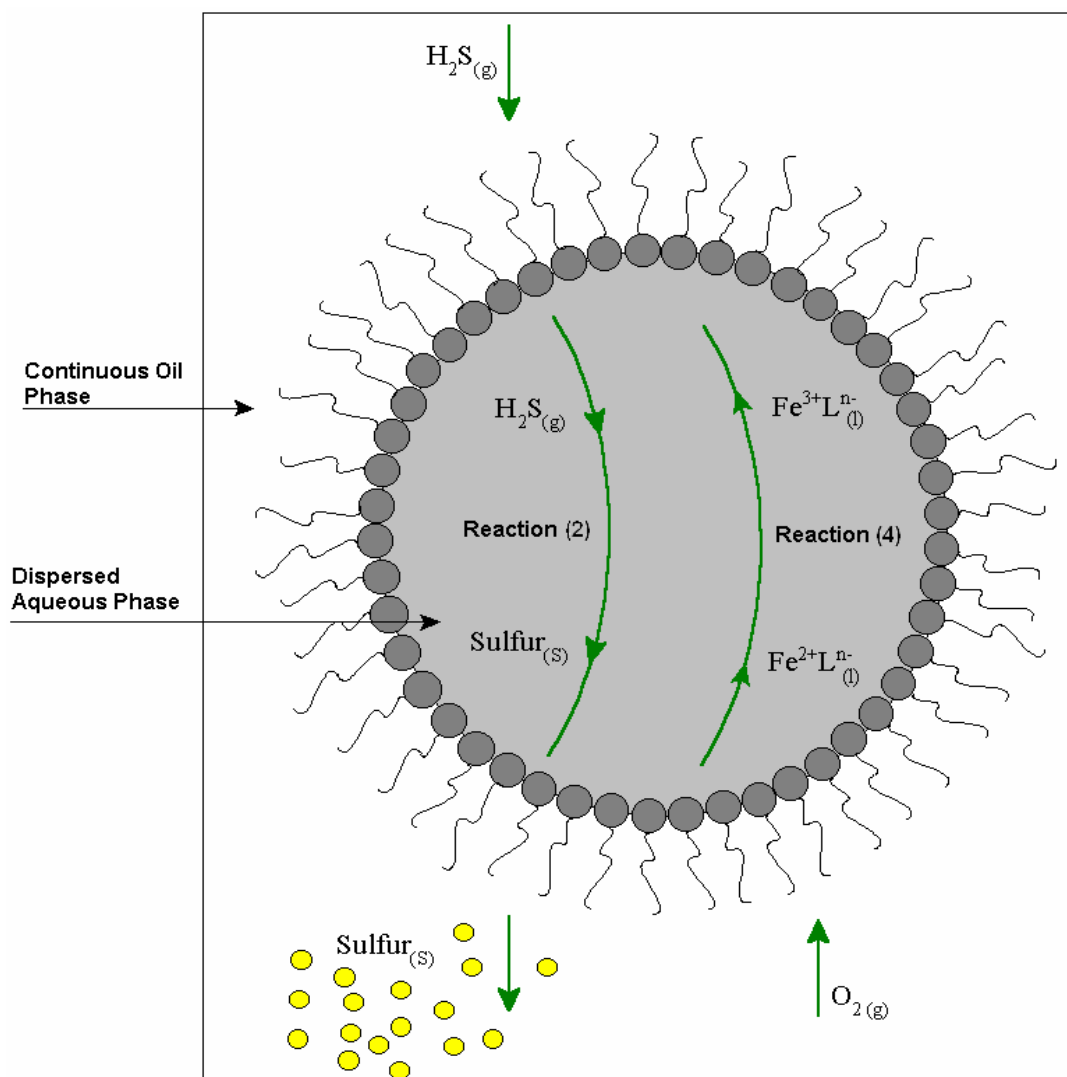


Figure 3.1. Schematic representation of synthesis of sulfur nanoparticles in w/o microemulsion system

3.1 XRD analysis of the sulfur particles

The XRD analysis of sulfur nanoparticles synthesized in w/o microemulsion and aqueous solution is shown in Figure 3.2. The position and intensities of the diffraction peaks of all samples were compared with standard alpha sulfur particle diffraction pattern.³³ The presence of sharp peaks in Figure 3.2b (and in the insight) indicates highly crystalline nature of the sulfur nanoparticles synthesized using w/o microemulsion system compared to particle synthesized by normal aqueous phase (Figure 3.2a). The determination of the mean particle diameter (D) was done by the XRD analysis using Debye-Scherrer formula,

$$D = \frac{k\lambda}{\beta \cos \theta} \quad (5)$$

Where D is the crystallite size, k is the Scherrer constant usually taken as 0.89, λ is the wavelength of the X-ray radiation (0.154056 nm for Cu $K\alpha$), and β is the full width half maximum (FWHM) of the diffraction peak measured at 2θ . The estimated crystallite size of the sample prepared in microemulsion from line broadening of the most intense diffraction peak is approximately 10 nm.

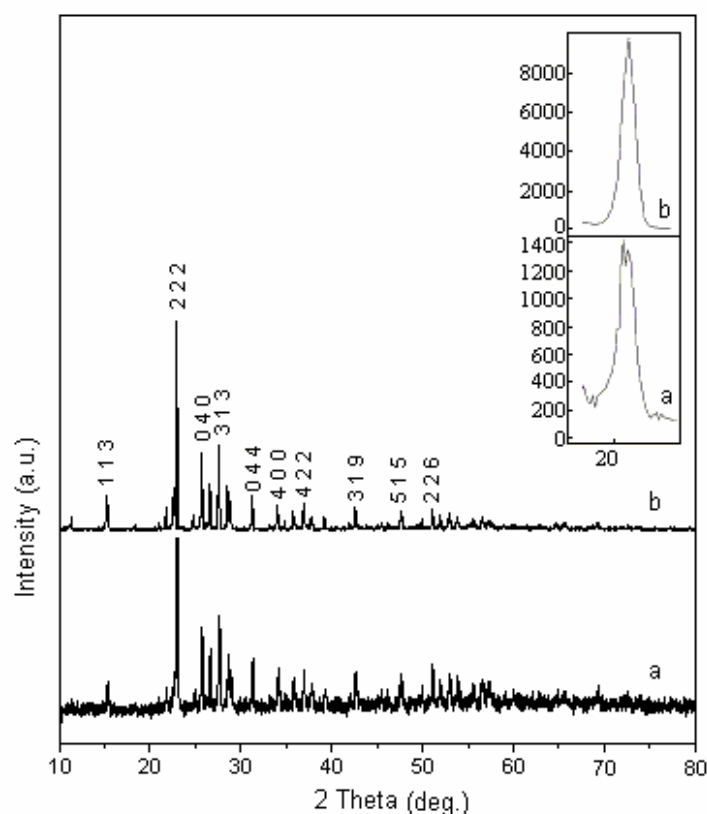


Figure 3.2 XRD of sulfur particle synthesized in: a) aqueous phase; b) w/o microemulsion. The insight shows highest intensity peaks magnification

3.2 EDS analysis

The synthesized nanoparticles were characterized by EDAX for the evaluation of their composition and purity. Figure 3.3 gives spectrum of the EDAX analysis. It is evident from the peaks that the product is completely pure and corresponds to sulfur

element only, which are synthesized in w/o microemulsion system and aqueous system.

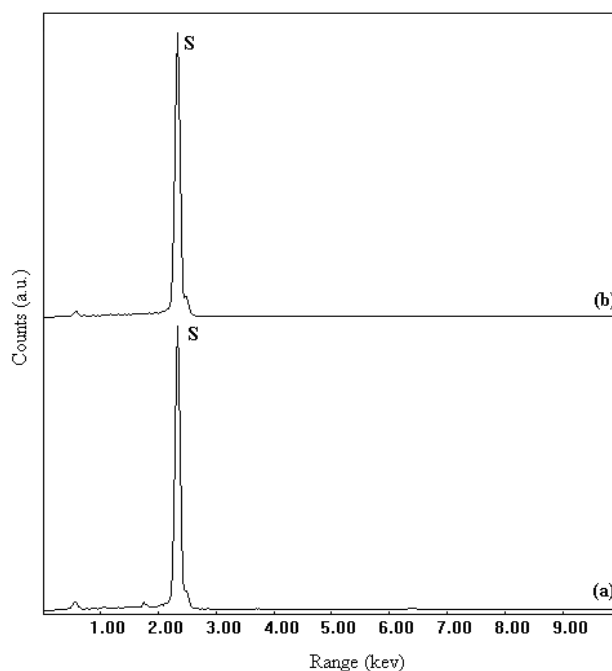


Figure 3.3 EDAX of sulfur nanoparticles synthesized in: a) aqueous phase; b) w/o microemulsion

3.3 TEM analysis

The morphology of the sulfur nanoparticles synthesized in w/o microemulsion system and aqueous system was analyzed using transmission electron microscope (Figure 3.4). Sulfur particles prepared in aqueous phase showed larger particle size and a wider particle size distribution (~ 80 - 100 nm) (Figure 3.4a). However, sulfur nanoparticles synthesized in w/o microemulsion system showed very fine particles of size ~ 10 nm and a relatively narrow particle size distribution (~ 5 - 15 nm) (Figure 3.4b). Figure 3.5 shows the histogram for the sulfur nanoparticles size distribution synthesized in w/o microemulsion.

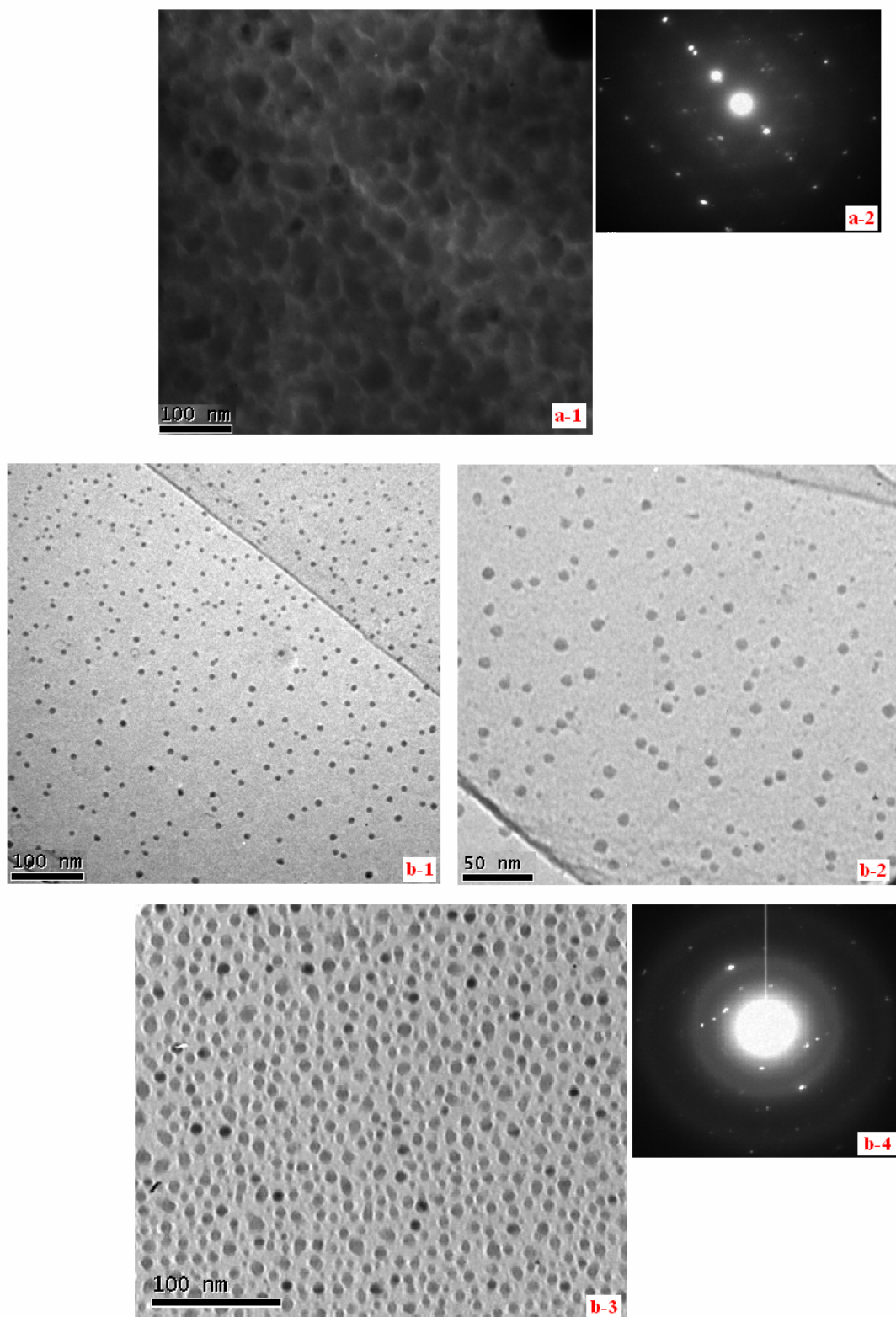


Figure 3.4 TEM analysis for sulfur nanoparticles synthesized in different systems: a-1) aqueous phase system; a-2) diffraction pattern of aqueous phase sulfur; b-1 to b-3) w/o microemulsion at various magnification; b-4) diffraction pattern of sulfur nanoparticle

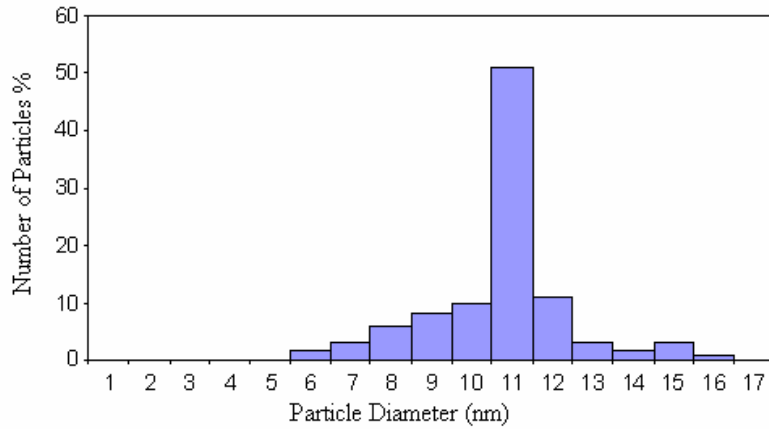


Figure 3.5 Histogram of particles size distribution for sulfur nanoparticles synthesized in w/o microemulsion

3.4 DLS Analysis

The mean particle size was determined by dynamic light scattering (DLS) for sulfur nanoparticles synthesized in w/o microemulsion system. DLS analysis shows the narrow size distribution with slight polydispersity of particles in the system. Figure 3.6 shows the average particles size of sulfur nanoparticles synthesized in w/o microemulsion system to be 10nm.

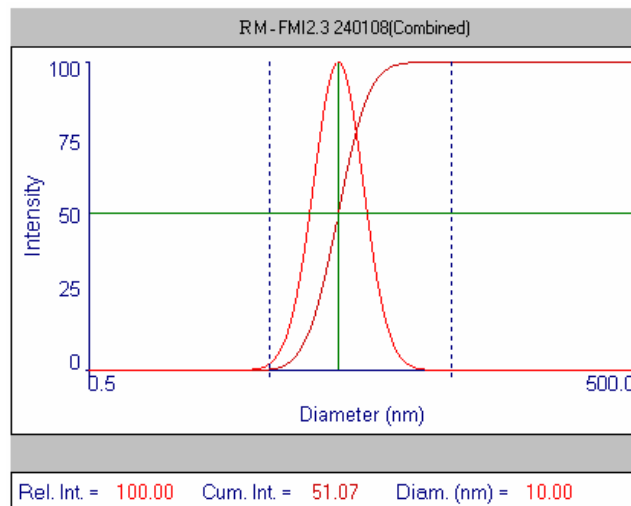


Figure 3.6 DLS analysis for sulfur nanoparticles synthesized in w/o microemulsion system

3.5 IR analysis

Figure 3.7 gives DRIRFT analysis of standard alpha sulfur and nanoparticles synthesized using w/o microemulsion system. The IR spectrum of the sulfur nanoparticles (Figure 3.7a) confirm presence of all characteristic peaks of alpha-sulfur at [463(s), 505(w), 550(m), 590(m), 617(m), 656(s), 683(m), 710(m), 845(s), 876(m), 903(m), 936(m), 986(w), 1052(w), 1298(m), 1513(m) cm^{-1}] when compared with standard alpha sulfur (Figure 3.7b).³⁴

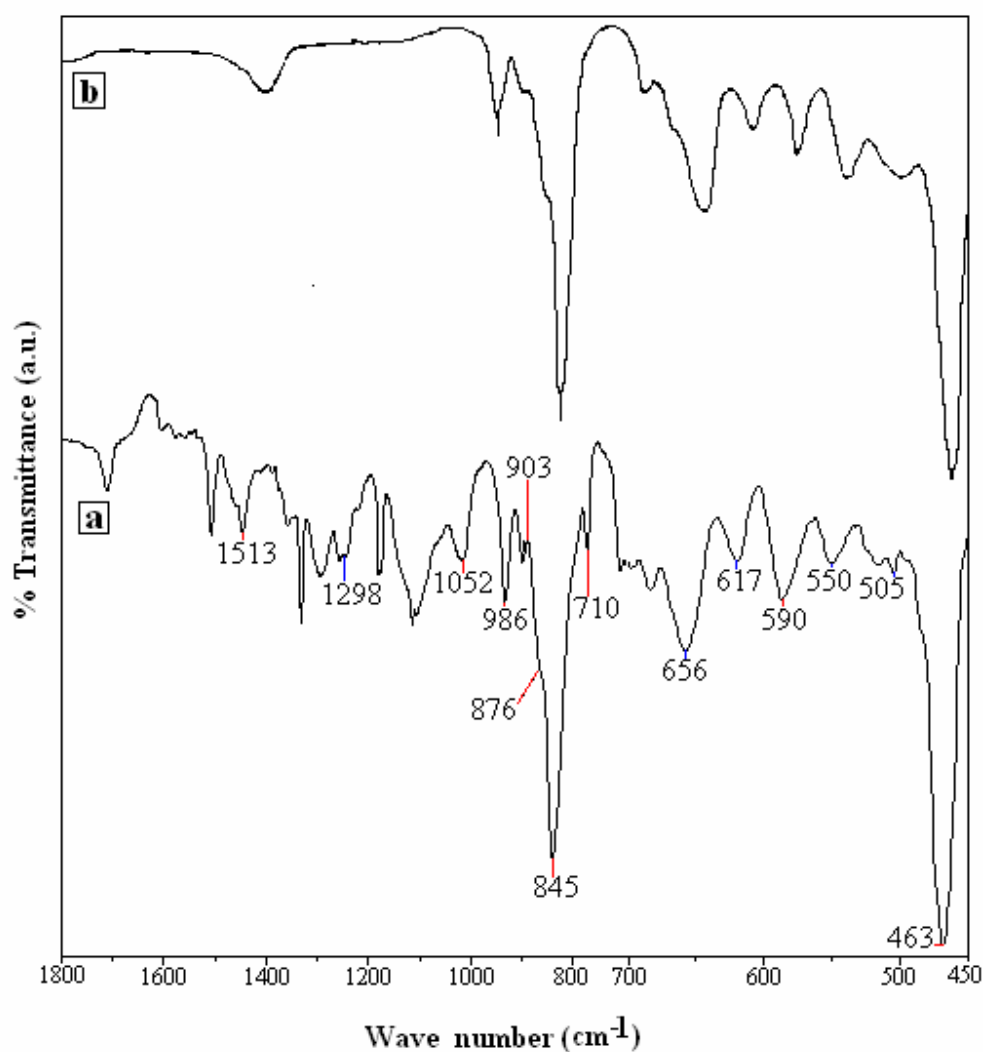


Figure 3.7 Diffused reflectance infra-red fourier transform analysis: a) sulfur nanoparticles; b) rhombic sulfur

3.6 Antimicrobial activity of sulfur nanoparticles

The sulfur element is known to possess potent antimicrobial activity⁴. Due to their smaller particle size (~10 nm), sulfur nanoparticles are expected to exhibit antimicrobial action at lower concentrations than sulfur particles synthesized in aqueous phase (80-100 nm). Furthermore, BET analysis shows that there was significant increase in surface area of sulfur nanoparticles (177 m²/g) compared to sulfur (48 m²/g) synthesized in aqueous phase only as shown in BET isotherms in Figure 3.8 and Figure 3.9, respectively.

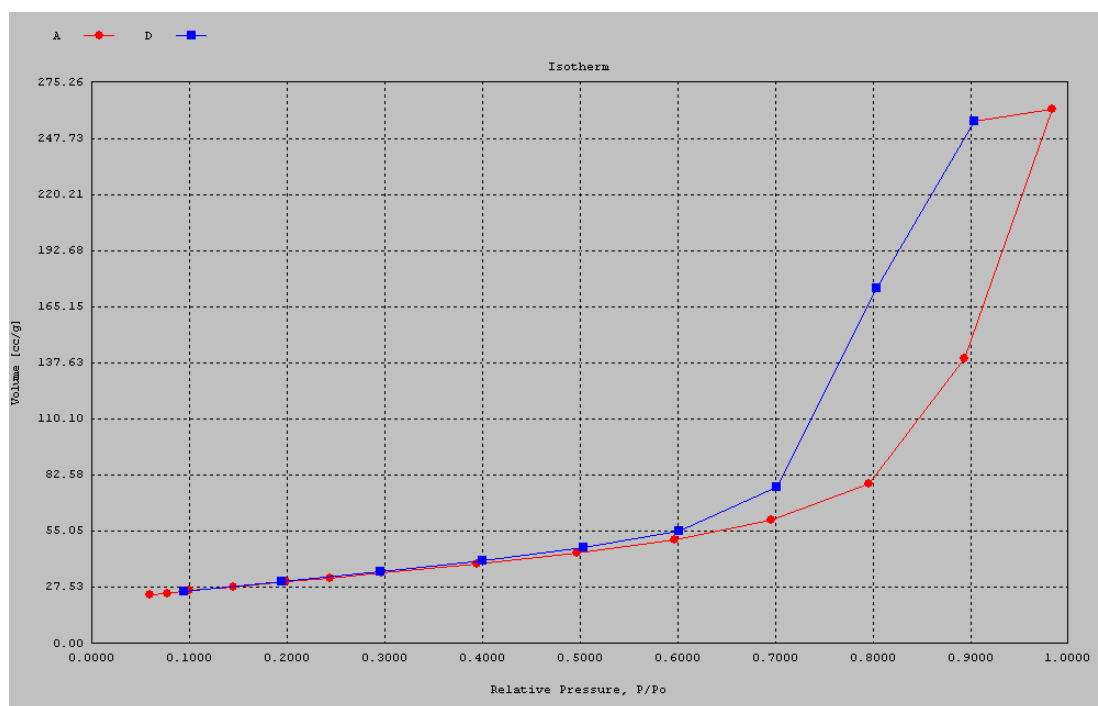


Figure 3.8 BET isotherm for the sulfur nanoparticles synthesized in w/o microemulsion

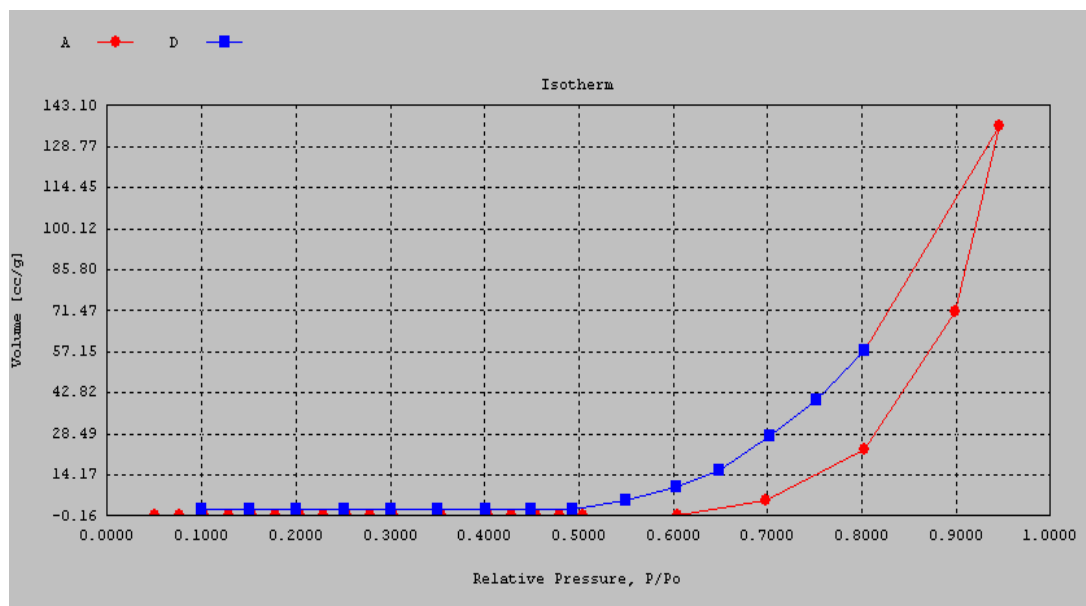


Figure 3.9 BET isotherm for the sulfur synthesized in aqueous phase only

The antimicrobial activity of sulfur nanoparticles (synthesized by reverse microemulsion system) was determined by plate assay. Here the efficiency of antimicrobial activity was measured in terms of diameter of inhibition zones.

Results of antimicrobial activities of nanoparticles and sulfur are summarized in Table 3.2. The inhibition zones for bacteria and yeast were determined at 30 $\mu\text{g/ml}$ and 150 $\mu\text{g/ml}$ of sulfur suspension. In bacterial strains, sulfur nanoparticles gave larger inhibition zones compared to that of sulfur. For example, in case of *Pseudomonas aeruginosa*, sulfur nanoparticles produced 7.3 and 25 mm inhibition zones at 30 $\mu\text{g/ml}$ and 150 $\mu\text{g/ml}$ sulfur concentrations, respectively. However sulfur produced no inhibition zone at 30 $\mu\text{g/ml}$ and 8.7 mm inhibition zone at 150 $\mu\text{g/ml}$. Similarly, in case of *Styphylococcus aureus*, larger inhibition zones were observed by sulfur nanoparticles than colloidal sulfur. Likewise sulfur nanoparticles were found to be more effective than sulfur in inhibiting growth of yeasts strains (*Candida albicans* NCIM 3102 and 3466). This indicates that at the same concentration, the sulfur nanoparticles have better antimicrobial activity against bacterial and yeast cultures than that of sulfur.

In case of Fungi, 30 µg/ml and 150 µg/ml suspensions of sulfur gave no inhibition zones. Therefore the antifungal activity was determined at higher concentrations. The distinct inhibition zones were observed when sulfur nanoparticles concentration was increased upto 1500 µg/ml and 3000 µg/ml (Table 3.2). At these concentrations, sulfur nanoparticles were found to inhibit growth of *Aspergillus flavus* and gave larger inhibition zones (14 and 22.5 mm, respectively). Whereas, at same concentrations the growth of *Aspergillus flavus* was completely unaffected when sulfur was used and no inhibition zones were observed. In case of *Aspergillus niger*, sulfur nanoparticles (at 1500 µg/ml and 3000 µg/ml concentrations) were found to retard normal fungal growth. Here the formation of spores (late stage of fungus growth cycle) was observed to be delayed by about 48 h. On the other hand, the growth of *Aspergillus niger* was found to be normal when sulfur was used. Thus the reduction in particle size enhances the effectiveness of sulfur particles as antimicrobial agent. These results are significant and indicate the greater efficacy of sulfur nanoparticles than normal sulfur particularly as an antifungal agent.

The antimicrobial/antifungal activity data for colloidal sulfur and sulfur nanoparticle were analyzed by two statistical tests namely p-value analysis and Student's t-test. First p-value analysis was conducted to test the statistical hypothesis that the observed experimental mean values are due to a chance occurrence or not. The p-values obtained using Minitab-15 software is listed in Table 3.2

Table 3.2 Antimicrobial activity of sulfur nanoparticles

Type of micro-organism	Microbial strain	Statistical analysis for zone of inhibition(mm)					
		Colloidal sulfur (80-100 nm) ^a			Sulfur nanoparticles synthesized in aqueous surfactant systems		
		Sulfur Nanoparticles (5-15 nm) ^a					
		Mean	p-value	t _c ^b	Mean	p-value	t _c ^b
Bacteria	PA						
	(a)30µg/ml (b)150µg/ml	Nil 8.7	0 <0.005	0 0	7.5 25	0.012 0.041	62.225 12.665
	SA						
	(a)30µg/ml (b)150µg/ml	Nil Nil	0 0	0 0	7.7 30	0.022 0.031	963.760 1415.784
Yeast	CA-3102						
	(a)30 µg/ml (b)150µg/ml	Nil 7.1	0 0.037	0 0	8.3 10	0.014 0.042	799.431 38.747
	CA-3466						
	(a)30 µg/ml (b)150µg/ml	Nil 7.3	0 0.023	0 0	8.3 11	0.035 0.031	736.867 100.434
Fungi	AF						
	(a)1500 µg/ml (b)3000 µg/ml	Nil Nil	0 0	0 0	15 22.5	0.021 0.031	708.678 4230.07
	AN						
	(a)1500 µg/ml (b)3000 µg/ml	Nil Nil	Growth retardation ^c Growth retardation ^c				

^a Average particle size; ^b formation of spores was observed to be delayed by about 48 h

It is seen that in all experiments $p > 0.05$ i.e. at 95% confidence level thus indicating that the experimental results are not due to chance. Specifically student t-test was performed to test the null hypothesis (H_0): $\mu_x = \mu_y$, where μ_x denotes the mean of antimicrobial/antifungal zone of inhibition for colloidal sulfur and μ_y denotes the mean of antimicrobial/antifungal zone of inhibition for sulfur nanoparticles synthesized in different aqueous surfactant systems. The results of the t-test are indicated in table II shows that $|t_c| \geq t_{2\alpha} (95\%) = 1.746$ (for 16 degree of freedom).^{35, 36} This suggests that $\mu_x \neq \mu_y$ and thus it can be inferred that the antimicrobial/antifungal activity of sulfur nanoparticles compared to colloidal sulfur is not due to chance.

To the best of our knowledge, the detail study of iron chelating property of malic acid has not yet been reported. Due to low biodegradability (e.g. BOD₅ of EDTA: 0.01%), the disposal of iron chelates used in Lo-CAT process raised serious environmental concern.²⁸ In order to overcome this environmental pollution, there is need to look for alternative iron chelating agents. The carboxylic acids are known to possess high rate of biodegradation (e.g. BOD₅ of malic acid: 65%) along with good iron chelating property. The results of the present investigation indicated that Fe⁺³-malic acid iron chelates in w/o microemulsion can effectively oxidize hazardous H₂S gas to produce sulfur nanoparticles.

Part –II Synthesis of sulfur nanoparticles in different aqueous surfactant systems

4. Results and Discussion

Different aqueous surfactant systems above CMC (0.01M, 50 ml each for CTAB and Tween-80 and 0.1M, 50 ml for SDS surfactant) were prepared. To the above aqueous surfactant systems 50ml of 0.05M Fe^{3+} -malic acid chelate solution (pH 7-7.5) was added with vigorous stirring. The oxidation of H_2S may occur inside the aqueous micelle or in the void volume between the micelles depends upon the micelle structure and number of aggregation for micelles at above concentration in presence of iron chelate solution as shown in Figure 3.10.

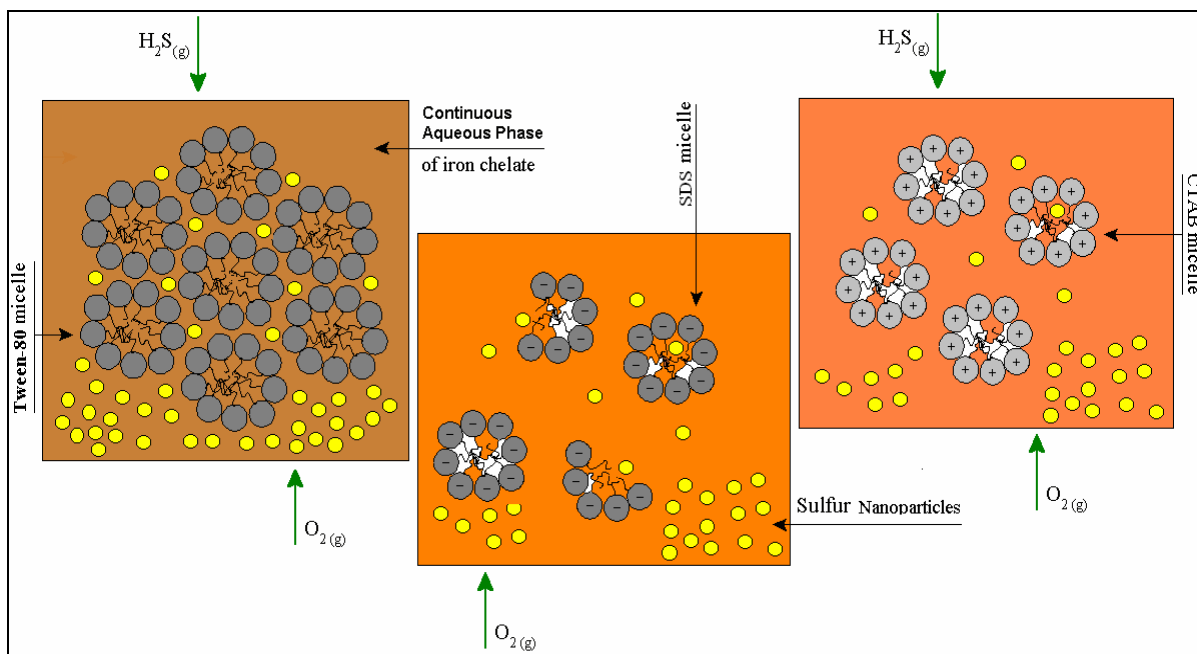


Figure 3.10 Schematic representation of synthesis of sulfur nanoparticles in various aqueous surfactant systems

The number of micelles in the solution was calculated depending on the concentration of surfactant used in the aqueous phase, size of surfactant molecule and nature of surfactants used for formation of micelles.

Table 3.3 The calculation for number of micelles in the solution

Aqueous Surfactant system	Concentration of surfactant in mole/m ³	Number of micelles/m ³	
		For closed packing from micelle radius	Calculated from concentration of surfactant
CTAB	0.01×10^{-3}	55.26×10^{24}	0.0634×10^{24}
SDS	0.1×10^{-3}	186.66×10^{24}	1.2044×10^{24}
Tween-80	0.01×10^{-3}	10.88×10^{24}	0.10037×10^{24}

From Table 3.3 it can be seen that number of micelles calculated from the size of surfactant molecule required for closed packing was very high than that of calculated from the concentration of surfactant considered for the experimental synthesis of nanoparticles. This may be one of the reasons for not getting very uniform shape nanoparticles of sulfur in the aqueous surfactant system as compared to w/o microemulsion system. The detail structural analysis of sulfur nanoparticles synthesized in aqueous surfactant system was carried out as follows.

4.1 XRD and EDS analysis of the sulfur particles

The XRD analysis of sulfur nanoparticles synthesized in aqueous surfactant system and aqueous solution (in absence of surfactant) is shown in Figure 3.11. The position and intensities of the diffraction peaks of all samples were compared with standard alpha sulfur particle diffraction pattern (JCPDS No. – 0824722).³³ The presence of sharp peaks in Figure 3.11b-d indicates highly crystalline nature of the sulfur

nanoparticles synthesized in aqueous surfactant systems of CTAB, SDS and Tween-80 respectively compared to particles synthesized in normal aqueous phase (Figure 3.11a.) (The peak intensity comparison between sulfur nanoparticles synthesized in aqueous surfactant system using CTAB surfactant and synthesized in aqueous phase only was elaborated). Though the particles were showing highly crystalline structure of nano particles — and TEM analysis also shows very fine particle size of nanosulfur — but due to no definite shape of nanoparticles it is very difficult to calculate the particles size using Debye-Scherrer formula.

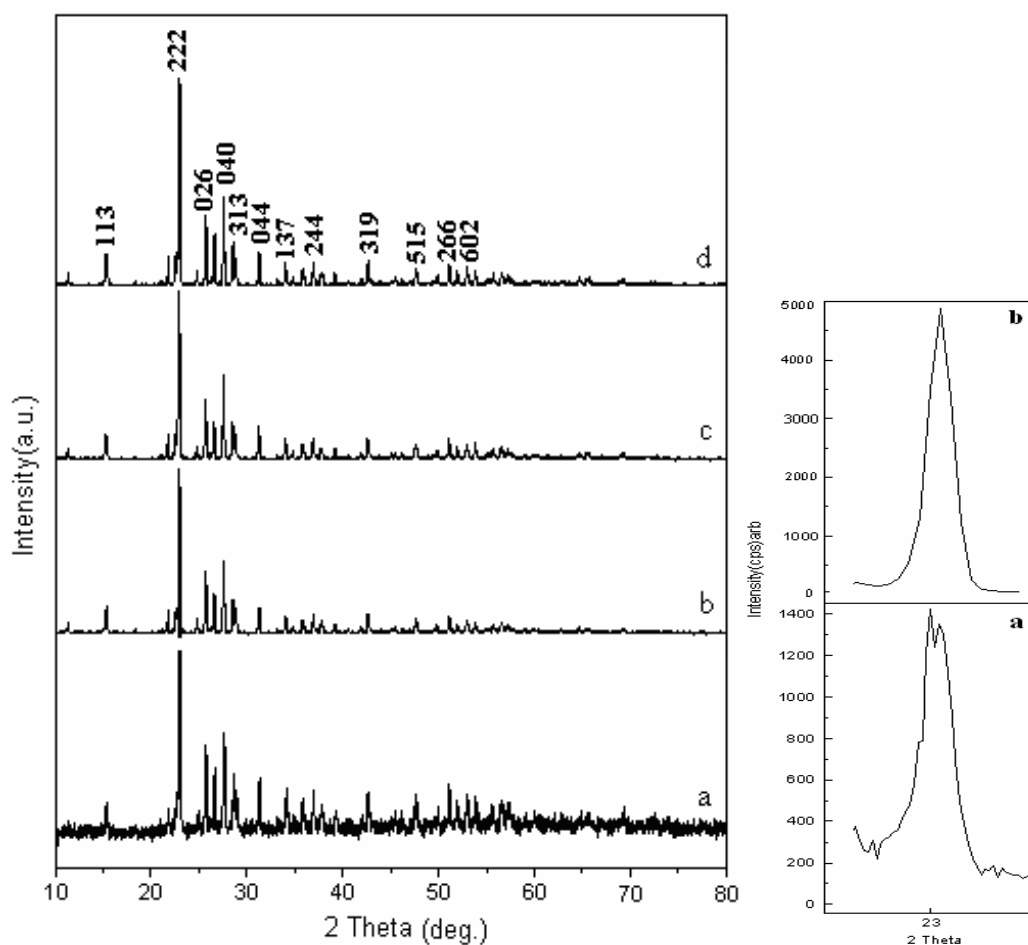


Figure 3.11 XRD of sulfur particle synthesis in: a) aqueous phase; b) CTAB; c) SDS; d) Tween-80

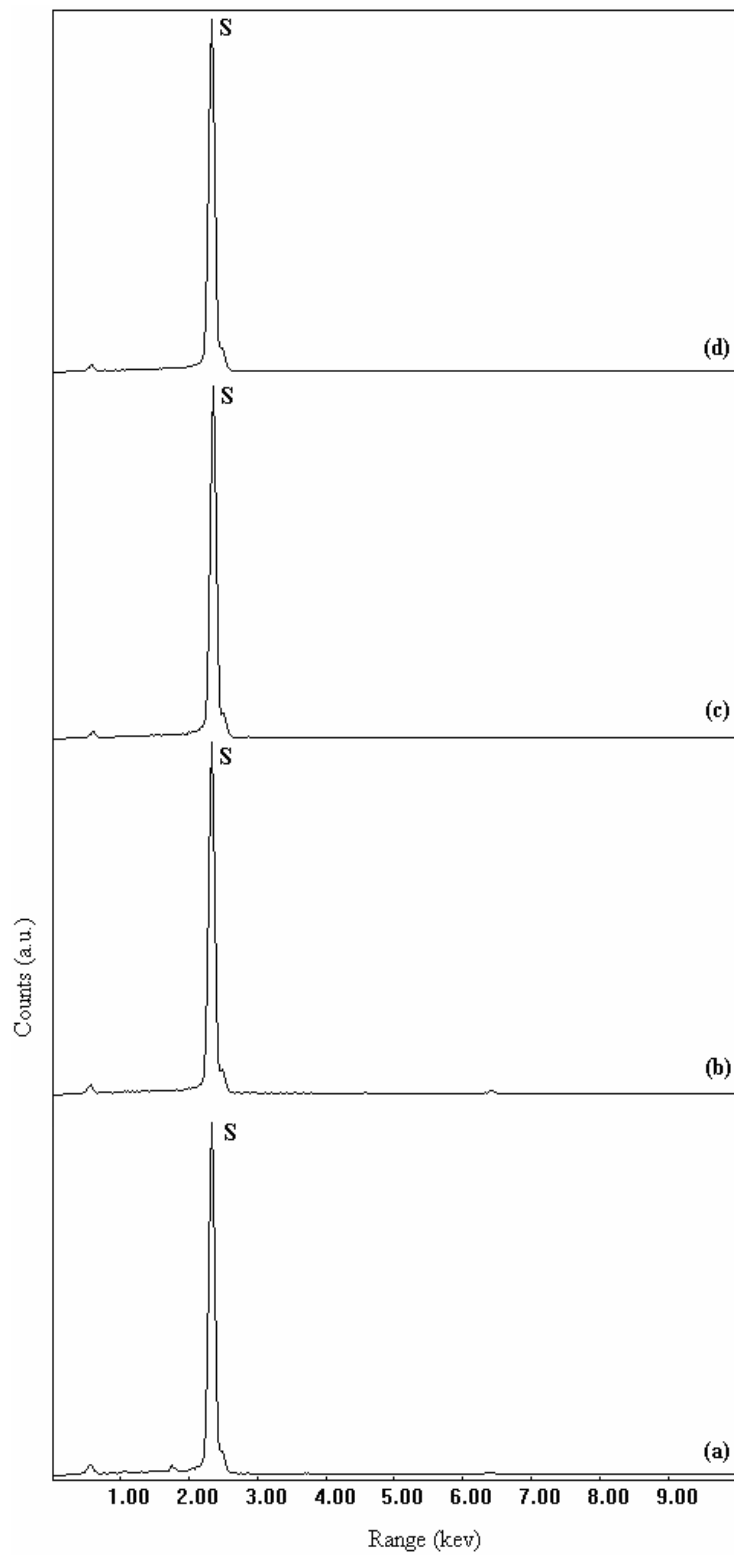


Figure 3.12 EDAX of sulfur nanoparticles synthesized in: a) aqueous phase; b) CTAB; c) SDS; d) Tween-80

Figure 3.12 gives spectrum of the EDAX analysis. It is evident from the peaks that the product is completely pure and corresponds to sulfur element only, which are synthesized in aqueous surfactant systems and normal aqueous systems.

4.2 TEM analysis

The morphology of the sulfur nanoparticles synthesized in aqueous surfactant systems and normal aqueous system was analyzed using transmission electron microscope (Figure 3.13). Sulfur particles prepared in aqueous phase showed larger particle size and a wider particle size distribution (~80-100 nm) (Figure 3.13a). However, TEM images of sulfur nanoparticles synthesized in Tween-80, CTAB, SDS, aqueous surfactant systems show uniform particle size distribution as indicated in Figure 3.13c, 3.13d and 3.13e respectively. The average particle size of the nanoparticles prepared in presence of CTAB, Tween-80 and SDS were 7 nm, 12 nm and 15 nm, respectively.

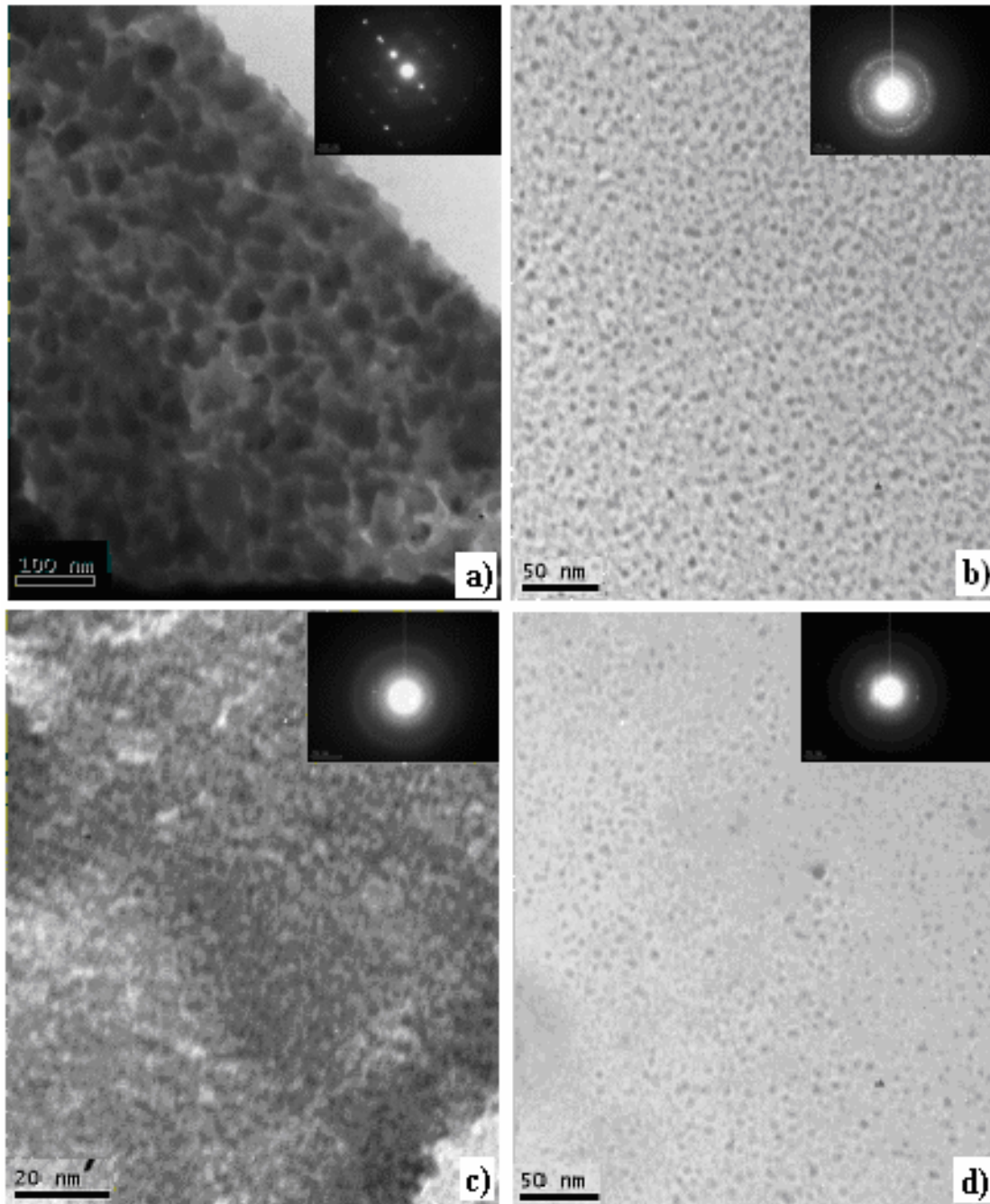


Figure 3.13 TEM analysis for sulfur nanoparticles synthesized in different systems: a) aqueous phase; b) Tween-80; c) CTAB; d) SDS surfactant system

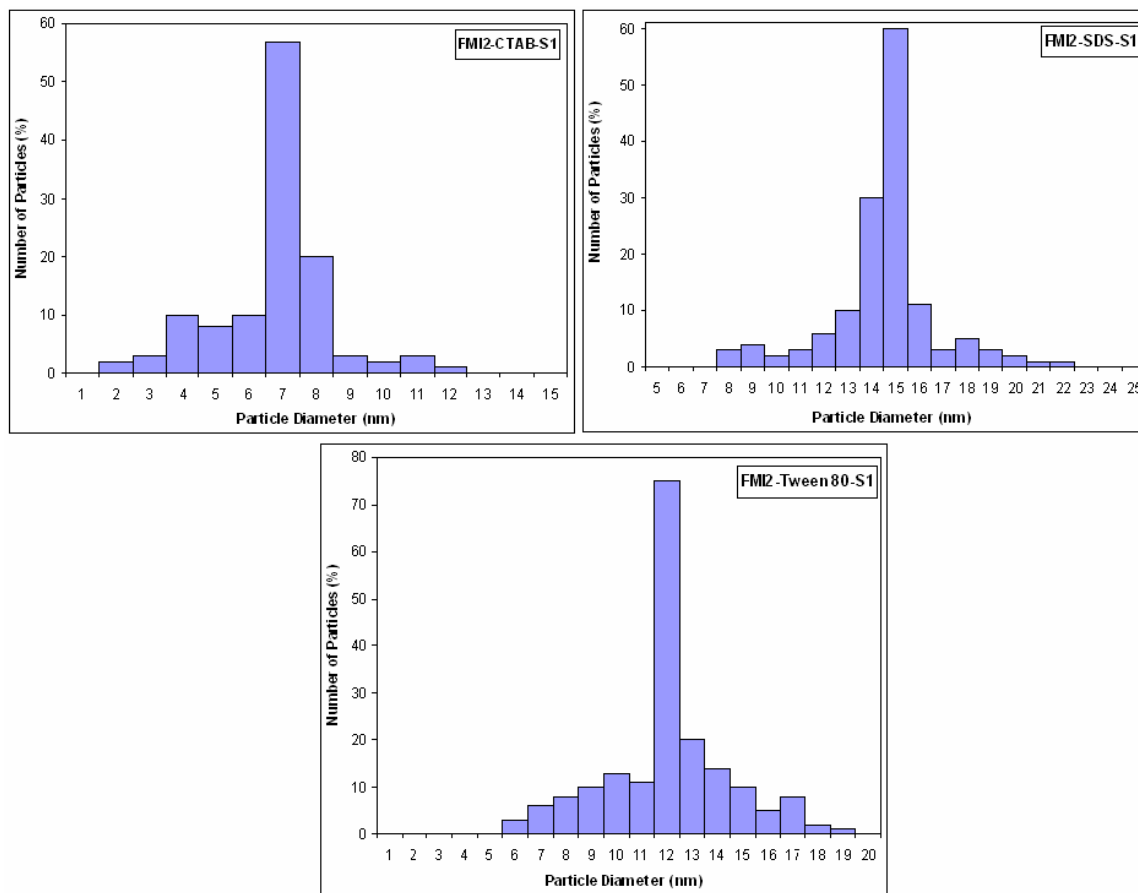


Figure 3.14 Histogram of particles size distribution for sulfur nanoparticles synthesized in different aqueous surfactant systems using: a) CTAB; b) Tween-80; c) SDS surfactant

4.3 DLS Analysis

The mean particle size was determined by dynamic light scattering (DLS) for sulfur nanoparticles synthesized in various surfactant systems. DLS analysis shows the narrow size distribution with highly monodispersity of particles in the CTAB aqueous surfactant system, whereas in Tween-80 and SDS aqueous surfactant system it shows slight polydispersity. Figure 3.15a-c shows the average particles size of sulfur nanoparticles synthesized in CTAB aqueous surfactant system to be 6.14nm, in Tween-80 surfactant system to be 11.84nm and in SDS surfactant system to be 13.55nm.

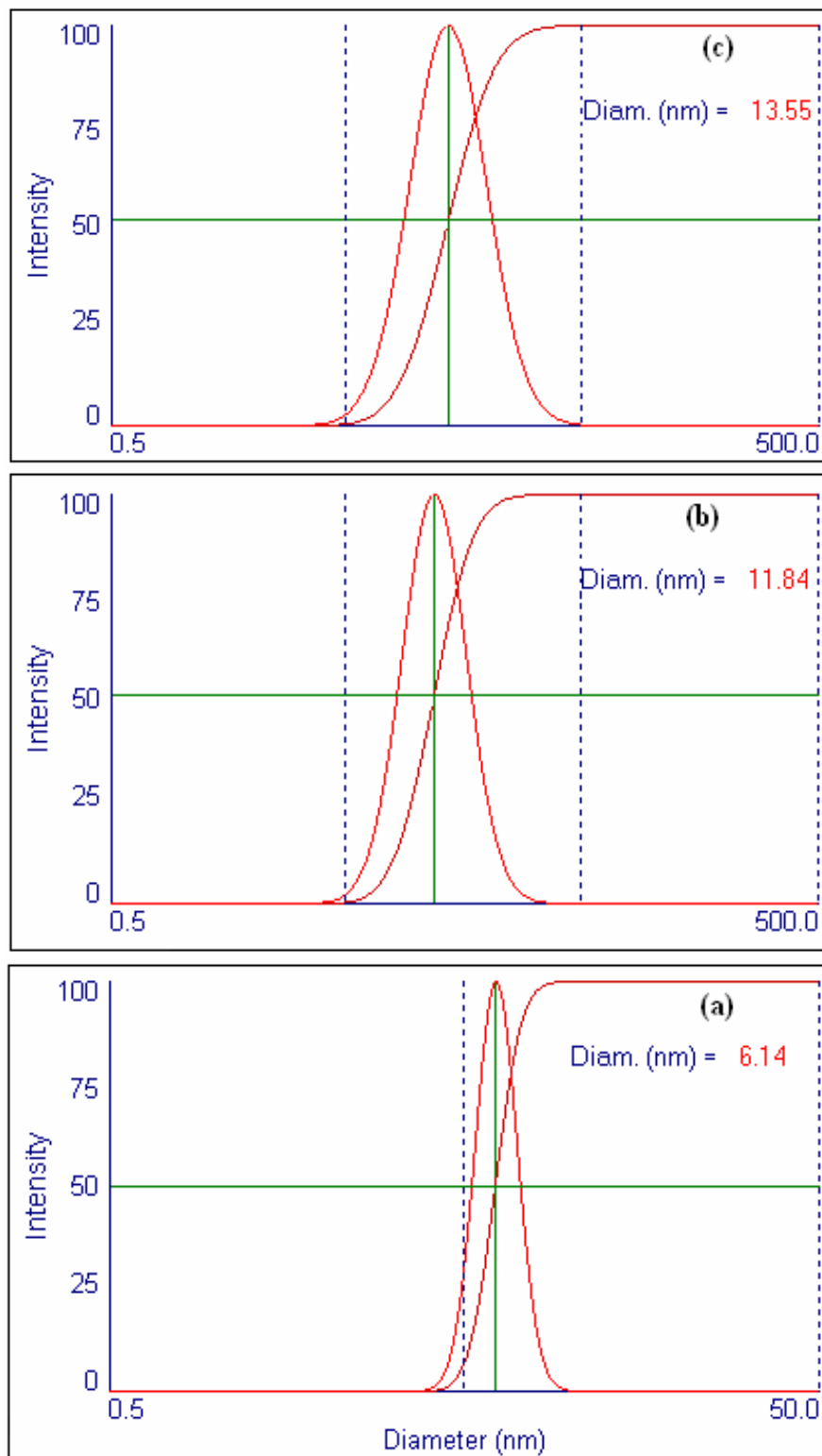


Figure 3.15 DLS analysis for sulfur nanoparticles synthesized in different systems: a) CTAB; b) Tween-80; c) SDS aqueous surfactant system

4.4 IR analysis

Figure 3.16 gives DRIRFT analysis of sulfur nanoparticles synthesized in aqueous surfactant systems using different surfactants. The IR spectrum of the sulfur nanoparticles indicate presence of all characteristic peaks of alpha-sulfur at [656(s), 683(m), 710(m), 845(s), 876(m), 903(m), 936(m), 986(w), 1052(w), 1298(m), 1513(m) cm^{-1}],³⁴ Figure 3.16a, 3.16b and 3.16c shows the sulfur nanoparticles synthesized in aqueous surfactant system using CTAB, Tween-80 and SDS surfactant system, respectively.

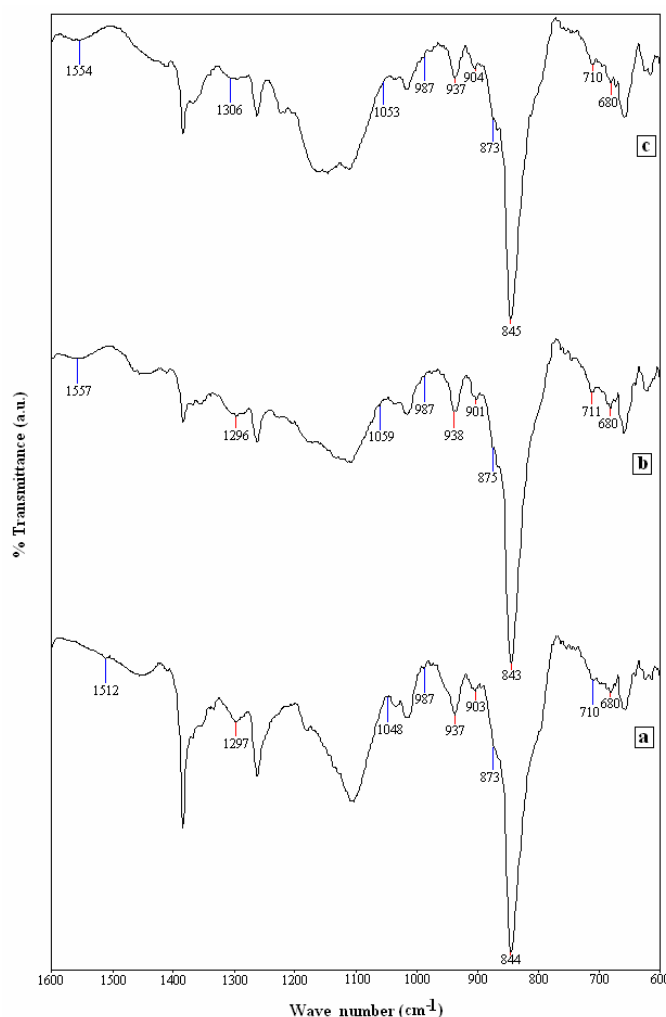


Figure 3.16 Diffused reflectance infra-red fourier transform analysis for sulfur nanoparticles synthesized in aqueous surfactant system using: a) CTAB surfactant; b) Tween-80 surfactant; c) SDS surfactant

4.5 Antimicrobial activity of sulfur nanoparticles

The antimicrobial/antifungal property of sulfur nanoparticles synthesized in different aqueous surfactant systems was carried out by following same method as used in the case of w/o microemulsion system. Due to their smaller particle size (~7nm, 12nm and 15nm), sulfur nanoparticles are expected to exhibit antimicrobial action at lower concentrations than sulfur particles synthesized in aqueous phase (80-100 nm). The results of antimicrobial activities of nanoparticle and sulfur are summarized in Table 3.4. The inhibition zones for bacteria and yeast were determined at 30 µg/ml and 150 µg/ml of sulfur suspension. In bacterial strains, sulfur nanoparticles gave larger inhibition zones compared to that of sulfur at the same concentration. In case of Fungi, 30 µg/ml and 150 µg/ml suspensions of sulfur gave no inhibition zones. Therefore the antifungal activity was determined at higher concentrations. The distinct inhibition zones were observed when sulfur nanoparticles concentration was increased upto 1500 µg/ml and 3000 µg/ml (Table 3). In case of *Aspergillus niger*, sulfur nanoparticles (at 1500 µg/ml and 3000 µg/ml concentrations) were found to retard normal fungal growth. Here the formation of spores was observed to be delayed by about 48 h. Thus the reduction in particle size enhances the effectiveness of sulfur particles as antimicrobial agent.

Also statistical analysis calculation was carried out to prove that the antimicrobial/antifungal activity of sulfur nanoparticles compared to colloidal sulfur is not due to chance, but it is due to the nanoscale size of sulfur particles (Table 3.4).

Table 3.4 Antimicrobial activity of sulfur nanoparticles synthesized in different aqueous surfactant system

Type of micro-organism	Microbial strain	Statistical analysis for zone of inhibition(mm)											
		Colloidal sulfur (80-100 nm) ^a			Sulfur nanoparticles synthesized in aqueous surfactant systems								
					CTAB (6nm) ^a			Tween-80 (12nm) ^a			SDS (15nm) ^a		
		Mean	p-value	t _c ^b	Mean	p-value	t _c ^b	Mean	p-value	t _c ^b	Mean	p-value	t _c ^b
Bacteria	PA												
	(a)30µg/ml	Nil	0	0	11	0.027	62.2	7	0.033	20.4	10	0.035	15.5
	(b)150µg/ml	8.7	<0.005	0	15	0.027	4.9	12	0.039	2.4	21	0.013	9.5
	SA												
	(a)30µg/ml	Nil	0	0	9	0.028	262.0	Nil	0	0	8	0.015	317.2
	(b)150µg/ml	Nil	0	0	11	0.044	205.9	Nil	0	0	10	0.015	102.6
Yeast	CA-3102												
	(a)30 µg/ml	Nil	0	0	16	0.023	1003.1	Nil	0	0	12	<0.005	1361.0
	(b)150µg/ml	7.1	0.037	0	18	0.047	151.4	Nil	0	-104.2	16	0.017	511.6
	CA-3466												
	(a)30 µg/ml	Nil	0	0	16	0.009	293.7	11	0.010	50.4	10	0.044	110.6
	(b)150µg/ml	7.3	0.023	0	20	0.033	442.9	18	0.011	165.0	19	0.023	50.7
Fungi	AF												
	(a)1500 µg/ml	Nil	0	0	15	0.053	808.0	12	0.021	156.0	14	0.037	162.1
	(b)3000 µg/ml	Nil	0	0	22	0.038	650.0	18	0.033	105.8	17	0.012	40.2
	AN												
	(a)1500 µg/ml	Nil	Growth retardation ^c										
	(b)3000 µg/ml	Nil	Growth retardation ^c										

PA- Pseudomonas areuginosa NCIM 2036; **SA-** Styphylococcus areus NCIM 2079; **CA-** Candida albicans NCIM 3102; **CA-** Candida albicans NCIM 3466; **AF-** Aspergillus flavus NCIM 535; **AN-** Aspergillus niger NCIM 545

^a Average particle size, ^bt_{2α} = 1.764 at α = 0.05, ^c formation of spores was observed to be delayed by about 48 h

Plate Assay for Antimicrobial and Antifungal Activity



Candida Tropicalis (Yeast)

Sulfur nanoparticles



Staphylococcus aureus (Bacteria)

Sulfur nanoparticles



**Pseudomonas aeruginosa
(Bacteria)**

Sulfur nanoparticles



**Pseudomonas aeruginosa
(Bacteria)**

Sulfur synthesized in aqueous phase only

Figure 3.17: Photographs of plate assay for antimicrobial and antifungal activity of sulfur nanoparticles and sulfur synthesized in aqueous phase only

5. Conclusions

The results of the present investigation indicated that Fe⁺³-malic acid iron chelates in w/o microemulsion system and different aqueous surfactant systems can effectively oxidize hazardous H₂S gas to produce sulfur nanoparticles. The described process gives highly crystalline pure α -sulfur with uniform shape and size of 10 nm of sulfur nanoparticles in w/o microemulsion system and average particle size of the nanoparticles prepared in aqueous surfactant system in presence of CTAB, Tween-80 and SDS surfactants were 7 nm, 12 nm and 15 nm respectively. The synthesized nanoparticles are showing very high antimicrobial and antifungal activity compare to sulfur synthesized in aqueous phase only. The sulfur nanoparticles synthesis was carried out at ambient temperature and atmospheric pressure and between pH 7-7.5. The described process serves mainly two objectives; waste utilization for preparation of commercially important product and reduction in environmental pollution. Besides reduction in environmental pollution (use of biodegradable chelating agents) and waste utilization (H₂S abatement), the described process also has high commercial significance.

References

- [1] Lide, D. R. "CRC Handbook of Chemistry and Physics". 85th ed.; CRC press: New York, **2004**, p. 30.
- [2] Merck Index, 13th ed., Merck & Co. Inc.: USA, **2001**, p.1599.
- [3] Leslie, K. S.; Millington, G. W. M.; Levell, N. J. "Sulphur & Skin: Satan to Saddam!". *J. of Cosmetic Dermatology*. **2004**, Vol. 13, p. 94.
- [4] Weld, J. T.; Gunther, A. "The Antibacterial Properties of Sulfur". *J. Exp. Med.* **1946**, p. 531.
- [5] Yu, X.; Xie, J.; Yang, J.; Wang, K. "All Solid-State Rechargeable Lithium Cells based on Nano-Sulfur Composite Cathodes". *J. of Power Sources*. **2004**, Vol. 132, p.181.
- [6] Zheng, W.; Liu, Y. W.; Hu, X. G.; Zhang, C. F. "Novel Nanosized Adsorbing Sulfur Composite Cathode Materials for the Advanced Secondary Lithium Batteries". *Electrochimica Acta*. **2006**, Vol. 51, p.1330.
- [7] Barkauskas, J.; Juskenas, R.; Mileriene, V.; Kubilius, V. "Effect of Sulfur on the Synthesis and Modification of Carbon Nanostructures". *Mater. Res. Bull.* **2007**, Vol. 42, p.1732.
- [8] Smorgonskaya, E. A.; Kyutt, R. N.; Shuman, V. B.; Danishevskii, A. M.; Gordeev, S. K.; Grechinskaya, A. V. "Small-Angle X-Ray Scattering in a Carbon-Sulfur Nanocomposite Produced from Bulk Nanoporous Carbon". *Phys. Solid State*. **2002**, Vol. 44, issue 10, p.1908.
- [9] Santiago, P.; Carvajal, E.; Mendoza, D.; Rendon, L. "Synthesis and Structural Characterization of Sulfur Nanowires". *Microsc. Microanal.* 2006, 12(supp.2).
- [10] J. Xu, W. Ji, J. "Characterization of ZnS Nanoparticles Prepared by New Route". *Mater. Sci. Lett.* **1999**, Vol. 2, p.115.
- [11] Khomane, R. B.; Manna, A.; Mandale, A. B.; Kulkarni, B. D. "Synthesis and Characterization of Dodecanethiol-Capped Cadmium Sulfide Nanoparticles in a Winsor II Microemulsion of Diethyl Ether/AOT/Water". *Langmuir*. **2002**, Vol. 18, p. 8237.

- [12] Kumar, A.; Jakhmola, A. "Photophysics and Charge Dynamics of Q-Pbs Based Mixed Zns/Pbs and Pbs/Zns Semiconductor Nanoparticles". *J. Colloid. Interf. Sci.* **2006**, Vol. 297, p. 607.
- [13] Zhu, J.; Zhu, Y.; Ma, M.; Yang, L.; Gao, L. "Simultaneous and Rapid Microwave Synthesis of Polyacrylamide–Metal Sulfide (Ag₂S, Cu₂S, HgS) Nanocomposites". *J. Phys. chem. C.* **2007**, Vol. 111, issue 10, p. 3920.
- [14] Kienle, L.; Duppel, V.; Schlecht, S. "Micro- And Nanostructure Of (Sn_{1-X}gex)S Mixed Crystals". *Soild State Sci.* **2004**, Vol. 6, p.179.
- [15] Chin, P. P.; Ding, J.; Yi, J. B.; Liu, B. H. "Synthesis of FeS₂ and FeS Nanoparticles by High-Energy Mechanical Milling and Mechanochemical Processing" *J. Alloy. Compd.* **2005**, Vol. 390, p. 255.
- [16] Bezverkhyy, I.; Afanasiev, P.; Marhic, C.; Danot, M. "Template free solution synthesis of sulfur microtubules". *Chem. Mater.* **2003**, Vol. 15, p. 2119.
- [17] Jia, C.; Liu, W.; Jin, C.; Zhang, B.; Yao, L.; Cai, W.; Li, X.; "A New Approach to Fabricate Sulfur Nanotubes". *Chem. Letters.* **2004**, Vol. 33, issue 5, p. 634.
- [18] Guo, Y. M.; Deng, Y. H.; Zhao, J. Z.; Wang, Z. C.; Zhang, H. B., "Synthesis and Characterization of Sulfur Nanoparticles by Liquid Phase Precipitation Method". *Acta Chimica Sinica*, **2005**, Vol 63, issue 4, p. 337.
- [19] Paul, B. K.; Moulik, S. P. "Uses and Applications of Microemulsions" *Current Sci.* **2001**, Vol. 80, p. 990.
- [20] Eriksson, S.; Nylen, U.; Rojas, S.; Moutonnet, M. "Preparation of Catalysts from Microemulsions and their Applications in Heterogeneous Catalysis". *Appl. Catal. A-Gen.* **2004**, Vol. 265, p.207.
- [21] Guo, Y.; Zhao, J.; Yang, S.; Yu, K.; Wang, Z.; Zhang, H. "Preparation and Characterization of Monoclinic Sulfur Nanoparticles by Water-In-Oil Microemulsions Technique". *Powder Technolo.* **2006**, Vol. 162, p. 83.
- [22] Jhon, S. E. "Recovery of Sulfur from Sour Acid Gas: A Review of the Technology". *Environ. Prog.* **2002**, Vol. 21, issue 3, p. 143.
- [23] Gaa, D.; Lagas, J. "Sulfur Recovery Solutions Global Trends". *Chem.Eng. World.* **2004**, Vol. 39, p. 43.

- [24] Dalrymple, D. A.; Trofe, T.W. “An Overview of Liquid Redox Sulfur Recovery”. *Chem. Eng. Prog.* **1989**, Vol. 85, p. 43.
- [25] Asai, S.; Konishi, Y.; Yabu, T. “Kinetics of Absorption of Hydrogen Sulfide into Aqueous Ferric Sulfate Solutions”. *AIChE J.* **1990**, Vol. 36, p. 1331.
- [26] C. Pagella, D. M. De Faveri, “H₂S Gas Treatment by Iron Bioprocess”. *Chem. Eng. Sci.* **2000**, Vol. 55, p. 2185.
- [27] A. B. Jensen, C. Webb, Enzyme. “Review- Treatment of H₂S containing gases: A review of microbiological alternatives”. *Microb. Technol.* **1995**, Vol. 17, p. 2.
- [28] Nagal, G. “Controlling H₂S Emissions”. *Chem Eng.* **1997**, Vol. 104, p. 125.
- [29] Demmink, J. F.; Wubs, H. J.; Beenackers, A. A. C. M. “Oxidative Absorption of Hydrogen Sulfide by a Solution of Ferric Nitrilotriacetic Acid Complex in a Cocurrent Down Flow Column Packed with SMV-4 Static Mixers”. *Ind. Eng. Chem. Res.* **1994**, Vol. 33, p. 2989.
- [30] Pandey, R. A.; Malhotra, S. “Desulphurization of Gaseous Fuels with Recovery of Elemental Sulphur: an overview”. *Crit. Rev. Env. Sci. Tec.* **1999**, Vol. 29, p. 229.
- [31] Karel, V. “*Handbook of Environmental Data on organic chemicals*”. 3rd ed.; VanNostrand Reinhold an international Thomson Publishing company: New York, **1996**.
- [32] Deshpande, A.S.; Sankpal, N. V.; Kulkarni, B. D. Indian Patent application number 1366/DEL/2003.
- [33] Joint Commission on Powder Diffraction Standards. Powder diffraction file, Inorganic phase. International center for diffraction data. PA, USA. JCPDS No. – 08247, p.410.
- [34] Strauss, H. L.; Greenhouse, J.A. “*Elemental sulfur Chemistry and physics*”. Meyer, B. Interscience Publishers, New York, **1965**, p. 241-250.
- [35] Prabhane, R.V.; Tambe, S.S.; Kulkarni, B. D. “ANN Modeling of DNA Sequences: New Strategies using DNA Shape Code”. *Computers and Chemistry.* **2000**, Vol. 24, issue 6, p. 699.
- [36] Mason, R. L.; Gunst, R. F.; Hess, J. L. “*Statistical design and analysis of experiments*”. 2nd ed. New York, **2003**.

||shri||

CHAPTER-4

NOVEL BIODEGRADABLE IRON CHELATE CATALYST FOR H₂S ABATEMENT: MODELING AND OPTIMIZATION OF BATCH REACTOR PROCESS USING ARTIFICIAL INTELLIGENCE STRATEGIES

Abstract

This study describes a new batch reactor process for the abatement of a common pollutant namely H₂S, to elemental sulfur using biodegradable Fe³⁺-malic acid (Fe³⁺-MA) chelate catalyst. The Fe³⁺-MA exhibits maximum sulfur recovery (499 mg/g of iron chelate) and purity (<99%). Further, process modeling and optimization of process operating variables and parameters have been conducted using an artificial intelligence based hybrid strategy involving *artificial neural networks* (ANN) and *genetic algorithms* (GA). Prior to the modeling, those process variables and parameters which significantly influence H₂S conversion were determined using *Plackett-Burman* (PB) design method. The ANN-GA hybrid strategy first utilizes an ANN to develop a process model predicting H₂S conversion and subsequently model's inputs are optimized using the GA formalism with a view to maximize H₂S conversion. The GA-optimized process conditions leading to a high ($\approx 97\%$) H₂S conversion was verified experimentally and the results obtained thereby show an excellent match with the GA maximized conversion.

Key words: H₂S abatement; Biodegradable iron chelates; Mechanically agitated batch reactor; Plackett-Burman design; Artificial neural networks - Genetic algorithm; Response surface method –Central composite design

1. Introduction

Hydrogen sulfide (H₂S) is a highly toxic and an undesirable gaseous component of natural gas and other waste gaseous streams. Catalytic conversion of H₂S to elemental sulfur can be achieved by various chemical¹⁻³ and biological^{4,5} methods. Liquid redox sulfur recovery⁶⁻⁹ processes absorb H₂S from gaseous streams and convert it to elemental sulfur.¹⁰⁻¹⁹ The use of biodegradable iron chelates²⁰ for catalytic conversion of H₂S was introduced earlier in this work. Among various chelates screened, the Fe³⁺-MA chelate exhibits maximum sulfur recovery and purity. The detail synthesis and characterization of biodegradable Fe³⁺-MA chelate system is discussed in Chapter 2. In this work the mechanically agitated batch reactor (MABR) using Fe³⁺-MA chelate as a catalyst for H₂S to elemental conversion is studied extensively.

To achieve maximum catalytic conversion of H₂S, it is necessary to design an optimal process operating strategy for the MABR. The commonly used optimization method, 'single factor at a time', does not account for the combined effect of all the influential factors since other factors are maintained arbitrarily constant. Moreover, this method is time consuming and requires a large number of experiments to determine the optimum levels of operating process variables and parameters. The limitations of the single factor optimization method can be overcome by developing a non-linear multivariate process model (since the process behavior is nonlinear) and employing it further for process optimization.

In the last two decades, an artificial intelligence paradigm viz., *artificial neural network* (ANNs) has emerged as an attractive tool for developing non-linear empirical models especially when the development of phenomenological or conventional empirical models either becomes impractical or cumbersome. The most

widely employed ANN paradigm is the *multi-layered perceptron* (MLP), which approximates non-linear relationships existing between multiple “causal (*input*)” process operating variables and parameters and the corresponding “dependent (*response/output*)” variables.²¹ Once an ANN-based process model with good generalization performance is constructed, its input space representing process operating variables and parameters can be optimized with a view to improve the process performance. The ANN models being exclusively data-driven, they cannot be guaranteed to be smooth in regions of sparse data. Hence, the standard gradient-based optimization methods, which require the objective function (being maximized/minimized) to be smooth, cannot be employed efficiently for optimizing the input space of an ANN model. Thus, it becomes essential to explore alternative non-linear optimization formalisms for optimizing inputs of an ANN model.

In recent years, *genetic algorithms* (GAs),^{22,23} which are artificial intelligence-based stochastic non-linear optimization formalisms, have been used with a great success in solving problems involving very large search spaces.^{24,25} The GAs are based on the principles of “survival-of-the-fittest” and “random exchange of memory during genetic propagation”, followed by biologically evolving species. The principal features, advantages and procedural details of GAs are described by, for instance, Lucasius et al.^{26,27} and Cheema et al.²⁸ Major advantages of GAs are: (i) they can work with objective functions that are not smooth, differentiable and continuous, and (ii) since they perform a global search of the solution space, GAs invariably arrive at the globally or near-globally optimal solution. These advantages make the GAs an ideal technique to solve diverse optimization problems in chemical engineering and technology including optimization of inputs of ANN-based process models.^{21,29,30}

Besides presenting a new process using Fe³⁺-MA biodegradable iron chelate catalyst for the H₂S abatement, the present study also aims at obtaining optimal process operating conditions for the maximum H₂S conversion. The stated task has been successfully completed using two different approaches. The first method was supported by three steps: (i) Plackett-Burman (PB) method has been used to select the most influential process operating variables and parameters, (ii) an ANN-based process model has been developed using the influential process variables and parameters as model inputs and H₂S conversion (%) as the model output and (iii) the input space of the ANN model is optimized using the GA formalism with a view of maximizing H₂S conversion to elemental sulfur.

The second approach for process optimization was carried out using Plackett-Burman design matrix for the same purpose as stated in approach one and Response Surface Method (RSM) [Centre Composite Design (CCD)] for optimization of the process for maximum H₂S abatement.

2. Materials

2.1 Chemicals

All chemicals were of analytical grade and used without further purification. Ferric chloride, ferric sulfate, ferric nitrate, gluconic acid, malic acid, citric acid and sodium hydroxide pellets were purchased from Merck India. All solutions were prepared in deionized Milli-Q water (H₂O with 18.2 Milli-Q cm resistivity, Millipore Corporation). Three H₂S cylinders: (i) 99.6% pure, (ii) 5000 ppm H₂S balanced by N₂ and (iii) 50000 ppm H₂S balanced by N₂ were procured from Vadilal chemicals.

2.2 Instrumentation

Online acquisition of process data was carried out using Ni DAQPad-6015 data acquisition system purchased from National Instrument. The stirring speed of the

impeller was set using AC Variable Frequency Drive ACS350-01E-02A4-4 with ACS-CP-C, purchased from ABB. The reactor temperature was regulated using Eurotherm temperature controller. The pressure inside the reactor was measured using WIKA make pressure transducer model S-10. UV analysis of various iron (III) chelates was carried out on the double beam UV spectrophotometer of Chemito make model Spectroscan 2700.

2.3 Computational techniques

The Plackett-Burman design computations and Response Surface Method (Central Composite Design) were performed using the Design Expert 7.1 software. The ANN and GA, software developed in-house at National Chemical Laboratory, Pune (India) on VC⁺⁺ and JAVA platforms were used.

2.4 Screening of Iron chelate solution

Various iron (III) salts were used as the iron source and the chelate complexes were synthesized using different carboxylic acids as chelating agents in various molar ratios at different pH ranges (see Table 2.2 from Chapter 2). The detail description of iron chelate synthesis and screening for capacity of H₂S removal and sulfur recovery is discussed in Chapter 2, Section 2.3 and 2.4. The result of screening of iron chelates exhibit the Fe³⁺-MA chelate complex gives maximum recovery of sulfur (499 mg/g of iron chelate) along with high purity (>99%) and reasonable reaction time as compared to other chelates. Hence, Fe³⁺-MA chelate complex was selected for the further detailed study involving ANN-based process modeling and GA-based process optimization.

3. Experimental

3.1 General method of sulfur recovery from H₂S gas

Figure 4.1 shows a schematic diagram of MABR used in the catalytic conversion of H₂S to elemental sulfur. The MABR was pressurized with H₂S gas wherein Fe³⁺-MA chelate solution oxidized the H₂S gas to elemental sulfur and simultaneously active ferric chelate was reduced to inactive ferrous chelate (Reaction 2). The MABR has liquid volume of 1.25 lit and is made of SS (10.21 cm ID and 28.30 cm height) with mechanically agitated disc impeller; the six bladed disc impeller (5.2 cm dia.) was located centrally in the liquid at an height of 3 cm above the reactor bottom. The second disc impeller of same size was located 5.20 cm above the liquid level in the gas phase volume. H₂S + N₂ gas mixture was added via a pre-mixer to reach the inlet H₂S concentrations varying between 5000 and 50000 ppm. The pressure and temperature transducers were connected to the reactor, enabling online and automatic data acquisition of the reactor performance. The real photographs 4.2 to 4.4 shows H₂S gas cylinders along with gas reservoir, mechanically agitated batch reactor, and online data acquisition system used for H₂S abatement.

The Iron (III) chelates were synthesized by dissolving a pre-calculated amount of iron salt (1 mol) into deionized water wherein chelating agents were added to the iron salt solutions in the molar ratio of 1:3. The solution was stirred for two hours at room temperature and the pH of the resulting solution was 2. Next, pH of the solution was adjusted in the range 7-7.5 by drop-wise addition of 5N NaOH solution.

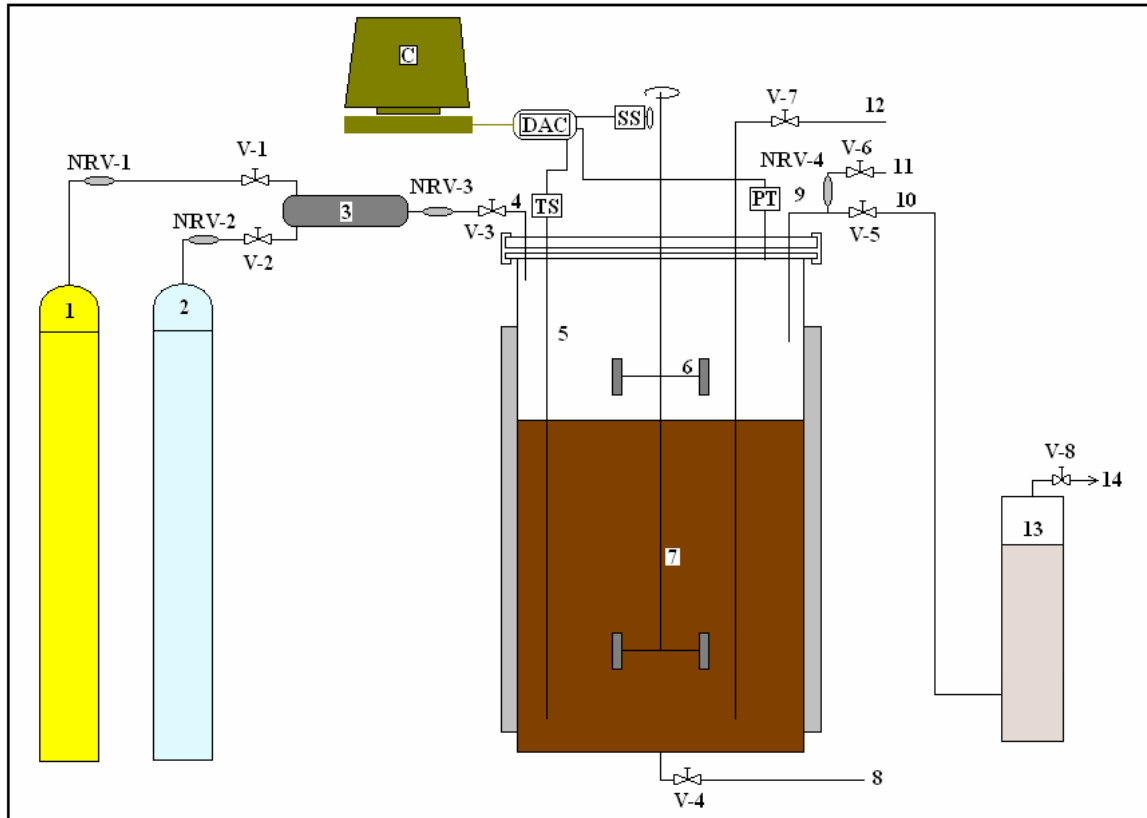


Figure 4.1. Simplified process flow diagram for catalytic conversion of H_2S to elemental sulfur. (1: H_2S cylinder; 2: N_2 cylinder; 3:pre-mixer; 4: gas inlet; 5: absorber; 6: double blade disc impeller; 7: iron chelate solution; 8: liquid outlet; 9: gas outlet; 10: gas outlet to NaOH scrubber; 11: gases sample port; 12: liquid sample port; 13: NaOH scrubber; 14: sweet gas outlet; V1-V8: valves; NRV 1-4: non-return valves; PT: pressure transducer; TS: temperature sensor; SS: stirring speed sensor; DAC: data acquisition card; C; Computer)



Figure 4.2 H_2S gas cylinders along with gas reservoir



Figure 4.3 Mechanically agitated batch reactor



Figure 4.4 Online data acquisition system used for H_2S abatement

During experimentation, inlet and outlet H₂S concentrations were measured by withdrawing gas samples (inlet: $V_G = 10 \text{ cm}^3$; outlet: $V_G = 20 \text{ cm}^3$) from sampling ports with a 25-cm long gas-tight syringe (see Figure 4.1). Each sample was then infused into a 25 cm³ rubber-cap vial containing 5 cm³ (V_B) buffer solution (pH = 10.00 ± 0.05) comprising potassium chloride, boric acid and sodium hydroxide. As a result, H₂S would immediately disperse into the buffer solution to form hydrosulfide ions (HS⁻). A UV spectrophotometer was used to estimate the HS⁻ concentration in the 5 cm³ buffer solution.¹⁷

Initially, degassed Fe³⁺-MA chelate solution was filled in the reactor. Next, in the evacuated reactor the mixture of H₂S and N₂ of desired concentration was pressurized and stirring of the impeller was started following which H₂S conversion to elemental sulfur begins. As this reaction progresses, the reactor pressure decreases. The reaction was stopped when pressure reached a constant value, which indicates maximum reactive absorption of H₂S into Fe³⁺-MA chelate solution. The initial and final gas and liquid samples were analyzed to measure the H₂S gas and iron chelate concentrations. The gas and liquid samples were immediately analyzed using UV-Vis spectrophotometer to quantify Fe³⁺-MA²⁻, Fe²⁺-MA²⁻ and HS⁻ contents. The Fe³⁺-MA²⁻ concentration was measured in the 300-350 nm band wherein HS⁻ exhibits zero absorbance. In this region, Fe²⁺-MA²⁻ absorptivity remains negligible compared to Fe³⁺MA²⁻, Fe²⁺MA²⁻ concentration was estimated by subtracting the final Fe³⁺MA²⁻ concentration from the initial one.

4. Part-I Process modeling and optimization using PB-ANN-GA hybrid Model

4.1 Plackett-Burman design

A number of process operating variables and parameters are known to influence the performance of an MABR. To ascertain these influences we scrutinized the effects of a number of variables and parameters on the catalytic oxidative absorption of H_2S in the MABR. The variables and parameters considered for scrutiny were: (i) initial Fe^{3+} -MA concentration ($C_{Fe,0}$), (ii) H_2S gas concentration in ppm ($C_{H_2S,0}$), (iii) reactor pressure (P), (iv) reactor temperature (T), (v) stirring speed of impeller (S) and (vi) reaction time (t). Other variables which are expected to influence H_2S abatement but were set constant throughout the investigation and thus excluded from the scrutiny were: pH of Fe^{3+} -MA chelate, reactor dimensions, reactor volume, liquid volume, gas volume, impeller dimensions and its position.

A fractional two-level factorial design approach featuring all six fixed-effect factors was implemented to evaluate their linear, quadratic and interaction effects on the average H_2S conversion (%) response. Initially, for screening of insignificant process variables and parameters a duplicated Plackett–Burman design matrix of eight experiments relevant to the determination of six *linearized* direct effects was implemented. In this PB design matrix, each process operating variable and parameter represents two levels, i.e. “upper” and “lower”. This gives the range covered by each variable and parameter. The ranges of process operating variables and parameters are as follows : (i) Fe^{3+} -MA concentration ($C_{Fe,0}$) : 1000-5000 ppm, (ii) H_2S gas concentration ($C_{H_2S,0}$) in the gas mixture ($N_2 + H_2S$) : 5000-50000 ppm, (iii) reactor initial gas pressure : 1-5 bar, (iv) reactor initial temperature : 25-85 °C, (v) stirring speed of impeller : 100-500 rpm and (vi) reaction time : 15-60 min. In addition to

these, the PB design matrix considers a dummy variable to introduce some redundancy required by the statistical procedure; this dummy variable is not assigned any value.

4.2 ANN-based modeling

The MLP neural network used in process modeling consists of four layers. The layers described as *input*, *hidden-1*, *hidden-2* and *output* layers, comprised, K , L , M and N number of processing nodes (neurons), respectively. All the nodes in a network layer are connected to each node in the subsequent layer with weighted connections. There also exists an additional node, known as the *bias* (with its output fixed at +1) in the input and hidden layers of an MLP network. The bias nodes do not have input connections and are linked using weighted connections only to the nodes in the subsequent layer.

The MLP network is a nonlinear function mapping device that determines the K -dimensional nonlinear function vector, \mathbf{f} , where $\mathbf{f}: X \rightarrow Y$. Here, X is a set of P number of K -dimensional input vectors ($X = \{\mathbf{x}_p\}$, $p = 1, 2, \dots, P$, where $\mathbf{x} = [x_1, x_2, \dots, x_k, \dots, x_K]^T$), and Y is the set of the corresponding N -dimensional output vectors ($Y = \{\mathbf{y}_p\}$; $p = 1, 2, \dots, P$), where $\mathbf{y} = [y_1, y_2, \dots, y_N]^T$. The combined set $\{X, Y\}$ is known as ‘example’ set containing P pairs of input vectors $\{\mathbf{x}_p\}$ and the corresponding output vectors $\{\mathbf{y}_p\}$. The precise form of \mathbf{f} is determined by: (i) network topology, (ii) choice of the activation function used for computing the outputs of the hidden and output nodes, and (iii) network weight matrices, W^{H1} , W^{H2} and W^O (these refer to the weights on the connections between input and hidden-1 layer nodes, hidden-1 and hidden-2 layers nodes and hidden-2 and output nodes, respectively). The nonlinear mapping executed by the MLP can be expressed as:

$$\mathbf{y} = \mathbf{f}(\mathbf{x}, W) \quad (5)$$

where, $W = \{W^{H1}, W^{H2}, W^O\}$. Given an example set, the weights of an MLP network model can be trained using an appropriate network training algorithm. The most widely used algorithm for MLP training is the *error-back-propagation* (EBP) algorithm.³¹ The details of training an optimal MLP model possessing good prediction and generalization abilities are described, for instance, in Bishop,³² Tambe et al.,³³ and Freeman et al.³⁴ The EBP training algorithm makes use of two adjustable parameters namely, the learning rate (η) ($0 < \eta \leq 1$), and momentum coefficient (α) ($0 < \alpha \leq 1$). The magnitudes of both these parameters are optimized heuristically along with the number of hidden layer neurons, L and M .

4.3 GA-Based Optimization of Inputs of ANN-Model

Having constructed an MLP-based process model, the GA method can be used to optimize model's input space (\mathbf{x}) representing process operating variables and parameters, with a view of maximizing the process performance, i.e. H₂S conversion (%). The underlying optimization objective is defined as: find the K -dimensional optimal decision variable vector, $\mathbf{x}^* = [x_1^*, x_2^*, \dots, x_k^*, \dots, x_K^*]^T$, such that it maximizes the objective function, $f(\mathbf{x}^*, W)$, representing H₂S conversion.

The GA-based search for an optimal solution (decision variable) vector, \mathbf{x}^* , begins with a randomly initialized population of probable (candidate) solutions. The solutions, coded in the form of binary or real-valued strings (*chromosomes*) are then evaluated to measure their fitness in fulfilling the optimization objective. Next, a main loop of following operations is executed: (i) selection of better (fitter) parent chromosomes to create a mating pool, (ii) crossover, i.e., the production of offspring solutions by crossing-over randomly the contents of individual parents of each parent pair in the mating pool and (iii) mutating randomly the elements of the offspring strings. An implementation of this loop produces a new population of candidate

solutions, which when compared with the current population, usually performs better at fulfilling the optimization objective. The best string that evolves after repeating the above-described loop till convergence forms the solution to the optimization problem.

5. Results and Discussion

5.1 Selection of influential process variables and parameters using Plackett–Burman design

Results for the duplicated Plackett–Burman design matrix are given in Table 4.1. A total of seven variables comprising six process variables and parameters and one dummy variable, were screened in eight duplicated experiments. These experiments were performed at different combinations of the high and low values of each variable.

The statistical calculations of the PB design matrix along with the corresponding variable-specific F-scores are given in Table 4.2. From the magnitudes of the F-score it is seen that there exist four dominating factors ($F > 1.0$), namely H₂S gas concentration ($C_{H_2S,0}$), reactor pressure (P), reactor temperature (T), stirring speed of impeller (S) and two less significant factors ($F < 1.0$) namely Fe³⁺-MA concentration ($C_{Fe,0}$) and reaction time (t). Among the less significant factors, Fe³⁺-MA concentration has lowest influence on the H₂S conversion. Accordingly, five variables and parameters barring the least significant Fe³⁺-MA chelate concentration were considered for the ANN based modeling.

Table 4.1 Experiments for Plackett-Burman design

Run No.	Process variables and parameters						Experimental H ₂ S Conversion (%)
	Fe ³⁺ Conc. (ppm)	H ₂ S Conc. (ppm)	Pressure (bar)	Temp (°C)	Stirring Speed (rpm)	Time (min)	
1	5000	50000	5.0217	25	500	15	87.22
2	5000	50000	5.08755	25	500	15	86.86
3	1000	50000	5.06055	85	100	60	82.30
4	1000	50000	5.1057	85	100	60	80.84
5	1000	5000	5.05185	85	500	15	82.81
6	1000	5000	5.04945	85	500	15	80.73
7	5000	5000	1.09605	85	500	60	54.56
8	5000	5000	1.0100	85	500	60	55.00
9	1000	50000	1.13445	25	500	60	87.51
10	1000	50000	1.08585	25	500	60	81.55
11	5000	5000	5.2053	25	100	60	49.47
12	5000	5000	5.0010	25	100	60	48.98
13	5000	50000	1.2135	85	100	15	58.07
14	5000	50000	1.10145	85	100	15	54.89
15	1000	5000	1.0506	25	100	15	2.96
16	1000	5000	1.05495	25	100	15	3.45

Table 4.2 Statistical calculations for PB design

Quantity	Fe ³⁺ Conc. (ppm)	H ₂ S Conc. (ppm)	Pressure (bar)	Temp (°C)	stirring speed (rpm)	Reaction time (min)	Dummy
y _{i+}	247.546	309.642	299.627	274.613	308.1429	270.1261	272.029
y _{i-}	251.097	189.002	199.017	224.031	190.5015	228.5183	226.615
Σ y _{i+} - y _{i-}	-3.5509	120.640	100.610	50.5825	117.6415	41.6079	45.4135
MSD	1.5761	1819.25	1265.30	319.823	1729.9391	216.4021	257.798
F _(Score)	0.00611	7.0569	4.9081	1.2406	6.7104	0.8394	1.0000

5.2 ANN-Based MABR Modeling

The MLP network architecture considered in modeling of the H₂S abatement process has five input nodes ($K = 5$) representing as many significant process operating variables [H₂S concentration (x_1), reactor pressure (x_2), reactor temperature (x_3), stirring speed of the impeller (x_4) and reaction time (x_5)] and one output node ($N = 1$) representing H₂S conversion (%) at the end of a batch run. Process data for the MLP-based modeling were generated by carrying out a number of H₂S abatement runs by systematically varying reactor operating conditions. Specifically, a total of 57 experiments were conducted and the corresponding data are tabulated in Table 4.3. The data corresponding to the stated 57 experiments were combined with the data from, 16 PB design experiments (Table 4.2) and the resultant set formed the example data set for the training of the MLP-based reactor model. Each of the 73 experimental data patterns comprised an input-output pair, where an input represents a 5-dimensional vector of process variables and parameters (x_1 - x_5) and output represents H₂S conversion (%). Each input-output variable in the example set was normalized to lie between 0.05 and 0.95.

Table 4.3 H₂S abatement reaction data used in ANN modeling

Run No.	H ₂ S Conc. (ppm)	Reactor pressure (bar)	Reactor temp. (°C)	Stirring Speed (rpm)	Fe ³⁺ Conc. (ppm)	Reaction Time (min)	H ₂ S conversion (%)
1	16212.87	2.09	40.71	200	5000	15	87.31
2	16212.87	2.12	40.11	200	5000	15	88.27
3	38727.27	2.06	39.94	200	5000	15	90.46
4	38727.27	2.03	40.01	200	5000	15	90.20
5	16212.87	4.07	40.25	200	5000	15	90.21
6	16212.87	4.01	40.23	200	5000	15	91.03
7	16212.87	2.10	69.20	200	5000	15	74.53
8	16212.87	2.07	69.26	200	5000	15	72.77
9	38727.27	2.11	69.35	200	5000	15	85.71
10	38727.27	2.08	69.32	200	5000	15	85.16
11	16212.87	4.10	69.96	200	5000	15	75.32
12	16212.87	4.16	69.77	200	5000	15	75.12
13	38727.27	4.05	69.37	200	5000	15	90.38
14	38727.27	4.00	69.45	200	5000	15	90.79

Table 4.3 continued.....

15	16296.30	2.12	39.57	400	5000	15	83.46
16	16296.30	2.15	39.52	400	5000	15	84.35
17	38740.46	2.05	39.17	400	5000	15	80.65
18	38740.46	2.03	39.12	400	5000	15	80.83
19	16296.30	4.32	40.46	400	5000	15	76.20
20	16296.30	4.26	40.47	400	5000	15	75.54
21	38745.39	4.05	39.63	400	5000	15	82.36
22	38745.39	4.00	39.65	400	5000	15	84.35
23	16296.30	2.08	69.38	400	5000	15	82.64
24	16296.30	2.05	69.33	400	5000	15	84.05
25	38740.46	2.10	69.48	400	5000	15	82.55
26	38740.46	2.07	69.52	400	5000	15	83.32
27	16296.30	4.36	69.74	400	5000	15	74.36
28	16296.30	4.30	69.82	400	5000	15	74.02
29	38740.46	4.14	70.16	400	5000	15	85.82
30	38740.46	4.09	70.10	400	5000	15	86.13
31	5000.00	3.08	54.66	300	5000	15	72.98
32	5000.00	3.04	54.60	300	5000	15	74.30

Table 4.3 continued.....

33	50000.00	3.03	54.94	300	5000	15	80.27
34	50000.00	3.00	55.07	300	5000	15	82.00
35	27772.00	1.03	54.86	300	5000	15	82.20
36	27772.00	1.02	54.96	300	5000	15	83.15
37	27428.57	5.19	55.17	300	5000	15	89.46
38	27428.57	5.12	55.11	300	5000	15	89.20
39	27500.00	3.02	30.17	300	5000	15	90.97
40	27500.00	2.98	30.11	300	5000	15	90.41
41	27428.57	3.09	85.17	300	5000	15	80.39
42	27428.57	3.05	85.22	300	5000	15	80.67
43	27428.57	3.03	54.73	100	5000	15	91.50
44	27428.57	3.08	54.83	500	5000	15	72.03
45	27428.57	3.04	55.17	500	5000	15	73.28
46	27428.57	3.05	54.71	300	5000	15	82.74
47	27428.57	3.01	54.75	300	5000	15	82.35
48	27428.57	3.08	55.15	300	5000	15	82.66
49	27428.57	3.17	55.38	300	5000	15	82.62
50	27428.57	3.05	54.71	300	5000	15	82.74

Table 4.3 continued.....

51	27428.57	3.01	54.75	300	5000	15	82.35
52	27428.57	3.05	54.71	300	5000	15	82.74
53	27428.57	3.01	54.75	300	5000	15	82.35
54	27428.57	3.08	55.15	300	5000	15	82.66
55	27428.57	3.17	55.38	300	5000	15	82.62
56	27428.57	3.10	55.08	300	5000	15	82.44
57	27428.57	3.06	55.87	300	5000	15	82.52

Ideally, an ANN model in addition to possessing good output prediction accuracy should also possess good generalization performance. The generalization ability refers to how accurately the model is capable of predicting outputs of a new set of inputs, which are not included in the ‘example’ set. To ensure that the ANN model is capable of generalization, the example input-output set was partitioned randomly into a *training* set (60 patterns) and a *test* set (13 patterns). While the training set was utilized for adjusting the weights (W) of the MLP model during its training, the test set was used for gauging the network’s generalization performance after each training iteration. The weights resulting in the least test set RMSE (root mean squared error) magnitude were chosen as the optimum weights. In the MLP training procedure, the logistic sigmoid activation function was used for computing outputs of the hidden and output layer nodes. While developing an optimal MLP model, the effect of varying number of hidden layer nodes and the EBP-algorithm specific parameters (learning rate, η , and momentum coefficient, α) on the training and test set RMSEs was studied rigorously. It was observed that an MLP architecture with three nodes each in hidden-1 and hidden-2 layers resulted in the least value for the test set RMSE (i.e., $E_{tst} = 0.424$). The values of η and α , which resulted in the minimum E_{tst} were 0.2 and 0.05, respectively; the corresponding RMSE value for the training set (E_{trn}) was 0.486. The average error (%) between the desired and model predicted H_2S conversion (%) for the training and test set data were 0.460 and 0.458, respectively; the values of the coefficient of correlation (CC) between the model-predicted and desired (experimental) H_2S conversion (%) pertaining to the training set (C_{trn}) and the test set (C_{tst}) were 0.998 and 0.999, respectively. The small and comparable magnitudes of the RMSE and average prediction error (%), and the high and comparable values of

CC for both the training and test set outputs suggest that the MLP-based MABR process model possesses excellent prediction and generalization characteristics. A comparison of the MLP model predicted and the corresponding experimental values of the H₂S conversion (%) is depicted in Figure 4.5.

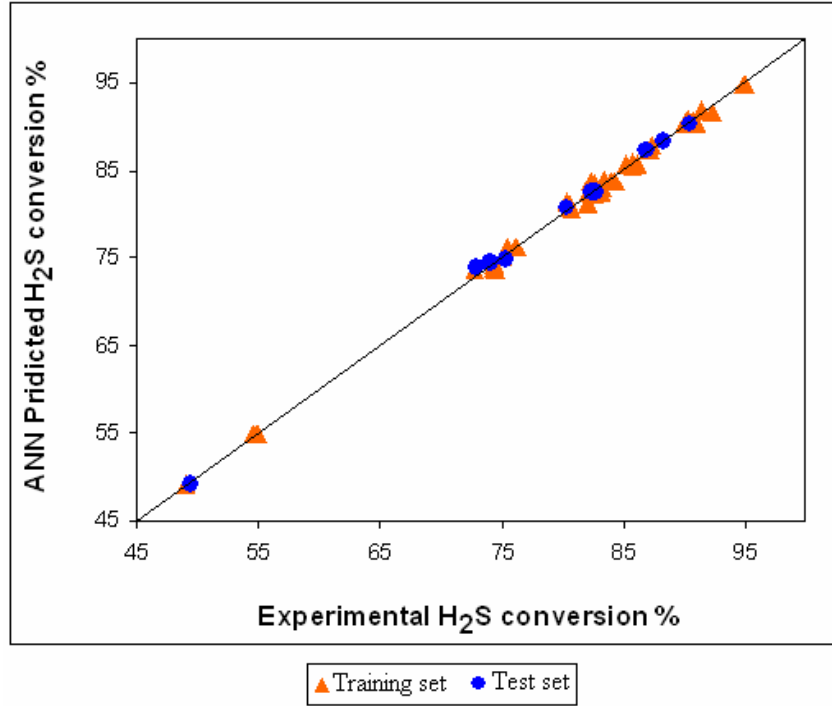


Figure 4.5 Parity plot of model-predicted and experimental H₂S conversion

5.3 GA-based Optimization of the MLP Model

The objective of the GA-based process optimization was to obtain the optimal values (\mathbf{x}^*) of the significant process operating variables and parameters in a manner such that the H₂S conversion (%) is maximized. This single objective optimization problem can be defined as given below in terms of an objective function comprising the MLP model that represents the nonlinear relationship between the five process variables and parameters, and the corresponding H₂S conversion (%):

$$\text{Maximize } y = f(\mathbf{x}, W) ; \quad x_k^L \leq x_k \leq x_k^U, \quad k = 1, 2, \dots, K \quad (6)$$

Where, f represents the objective function (MLP model); y refers to the H₂S conversion; the K -dimensional decision vector, \mathbf{x} , denotes the MABR operating variables and parameters to be optimized ($K= 5$) and x_k^L and x_k^U respectively represent the lower and upper bounds on x_k .

In the current study, a real coded GA was used for the estimation of optimal decision variable vector \mathbf{x}^* . A positive feature of the real-coding strategy is that it allows continuous values of the decision variables to be optimized. This is in contrast to the binary coding that allows only discrete-valued decision variables. The values of the GA-specific parameters used in the H₂S conversion maximization simulations were: l_{chr} (chromosome length) = 5, N_{pop} (population size) = 50, p_{cr} (crossover probability) = 0.95, p_{mut} (mutation probability) = 0.05, and N_g^{max} (maximum number of generations over which GA evolved) = 500. The procedure for computing the fitness score of a candidate solution in a population involves: (i) application of the five dimensional solution vector to the MLP model and computing the corresponding model output (H₂S conversion), and (ii) evaluation of the fitness by following equation,

$$\varepsilon_j = \hat{y}_{pred}^j ; j = 1, 2, \dots, N_{pop} \quad (7)$$

where ε_j denotes the fitness score of the j^{th} candidate solution vector and \hat{y}_{pred}^j refers to the MLP model predicted H₂S conversion (%) when j^{th} solution is used as the model input. During GA-implementation, the search for an optimal solution was restricted to the following ranges of the five influential process operating variables and parameters: (i) H₂S concentration (ppm) (x_1): [5000, 50000], (ii) reactor pressure (bar) (x_2): [1, 5], (iii) reactor temperature (°C) (x_3): [25, 85], (iv) stirring speed of impeller (rpm) (x_4): [100, 500] and (v) reaction time (min) (x_5): [15, 60].

In the case of a non-linear objective function, it is possible that the optimization algorithm obtains a locally optimal solution instead of the globally optimal one. Thus, for an objective function maximization problem (as in the present study), a thorough exploration of the solution space was necessary to secure a solution that corresponds to the tallest local or the global maximum. Accordingly, the GA-based optimization simulations were repeated by using each time a different randomly initialized population of candidate solutions. Dissimilar initial populations ensure that each time the GA begins its search for an optimal solution from a different search sub-space, which helps in locating the tallest local or the global maximum on the objective function surface. Accordingly, the two best solutions (GA-1 and GA-2) obtained after conducting numerous (≈ 20) GA-trials are given in Table 4.4

Table 4.4 GA-optimized solutions and their experimental validation

Run		H ₂ S Conc. (ppm)	Pressure (bar)	Temp (°C)	Stirring Speed (rpm)	Fe ⁺³ Conc. (ppm)	Reaction Time (min)	H ₂ S conversion (%)
GA optimized solution -1	GA-1	33300.8	3.95	22.81	103.82	5000	19.22	97.46
Validation Experiment-1	GA-1	33267.71	4.07	22.80	104.00	5000	19.00	97.13
GA optimized solution -2	GA-2	19414.9	1.90	21.65	77.78	5000	12.54	97.26
Validation Experiment -2	GA-2	19465.64	1.94	22.00	80.00	5000	13.00	95.84

It can be observed from the Table 5 that the GA has converged to dissimilar optimal solutions albeit leading to closely matching maximized values (97.26% and 97.46%) of H₂S conversion. Next, the best solution provided by the GA (i.e. GA-1) was verified experimentally by carrying out an H₂S abatement run using the respective optimum reactor conditions (see Table 4.4). The H₂S conversion (%) value obtained in this experiment was 97.13%, which is in close agreement with the GA-

optimized H₂S conversion of 97.46%. The 2nd best solution given by the GA (GA-2) was also verified similarly and as can be seen in Table 4.5, the results corresponding to this experiment also matched with the GA-optimized solution leading to 95.84% H₂S conversion. It is thus seen that application of the ANN-GA hybrid modeling-optimization strategy has resulted in 5.63% improvement over the best H₂S conversion of 91.5% (see experiment 43 in Table 4.4), obtained in non-optimized experiments.

6. Part-II Process modeling and optimization using PB-RSM

6.1 Plackett-Burman design

A fractional two-level factorial design approach featuring all fixed-effect factors was implemented to evaluate their linear, quadratic and interaction effects on the average H₂S conversion (%) response. The Plackett-Burman design approach was carried out in the same way as discussed in the section 4.1 of Part-I.

6.2 Response Surface Method (Central Composite Design)

Response surface methodology (RSM) is a collection of mathematical and statistical techniques that are useful for modelling and analysis of problems in which output or response influenced by several variables and the goal is to find the correlation between the response and the variables³⁵⁻³⁷. It can be used for optimizing the response. It is an empirical modelization technique devoted to the evaluation of relations existing between a group of controlled experimental factors and the observed results of one or more selected criteria. A prior knowledge of the studied process is thus necessary to achieve a realistic model. According Plackett-Burman design which was analyzed in the Section 7.1, gives the detail information about the factors that are influencing H₂S conversion. The statistical calculations of the PB design matrix along with the corresponding variable-specific F-scores analyzed in Table 4.2; shows that

Fe³⁺-MA chelate concentration and reaction time (t) — having very less F_{score} value — are the non-influential factors on the H₂S conversion. Therefore, will be considered constant value for further runs. So, four variables and parameters barring the least significant were considered for the RSM based CCD. The CCD gives total 30 experimental runs for four variables and parameters (k = 4); namely H₂S gas concentration (C_{H₂S,0}), reactor pressure (P), reactor temperature (T), stirring speed of impeller (S). The number of experimental runs is distributed as follows,

$$\text{Total number of runs} = n_f + n_{of} + n_e + n_{0e} \quad (8)$$

Where, n_f: experiments in factorial design = 16

n_{of}: center points in factorial design = 4

n_e: experiments in star design = 8

n_{0e}: center points in star design = 2

Table 4.5. The coded values for the independent variables and parameters.

No.	Variables and Parameters	Coded values				
		-2	-1	0	1	2
1	H ₂ S conc. (ppm)	5000	16250	27500	38750	50000
2	Pressure (bar)	1	2	3	4	5
3	Temperature (°C)	25	40	55	70	85
4	Stirring Speed of impeller (rpm)	100	200	300	400	500

The operating ranges of the variables and parameters are same as considered for PB design.

The response variable was fitted by a second order model in order to correlate the response variable to the independent variables. The general form of the second degree polynomial equation is:

$$Y_i = \beta_o + \sum_{j=4}^4 \beta_j x_j + \sum_{i<j} \beta_{ij} x_i x_j + \sum_{j=4}^4 b_{jj} x_j^2 \quad (9)$$

Where Y_i is the predicted response, x_i, x_j are input variables which influence the response variable Y ; β_o is the offset term; β_i is the i th linear coefficient; β_{ii} the i th quadratic coefficient and β_{ij} is the ij^{th} interaction coefficient.

x_i is the dimensionless value of an independent variable defined as:

$$x_i = \frac{(x_i - x_o)}{\Delta x_i} \quad (10)$$

where x_i is the real value of an independent variable; x_o is the real value of an independent variable at the center point; Δx_i is the step change.

Analysis of variance (ANOVA) is the statistical analysis used to check the significance of the equation with the experimental data. This analysis included the Fisher's F -test (overall model significance), its associated probability $p(F)$, correlation coefficient R , determination coefficient R^2 which measures the goodness of fit of regression model. For each variable, the quadratic models were represented as contour plots (2D). The optimal combination was determined from contour plot.

7. Results and Discussion

7.1 Selection of influential process variables and parameters using Plackett–Burman design

Results for the duplicated Plackett–Burman design matrix are well discussed in Section 6.1 of Part-I. The statistical calculations of the PB design matrix along with the corresponding variable-specific F -scores are given in Table 4.2. From the magnitudes of the F -score it is seen that there exist four dominating factors ($F > 1.0$), namely H₂S gas concentration ($C_{H_2S,0}$), reactor pressure (P), reactor temperature (T), stirring speed of impeller (S) and two less significant factors ($F_{score} < 1.0$) namely Fe⁺³-MA concentration ($C_{Fe,0}$) ($F_{score} = 0.00611$) and reaction time (t) ($F_{score} = 0.8394$).

Accordingly, four variables and parameters barring the least significant Fe³⁺-MA chelate concentration and reaction time (t) were considered for the RSM based CCD.

7.2 Response Surface method (Central Composite Design) for process modeling and optimization

The 30 experiments were conducted in duplicate and the values of % H₂S conversion with design matrix were tabulated in Table 4.6.

Table 4.6 RSM based Central Composite design matrix of independent variables and parameters and their corresponding experimental and predicted % H₂S conversion

Std. Run	H ₂ S Conc. (ppm)	Reactor pressure (bar)	Reactor Temp (°C)	Stirring speed (rpm)	Fe ⁺³ Conc. (ppm)	Reaction Time (min)	Experimental % H ₂ S conversion	Predicted % H ₂ S conversion
1	16212.87	2.09	40.71	200	5000	15	87.31	88.62
2	16212.87	2.12	40.11	200	5000	15	88.27	88.93
3	38727.27	2.06	39.94	200	5000	15	90.46	87.34
4	38727.27	2.03	40.01	200	5000	15	90.20	87.00
5	16212.87	4.07	40.25	200	5000	15	90.21	91.45
6	16212.87	4.01	40.23	200	5000	15	91.03	91.28
7	38750.00	4.08	39.92	200	5000	15	92.90	92.91
8	38750.00	4.02	39.90	200	5000	15	93.02	93.16
9	16212.87	2.10	69.20	200	5000	15	74.53	77.49
10	16212.87	2.07	69.26	200	5000	15	72.77	75.45
11	38727.27	2.11	69.35	200	5000	15	85.71	79.83
12	38727.27	2.08	69.32	200	5000	15	85.16	78.85
13	16212.87	4.10	69.96	200	5000	15	75.32	80.27
14	16212.87	4.16	69.77	200	5000	15	75.12	80.14
15	38727.27	4.05	69.37	200	5000	15	90.38	89.34
16	38727.27	4.00	69.45	200	5000	15	90.79	90.00
17	16296.30	2.12	39.57	400	5000	15	83.46	82.16
18	16296.30	2.15	39.52	400	5000	15	84.35	82.35
19	38740.46	2.05	39.17	400	5000	15	80.65	79.51
20	38740.46	2.03	39.12	400	5000	15	80.83	80.00
21	16296.30	4.32	40.46	400	5000	15	76.20	78.27
22	16296.30	4.26	40.47	400	5000	15	75.54	77.50
23	38745.39	4.05	39.63	400	5000	15	82.36	82.36

Table 4.6 continued.....

24	38745.39	4.00	39.65	400	5000	15	84.35	84.35
25	16296.30	2.08	69.38	400	5000	15	82.64	78.16
26	16296.30	2.05	69.33	400	5000	15	84.05	79.90
27	38740.46	2.10	69.48	400	5000	15	82.55	79.13
28	38740.46	2.07	69.52	400	5000	15	83.32	80.23
29	16296.30	4.36	69.74	400	5000	15	74.36	74.21
30	16296.30	4.30	69.82	400	5000	15	74.02	74.10
31	38740.46	4.14	70.16	400	5000	15	85.82	81.92
32	38740.46	4.09	70.10	400	5000	15	86.13	82.00
33	5000.00	3.08	54.66	300	5000	15	72.98	76.00
34	5000.00	3.04	54.60	300	5000	15	74.30	77.35
35	50000.00	3.03	54.94	300	5000	15	80.27	82.41
36	50000.00	3.00	55.07	300	5000	15	82.00	83.24
37	27772.00	1.03	54.86	300	5000	15	82.20	81.23
38	27772.00	1.02	54.96	300	5000	15	83.15	82.34
39	27428.57	5.19	55.17	300	5000	15	89.46	86.85
40	27428.57	5.12	55.11	300	5000	15	89.20	86.19
41	27500.00	3.02	30.17	300	5000	15	90.97	94.13
42	27500.00	2.98	30.11	300	5000	15	90.41	93.00
43	27428.57	3.09	85.17	300	5000	15	80.39	82.56
44	27428.57	3.05	85.22	300	5000	15	80.67	82.90
45	27428.57	3.03	54.73	100	5000	15	91.50	87.09
46	27428.57	2.99	54.74	100	5000	15	92.27	88.22
47	27428.57	3.08	54.83	500	5000	15	72.03	73.21
48	27428.57	3.04	55.17	500	5000	15	73.28	73.30
49	27428.57	3.05	54.71	300	5000	15	82.74	82.44
50	27428.57	3.01	54.75	300	5000	15	82.35	82.35

Table 4.6 continued.....

51	27428.57	3.08	55.15	300	5000	15	82.66	82.70
52	27428.57	3.17	55.38	300	5000	15	82.62	82.50
53	27428.57	3.05	54.71	300	5000	15	82.74	82.44
54	27428.57	3.01	54.75	300	5000	15	82.35	82.18
55	27428.57	3.05	54.71	300	5000	15	82.74	82.44
56	27428.57	3.01	54.75	300	5000	15	82.35	82.18
57	27428.57	3.08	55.15	300	5000	15	82.66	82.70
58	27428.57	3.17	55.38	300	5000	15	82.62	82.50
59	27428.57	3.10	55.08	300	5000	15	82.44	82.44
60	27428.57	3.06	55.87	300	5000	15	82.52	82.52

For analysis the data, the checking of goodness of fit of the model is very much required. The model adequacy checking includes the test for significance of the regression model, test for significance on model coefficients, and test for lack of fit. For this purpose, analysis of variance (ANOVA) is performed, shown in Table 4.7.

Table 4.7 Analysis of variance (ANOVA)

Source	Sum of squares	DF	Mean Squire	F-value	Prob > F
Model	927.04	14	66.22	11.53	< 0.0001 ^a
A	179.47	1	179.47	31.26	< .0001 ^a
B	10.76	1	10.76	1.87	0.1912 ^b
C	133.91	1	133.91	23.32	0.0002 ^a
D	242.63	1	242.63	42.26	< 0.0001 ^a
A ²	36.10	1	36.10	6.29	0.0242 ^a
B ²	26.63	1	26.63	4.64	0.0480 ^a
C ²	21.38	1	21.38	3.72	0.0728 ^b
D ²	0.11	1	0.11	0.019	0.8926 ^b
AB	49.53	1	49.53	8.63	0.0102 ^a
AC	46.21	1	46.21	8.05	0.0125 ^a
AD	20.68	1	20.68	3.60	0.0771 ^a
BC	0.12	1	0.12	0.022	0.8850 ^b
BD	41.31	1	41.31	7.20	0.0171 ^a
CD	106.14	1	106.14	18.49	0.0006 ^a
Residual	86.13	15	5.74		
Lack of Fit	86.08	10	8.61	882.86	< 0.0001 ^a
Pure Error	0.049	5	9.750E-003		
Cor Total	1013.17	29			

^a Significant at "Prob > F" less than 0.05;

^b Insignificant at "Prob > F" more than 0.05

The Model F-value of 11.53 implies the model is significant. There is only a 0.01% chance that a "Model F-Value" this large could occur due to noise. Values of

"Prob > F" less than 0.0500 indicate model terms are significant. In this case A, C, D, A², B², AB, AC, BD, CD are significant model terms. Values greater than 0.1000 indicate the model terms are not significant. If there are many insignificant model terms (not counting those required to support hierarchy), model reduction may improve model. The "Lack of Fit F-value" of 882.86 implies the Lack of Fit is significant. There is only a 0.01% chance that a "Lack of Fit F-value" this large could occur due to noise. Significant lack of fit is bad. The fit summary recommended that the quadratic model is statistically significant.

Regression analysis of the data gives second degree polynomial equation in terms of actual factors for the calculation of response i.e. % H₂S conversion:

$$\begin{aligned} \text{\% H}_2\text{S conversion} = & +82.50500 + 2.73458 * A + 0.66958 * B - 2.36208 * C - 3.17958 * \\ & D - 1.14719 * A^2 + 0.98531 * B^2 + 0.88281 * C^2 + 0.062812 * D^2 \\ & + 1.75938 * A * B + 1.69938 * A * C - 1.13687 * A * D - \\ & 0.088125 * B * C - 1.60687 * B * D + 2.57563 * C * D. \end{aligned} \quad (11)$$

Where, A: Initial H₂S Conc. (ppm); B: Reactor Pressure (bar); C: Temperature (°C); D: stirring Speed of impeller (rpm).

A low value of the coefficient of variation (2.88%) indicates the very high degree of precision and a good reliability of the experimental values. The fit of the model was also expressed by the coefficient of determination R², which was found to be 0.9150, indicating that 91.5% of the variability in the response could be explained by the model. The results obtained from the experiments are compared with the predicted value calculated from the model in Figure 4.6. It can be seen that the regression model is reasonably well fitted with the observed values.

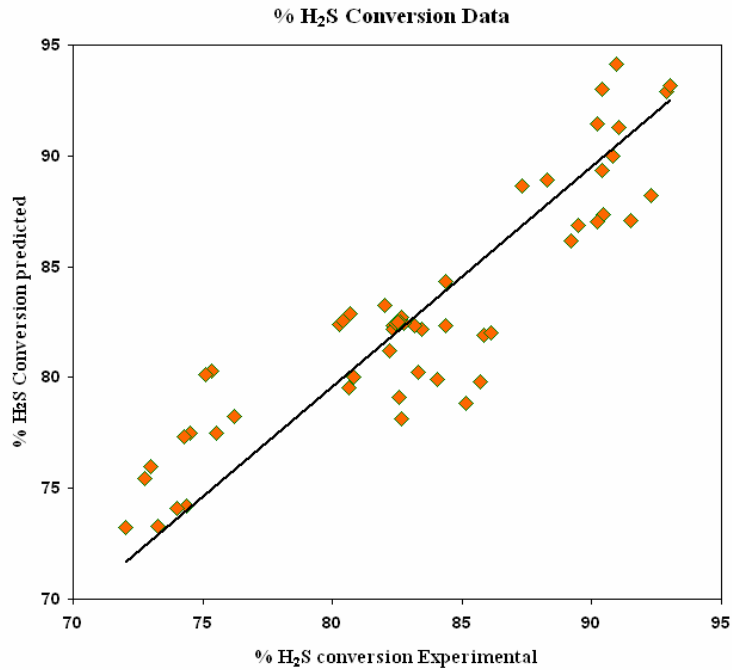
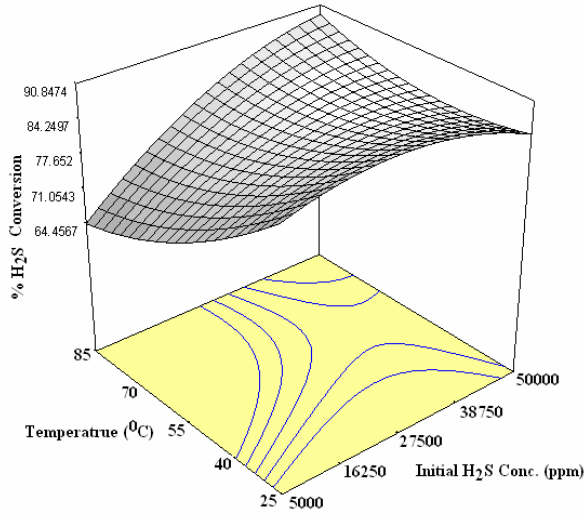
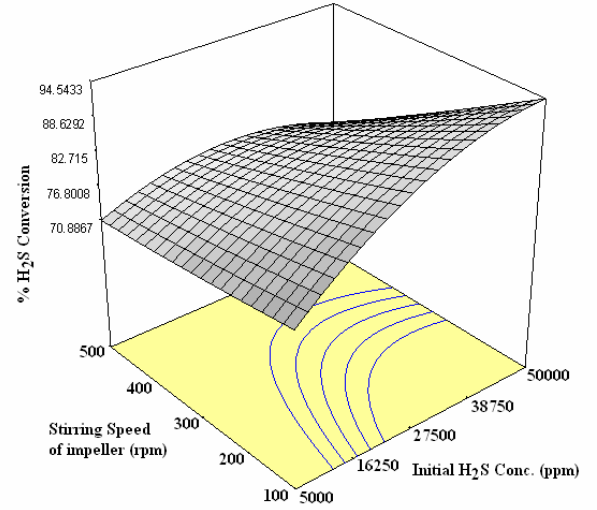


Figure 4.6 Plot of RSM model predicted H_2S % conversion v/s experimental results

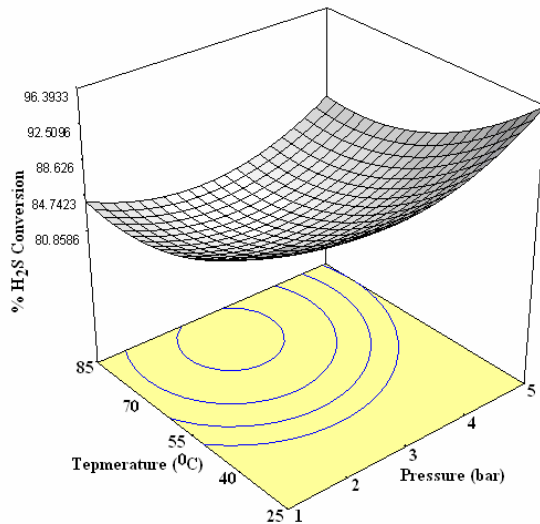
The effect of variables and parameters on the % H_2S conversion for different runs was illustrated by various contour plots. From the ANOVA analysis the significant process variables and parameters are showing interaction between each other. The contour plot 4.1 was used to determine % H_2S conversion over interactive variables of initial H_2S concentration and temperature. As the temperature of the increases the % H_2S conversion decreases as the solubility of gases decreases in high temperature, where, as H_2S concentration increase form 5000 to 50000 ppm there was initially increase in % H_2S conversion till 27500 ppm H_2S concentration. But as concentration increases then % H_2S conversion decreases. The contour plot 4.2 shows the interaction between initial H_2S concentration with stirring speed of impeller on the % H_2S conversion. When initial H_2S concentration was kept low, there was not much effect of stirring speed of impeller on % H_2S conversion, but as initial H_2S concentration was increased the % H_2S conversion was increased from 64% to 92% with varying stirring speed of impeller.



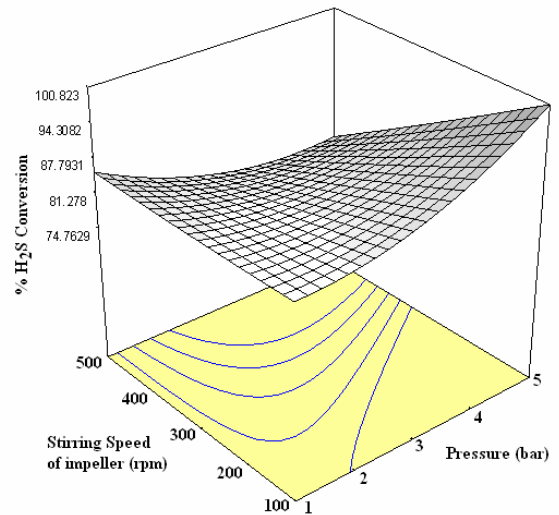
Contour plot - 4.1



Contour plot - 4.2

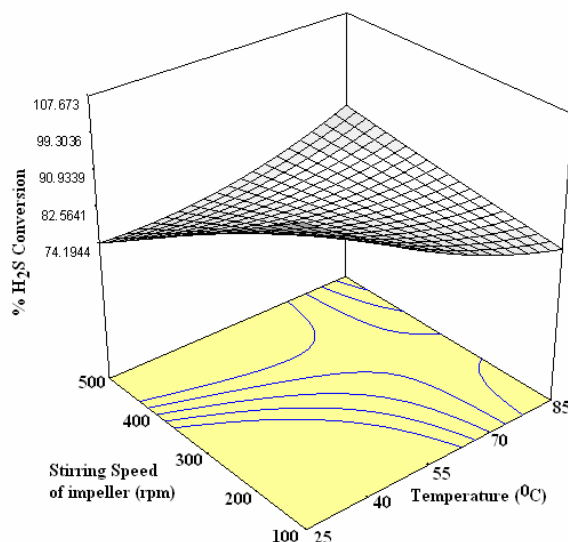


Contour plot - 4.3



Contour plot - 4.4

The effect of interdependency of reactor pressure and temperature on response of % H_2S conversion was shown by contour plot 4.3. The % H_2S conversion was maximum at moderate pressure and at lower temperature. The effects of pressure, temperature and stirring speed of impeller on the % H_2S conversion was shown by contour plot 4.4 and 4.5, respectively.



Contour plot – 4.5

The optimized conditions for the four variables and parameters were calculated by RSM based CCD method was method was tabulated. Table 4.8 gives the three optimized conditions runs for process.

Table 4.8 RSM-optimized solutions and their experimental validation

RSM optimized solution	Run	H ₂ S Conc. (ppm)	Pressure (bar)	Temp. (°C)	Stirring Speed (rpm)	Fe ⁺³ Conc. (ppm)	Reaction Time (min)	H ₂ S % conversion
Predicted run	RSM-1	29862.5	4.18	38.80	169	5000	15	97.0668
Experimental Run	RSM-1	29267.71	4.07	37.80	170	5000	15	97.1382
Predicted run	RSM-2	42575	3.99	40.00	181	5000	15	95.6337
Experimental Run	RSM-2	42445	4.06	40.00	180	5000	15	94.1229
Predicted run	RSM-3	27050	1	70	500	5000	15	94.8731
Experimental Run	RSM-3	27485	1.03	70	500	5000	15	92.8429

The predicted response by RSM was experimentally verified for all three runs. The predicted optimized conditions exhibits the % H₂S conversion of 97% can be achieved at moderate conditions of temperature, pressure, stirring speed of impeller in very less reaction time. Also this process can be used for wide range of initial H₂S

concentration. The agreement between predicted value and experimental value confirms the significance of the model.

8. Conclusions

This work reports a new mechanically agitated batch reactor process involving biodegradable Fe³⁺-Malic acid chelate catalyst for the abatement of environment polluting and toxic hydrogen sulfide gas. The process converts H₂S to elemental sulfur with maximum sulfur recovery (499 mg/gm of iron chelate). Having established the effectiveness of Fe³⁺-MA chelate for H₂S abatement process modeling and optimization was performed using an artificial intelligence based hybrid strategy integrating artificial neural networks and genetic algorithms. In the implementation of this strategy, a process model was developed using an ANN following which the input space of that model—representing significant process operating variables and parameters—was optimized using the GA method with a view of maximizing H₂S conversion (%). The two optimized sets of process conditions obtained using the hybrid ANN-GA strategy were successfully validated in fresh experiments. The best set of optimized process conditions has resulted in 5.63% improvement in the H₂S conversion over that given by the best set of non-optimized process conditions.

References

- [1] John, S. E. "Recovery of Sulfur from Sour acid Gas: A Review of the Technology". *Environ. Prog.* **2002**, Vol. 21, p. 143.
- [2] Gaa, D.; Lagas, J. "Sulfur Recovery Solutions Global Trends". *Chem. Eng. World.* **2004**, Vol. 39, p. 43.
- [3] Asai, S.; Konishi, Y.; Yabu, T. "Kinetics of Absorption of Hydrogen Sulfide into Aqueous Ferric Sulfate Solutions". *AIChE J.* **1990**, Vol. 36, p. 1331.
- [4] Pagella, C.; De Faveri, D. M. "H₂S gas Treatment by Iron Bioprocess". *Chem. Eng. Sci.* **2000**, Vol. 55, p. 2185.
- [5] Jensen, A. B.; Webb, C. "Treatment of H₂S Containing Gases: A review of microbiological alternatives". *Enzyme. Microb. Technol.* **1995**, Vol. 17, p. 2.
- [6] Dalrymple, D. A.; Trofe, T.W. "An Overview of Liquid Redox Sulfur Recovery". *Chem. Eng. Prog.* **1989**, Vol. 85, p. 43.
- [7] McManus, D.; Martell, A. E. "The Evolution, Chemistry an Application of Chelated Iron Hydrogen Sulfide Removal and Oxidation Processes". In 6th International Symposium on the Activation of Dioxygen and Homogenous Oxidation, Noordwijkerhout, The Netherlands, **1996**.
- [8] Oostwouder, S. P.; Hodge, V. B. "Sulferox Process Technology and Application update". In *Sulfur Recovery Conference*. GRI, **1995**.
- [9] Hua, G. X.; Mcmanus, D.; Woollins, J. D. "The Evolution, Chemistry and Applications of Homogeneous Liquid Redox Sulfur Recovery Techniques". *Comments in Inorganis Chemistry.* **2001**, Vol. 22, p. 327.
- [10] Bedell, S. A.; Kriby, L. H.; Buenger, C. W.; McGaugh, M. C. "Chelates' Role in Gas Treating". *Hydrocarb. Process.* **1988**, Vol. 67, p. 63.
- [11] McManus, D.; Martell, A. E. "The Evolution, Chemistry and Applications of Chelated Iron Hydrogen Sulfide Removal and Oxidation Processes". *J.Mol. Catal. A-Chem.* **1997**, Vol. 117, p. 289.
- [12] Demmink, J. F.; Wubs, H. J.; Beenackers, A. A. C. M. "Oxidative Absorption of Hydrogen Sulfide by a Solution of Ferric Nitrilotriacetic Acid Complex in a Cocurrent Down Flow Column Packed with SMV-4 Static Mixers". *Ind. Eng. Chem. Res.* **1994**, Vol. 33, p. 2989.

- [13] Pandey, R. A.; Malhotra, S. "Desulphurization of Gaseous Fuels with Recovery of Elemental Sulphur: an overview". *Crit. Rev. Env.Sci.Tec.* **1999**, Vol. 29, p. 229.
- [14] Nagal, G. "Controlling H₂S Emissions". *Chem Eng.* **1997**, Vol. 104, p.125.
- [15] Pieters, H. A. J.; Krevelen, D. W. "The Wet Purification of Coal Gas and similar Gases by the Staatsmijnen-otto-process". Elsevier, **1946**.
- [16] Martell, A.E.; Motekaitis, R. J.; Chen, D.; Hancock, R. D.; McManus, D. "Selection of new Fe(III)/Fe(II) chelating agents as catalysts for the oxidation of hydrogen sulfide to sulfur by air". *Can. J. Chem.* **1996**, Vol. 74, p. 1872.
- [17] Piché, S.; Ribeiro, N.; Bacaoui, A.; Larachi, F. "Assessment of a redox alkaline/iron-chelate absorption process for the removal of dilute hydrogen sulfide in air emissions". *Chem. Eng. Sci.* **2005**, Vol. 60, p. 6452.
- [18] Karel, V. *Handbook of Environmental Data on organic chemicals*; Van Nostrand Reinhold an international Thomson Publishing company, New York: **1996**.
- [19] Gautier-Luneau, I.; Merle, C.; Phanon, D.; Lebrun, C.; Biaso, F.; Serratrice, G.; Pierre, J. "New Trends in the Chemistry of Iron (iii) Citrate Complexes: Correlations between X-ray Structures and Solution Species Probed by Electrospray Mass Spectrometry and Kinetics of Iron Uptake from Citrate by Iron Chelators". *Chem. Eur. J.* **2005**, Vol. 11, p. 2207.
- [20] Deshpande, A. S.; Sankpal, N. V.; Kulkarni, B. D. Indian Patent application number 1366/DEL/**2003**.
- [21] Nandi, S.; Ghosh, S.; Tambe, S. S.; Kulkarni, B. D. "Artificial neural-network assisted stochastic process optimization strategies". *AIChE J.* **2001**, Vol. 47, p. 126.
- [22] Goldberg, D. *Genetic algorithms in search, optimization, and machine learning* Addison-Wesley: NY, **1989**.
- [23] Davis, L. *Handbook of genetic algorithms*. Van Nostrand Reinhold: NY, **1991**.
- [24] Ramanathan, S.P.; Mukherjee, S.; Dahule, R. K.; Ghosh, S.; Rahman, I.; Tambe, S. S. "Optimization of continuous distillation columns using stochastic optimization approaches". *Trans Inst Chem Eng.* **2001**, Vol. 79, p. 310.
- [25] Sumanwar, V. S.; Jayaraman, V. K.; Kulkarni, B. D.; Kusumakar, H. S.; Gupta, K.; Rajesh, J. "Solution of constrained optimization problems by multi objective genetic algorithms". *Comp Chem Eng.* **2002**, Vol. 26, p. 1481.

- [26] Venkatasubramanian, V.; Sundaram, A. *Genetic algorithms: introduction and applications*. In: *Encyclopaedia of computational chemistry*. Wiley: Chichester, UK, **1998**.
- [27] Lucasius, C.B.; Kateman, G. "Understanding and using genetic algorithms. Part I. Concepts, properties and context". *Chem Intell Lab Syst.* **1993**, Vol.19, p.1.
- [28] Lucasius, C.B.; Kateman, G. "Understanding and using genetic algorithms. Part II. Representation, configuration and hybridization". *Chem Intell Lab Syst.* **1994**, Vol. 25, p. 99.
- [29] Cheema, J. J. S.; Sankpal, N. V.; Tambe, S. S.; Kulkarni, B. D. "Genetic programming assisted stochastic optimization strategies for optimization of glucose to gluconic acid fermentation". *Biotechnol Prog.* **2002**, Vol. 18, p. 1356.
- [30] Baishan, F.; Hongwen, C.; Xiaolan, X.; Ning, W.; Zongding, H. "Using genetic algorithms coupling neural networks in a study of xylitol production: medium optimization". *Process Biochem.* **2003**, Vol. 38, p. 979.
- [31] Rumelhart, D.; Hinton, G. Williams R. "Learning representations by back propagating errors". *Nature.* **1986**, p.323.
- [32] Bishop, C. "Neural networks and their applications". *Rev Sci Instrum* 1803, p.65.
- [33] Tambe, S. S.; Kulkarni, B. D.; Deshpande, P. B. *Elements of artificial neural network with selective applications in chemical and biological sciences Simulation and Advance Control Inc.* Louisville, KY, USA: **1996**.
- [34] Freeman, J. A.; Skapura, D. M. *Neural networks: algorithms, applications, and programming techniques Reading*. Addison-Wesley: MA, **1991**.
- [35] Kiran, B.; Kaushik, A.; Kaushik, C. P. "Response surface methodological approach for optimizing removal of Cr (VI) from aqueous solution using immobilized cyanobacterium". *Chemical Engineering Journal.* **2007**, Vol.126, p.147.
- [36] Parappagoudar, M. B.; Pratihari, D. K.; Datta, G. L. "Non-linear modelling using central composite design to predict green sand mould properties". *Proc. IMechE, J. Engineering Manufacture.* **2007**, Vol. 221 Part B, p. 881.
- [37] Jiunn-Jyi Lay. "Modeling and Optimization of Anaerobic Digested Sludge Converting Starch to Hydrogen". *Biotechnology and Bioengineering,* **2000**, Vol. 68, issue. 3, p. 269.

||shri||

CHAPTER-5

CONCLUSIONS

It is not easy for the earth to replenish her at a pace that she may be relieved of all the pollution we impose upon her”.

The abatement of highly toxic odorous hydrogen sulfide gas is a challenging task. The use of liquid redox sulfur recovery processes are most popular and widely used processes for gas sweetening. The iron (III) was chelated using polyaminopolycarboxylic acids e.g. EDTA, HEDTA, NTA, CDTA, etc. which catalytically converts H₂S into elemental sulfur precipitate. However, very low rate of biodegradation of these commercial chelating agents in the blow down raises the question about environmental pollution.

The main theme of our research work is to replace these commercial chelating agents with some biodegradable chelating agents like simple carboxylic acids which have good chelating property along with higher rates of biodegradation. Taking into consideration the above problem, the screening of some carboxylic acid as chelating agents for iron chelation was carried out. The iron chelates using gluconic acid, malic acid and citric acid as chelating agents were synthesized and used for H₂S to elemental sulfur conversion. Based on the study on the screening of synthesized iron chelates, FeCl₃-malic acid chelate system has been observed to give maximum recovery of sulfur (499 mg/g of iron chelate) along with high purity (> 99%) and reasonable extent of reaction time (15 min). Further study was carried out to decipher the detailed structural characterization of this Fe⁺³-MA chelate using IR, ESI-MS,

TG/DTA techniques which corroborates emphasis the bimetallic iron chelate formation with six malic acid molecules.

The second part of the thesis is focused on the sulfur nanoparticle synthesis, characterization and their applications. Sulfur finds extensive applications in various industries. In our work we first time report the sulfur nanoparticles synthesis using biodegradable iron chelates from hazardous H₂S gas. The synthesis was carried out in reverse microemulsion and aqueous surfactant systems. The sulfur nanoparticles so synthesized are highly mono-dispersed, uniform in shape and size of 5-15nm range. Sulfur is known for its antimicrobial and antifungal activity. The statistical analysis of the experimental data on sulfur activity confirms the high antimicrobial and antifungal activity of sulfur nanoparticles compared with normal sulfur. The analysis also confirms this is due to the actual nano-size, shape and high surface area of nano-sulfur.

The performance of novel biodegradable Fe⁺³-MA chelate for catalytic conversion of H₂S to elemental sulfur was studied in mechanically agitated batch reactor. To achieve maximum catalytic conversion of H₂S, it is necessary to design an optimal process operating strategy for the MABR. The process variables and parameters which significantly influence H₂S conversion were determined using *Plackett-Burman* (PB) design method. Then modeling and optimization of the process operating variables and parameters were conducted using an artificial intelligence based hybrid strategy involving *artificial neural networks* (ANN) to develop model predicting H₂S conversion. Then this model's inputs are optimized using the GA formalism with a view to maximize H₂S conversion. The interactive effects of the process variables and parameters were studied using *Plackett-Burman* (PB) – *Response Surface Method using Central Composite Design* RSM (CCD). The

optimized sets of process conditions obtained using the hybrid ANN-GA and PB-RSM (CCD) strategy were successfully validated in fresh experiments. The GA-optimized process conditions leading to a high ($\approx 97\%$) H_2S conversion was verified experimentally.

The objective of replacement of commercial chelating agents by novel biodegradable iron chelates for maximum catalytic conversion of H_2S to elemental sulfur at ambient temperature and atmospheric pressure was achieved. The reported biodegradable iron chelate system serves many objectives; as reduction of aqueous pollution (by using biodegradable iron chelate), treatment for gaseous waste (removal of H_2S) and recovery of commercially important product (sulfur recovery).

List of Publications

Publications:

- 1) A. S. Deshpande, R. B. Khomane, B.K. Vaidya, R. M. Joshi, A. S. Harle, B. D. Kulkarni, 2008, "Sulfur Nanoparticles Synthesis and Characterization from H₂S gas, using Novel Biodegradable Iron Chelates in Reverse Microemulsion." *Nanoscale Res Lett*, Vol.3, P.221–229, 2008.
- 2) A. S. Deshpande, R. B. Khomane, A. S. Harle, B. D. Kulkarni, 2008, "Sulfur Nanoparticles Synthesis and Characterization from H₂S gas, using Novel Biodegradable Iron Chelates in Aqueous surfactant systems." *Mater. Res. Soc. Symp. Proc.* Vol. 1103, MM01-03, 2008.
- 3) R. B. Jotania, R. B. Khomane, A. S. Deshpande, C. C. Chauhan, and B. D. Kulkarni, "Physical and Magnetic Properties of Barium Calcium Hexaferrite Nanoparticles Synthesized by Water-in-oil Reverse Micelle and Co-precipitation Techniques", *J. Sci Res.* Vol.1, issue 1, P. 1-13, 2009.
- 4) S. S. Mandal, A. S. Deshpande, S.Mayadevi, "Physico-chemical Properties of Layered Double Hydroxide Materials Synthesized in Reverse Microemulsion System: Influence on Fluoride Removal." *Mater. Res. Soc. Symp. Proc.* Vol. 1151, SS01-05, 2009.

Patent:

- 1) Aniruddha S. Deshpande, Narendra, V. Sankpal, Bhaskar D. Kulkarni, "Process Recovery of Sulfur from Sour/Natural Gas using Biodegradable Carboxylic Acid Metal Chelates". Indian patent filled application No. 1366/DEL/2003.

Presentations:

- 1) A. S. Deshpande, R. B. Khomane, A. S. Harle, B. D. Kulkarni, 2008, "Sulfur Nanoparticles Synthesis and Characterization from H₂S gas, using Novel Biodegradable Iron Chelates in Aqueous surfactant systems." presenting at MRS spring meeting Moscone West Convention Center in San Francisco, California. USA.
- 2) A. S. Deshpande, R. B. Khomane, B.K. Vaidya, R. M. Joshi, A. S. Harle, B. D. Kulkarni, 2008, "Sulfur Nanoparticles Synthesis and Characterization from H₂S gas, using Novel Biodegradable Iron Chelates in Reverse Microemulsion." presented at VC-IAN 2008, Orlando, Florida, USA.

- 3) A. S. Deshpande, B. D. Kulkarni, "Gas Phase Synthesis of Sulfur Nanoparticles", a poster presented on National Science Day (28th Feb 2007) at National Chemical Laboratory, Pune-India.
-

Manuscripts communicated and under preparation:

- 1) A. S. Deshpande, Y.P. Badhe, P.P.Barve, S.S.Tambe, "Novel Biodegradable Iron Chelate Catalyst for H₂S Abatement: Modeling and Optimization of Batch Reactor Process using Artificial Intelligence Strategies", Submitted to I&ECR, Manuscript ID ie-2008-01846p, Dec-2008
- 2) A. S. Deshpande, L. B. Kunde, S. B. Umbarkar, M. K. Dongre, B. D. Kulkarni, "Structural Characterization of Iron(III) Chelates Synthesized using Biodegradable Carboxylic Acid: for Catalytic Oxidation of H₂S".